Loan Copy

#1

DOCUMENT OFFICE 26-327
RESEARCH LABORATORY OF ELECTRONICS
MASSACHUSETTS INSTITUTE OF TECHNOLOGY

A MODEL FOR FIRING PATTERNS OF AUDITORY NERVE FIBERS

418

THOMAS F. WEISS

TECHNICAL REPORT 418

MARCH 2, 1964

MASSACHUSETTS INSTITUTE OF TECHNOLOGY
RESEARCH LABORATORY OF ELECTRONICS
CAMBRIDGE, MASSACHUSETTS

The Research Laboratory of Electronics is an interdepartmental laboratory in which faculty members and graduate students from numerous academic departments conduct research.

The research reported in this document was made possible in part by support extended the Massachusetts Institute of Technology, Research Laboratory of Electronics, jointly by the U.S. Army (Electronics Materiel Agency), the U.S. Navy (Office of Naval Research), and the U.S. Air Force (Office of Scientific Research) under Contract DA36-039-AMC-03200(E); and in part by Grant DA-SIG-36-039-61-G14; additional support was received from the National Science Foundation (Grant G-16526) and the National Institutes of Health (Grant MH-04737-03).

Reproduction in whole or in part is permitted for any purpose of the United States Government.

MASSACHUSETTS INSTITUTE OF TECHNOLOGY
RESEARCH LABORATORY OF ELECTRONICS

Technical Report 418 March 2, 1964

A MODEL FOR FIRING PATTERNS OF AUDITORY NERVE FIBERS

Thomas F. Weiss

Submitted to the Department of Electrical Engineering, M. I. T., May 24, 1963, in partial fulfillment of the requirements for the degree of Doctor of Philosophy.

(Manuscript received October 25, 1963)

Abstract

Recent electrophysiological data obtained from auditory nerve fibers of cats have made possible the formulation of a model of the peripheral auditory system. This model relates the all-or-none activity of these fibers to acoustic stimuli. The constituents of the model are intended to represent the major functional constituents of the peripheral system. These constituents are: (i) a linear mechanical system intended to represent the outer, middle, and the mechanical part of the inner ear; (ii) a transducer intended to represent the action of the sensory cells; and (iii) a model neuron intended to represent the nerve excitation process. A general-purpose digital computer has been used to determine the response of the model to a variety of acoustic stimuli. These results have been compared with data obtained from auditory nerve fibers.

TABLE OF CONTENTS

I. INTRODUCTION

The passing of a century of research in audition has produced fundamental changes of attitude on the part of the physiologist. The speculative views of antiquity have been replaced by the empiricism of the late nineteenth and twentieth centuries. We quote from M. J. P. Flourens[2] (1794-1867):

> "Almost every physiologist will admit that we are in complete ignorance as to the usage of the various parts of the ear. Those who do not hold this view are hard pressed to disguise their ignorance by suppositions, conjectures or by some of those words which are used everywhere but which, according to Fontenelle, have no other merit than that of having been considered as real things for a long time. Reasoning alone serves poorly if the question to decide is a question of fact. Everywhere people have started by theorizing instead of doing the necessary experiments. Even in physiology the time has come to proceed in the opposite direction, and to multiply, to repeat, to accumulate experiments in order to end up some day with theories..."

While it is probably true that neurophysiology is still in a developmental stage in which the careful gathering of relevant data is pre-eminent, we feel that it is never too early to organize empirical data along formal and conceptual lines. It is the belief of the writer that such organization of empirical evidence often leads both to deeper insight into the phenomena under investigation and to the suggestion of new and pertinent experiments. In a sense, Flourens' advice has been heeded, and it is now time to produce the theories that he considered to be speculative and premature in his time.

We feel that the primary requisite of a model or theory is precision. The model may well be a crude representation of the system (or phenomenon) under investigation, but it must itself be precise in order for it to be verifiable. It must be possible to test the model in at least a gedanken experiment sense. There are other desirable features of models, beyond their precision, but we shall not belabor the point.

Electrophysiological data obtained recently from single nerve fibers in the auditory nerve (of cats) have made possible the formulation and testing of a model of the peripheral auditory system. This model is intended to relate the all-or-none potentials of these fibers to acoustic stimuli. The initial encoding of acoustic events in the external environment of man (and other species) into all-or-none neural events is accomplished in the peripheral system, and these neural events are transmitted to the central system through the auditory nerve. Understanding both the performance of "higher auditory centers" in the central nervous system and the over-all behavior of the organism appears to us to be predicated on an understanding of the peripheral system.

In this report the discussion of the formulation and testing of the model is organized in six sections. Section II gives a brief discussion of the anatomy of the peripheral auditory system and is intended to introduce some of the terminology associated with the peripheral system. Section III is a discussion of some

of the known physiological mechanisms of the peripheral auditory system. The physiological bases for the model described in Section IV are contained in Section III. A discussion of the results of testing the model is presented in Section V, and concluding remarks are found in Section VI.

II. ANATOMY OF THE PERIPHERAL AUDITORY SYSTEM

The gross anatomy of the peripheral auditory system of man (and other higher species) is relatively well known (see, for instance, Polyak[48]) and only the briefest description need be given here. For our purposes, we can divide the auditory system into four parts (as shown in Fig. 1) – the outer, middle, and inner ear, constituting the peripheral auditory system, and the central nervous system.

Figure 2 shows a schematic diagram of the peripheral system. Airborne sound enters the outer ear past the auricle (the externally visible ear-lobe structure) by way of the external auditory meatus (a canal that is 2.5 cm long in man) and impinges on the tympanic membrane (or eardrum). The sound waves set the tympanic membrane in motion. This motion is transmitted to the middle ear, which contains a set of three tiny bones, the ossicles. The three-ossicle chain, malleus to incus to stapes, transmits the motion of the tympanic membrane to another membrane, the "oval window," which is the mechanical input to the inner ear. The auditory part of the inner ear comprises the cochlea, a functionally and morphologically complex system that converts the mechanical motion of the stapes into spike potentials. The 3×10^4 nerve fibers[21] emerging from the cochlea go directly into the central nervous system as a part of the VIIIth Cranial nerve at the level of the medulla oblongota.

The detailed anatomy of the cochlea is the most complex part of the peripheral system. It is in the cochlea that the mechanical forces and motions are converted into neural signals. As shown in Fig. 3, the cochlea is in the form of a spiral tube, that is, a tube wound on a cone in such a way that the axis of the tube is helical. The interior of this helix is called the modiolus and contains the nerve fibers as they emerge from the tube, or cochlear canal. The number of revolutions of the canal differs in different species: 2 3/4 cochlear turns in man, 3 in cat, and 4 1/2 in guinea pig. The lengths of the axes of the canal are 35 mm, 23 mm, and 18 mm, respectively. The canal diameter decreases from the basal end of the cochlea (near the base of the cone) to the apical end. In man this variation is from 2.5 mm to 1.2 mm.

The cross section of the cochlear canal (shown schematically in Fig. 4) is divided by a multimembraneous "cochlear partition." This partition separates the cochlear canal into two canals filled with fluid, the perilymph. These two canals, the scala vestibuli and scala tympani, are connected through a hole (0.15 mm^2 in man), called the helicotrema, in the apex of the cochlear partition. Perilymph can thus flow from scala vestibuli to scala tympani, and vice versa, through the helicotrema. At the basal end of the cochlea the two scalae are each sealed by a membrane. The oval window seals the scala vestibuli, and the round window seals the scala tympani. It is the oval window that is displaced directly by the motion of the footplate of the stapes.

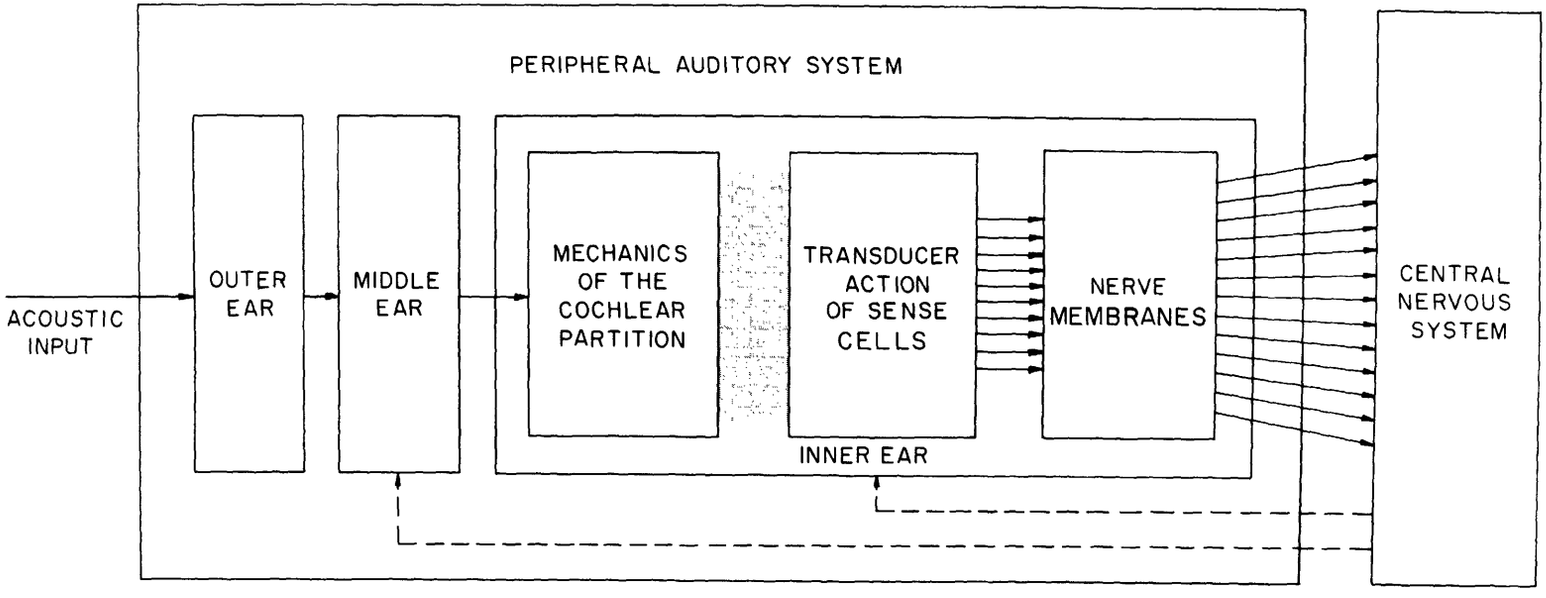

Fig. 1. Block diagram representation of a model of the peripheral auditory system. The shaded area represents the motion of the cochlear partition as a continuous function of space and time. Arrows emerging from the block labelled "Transducer Action of Sense Cells" represent the outputs of the sensory cells that are considered to be spatially discrete. Arrows emerging from the block labelled "Nerve Membranes" represent afferent auditory nerve fibers. Dashed lines represent efferent pathways emerging from the central nervous system and terminating in the peripheral auditory system.

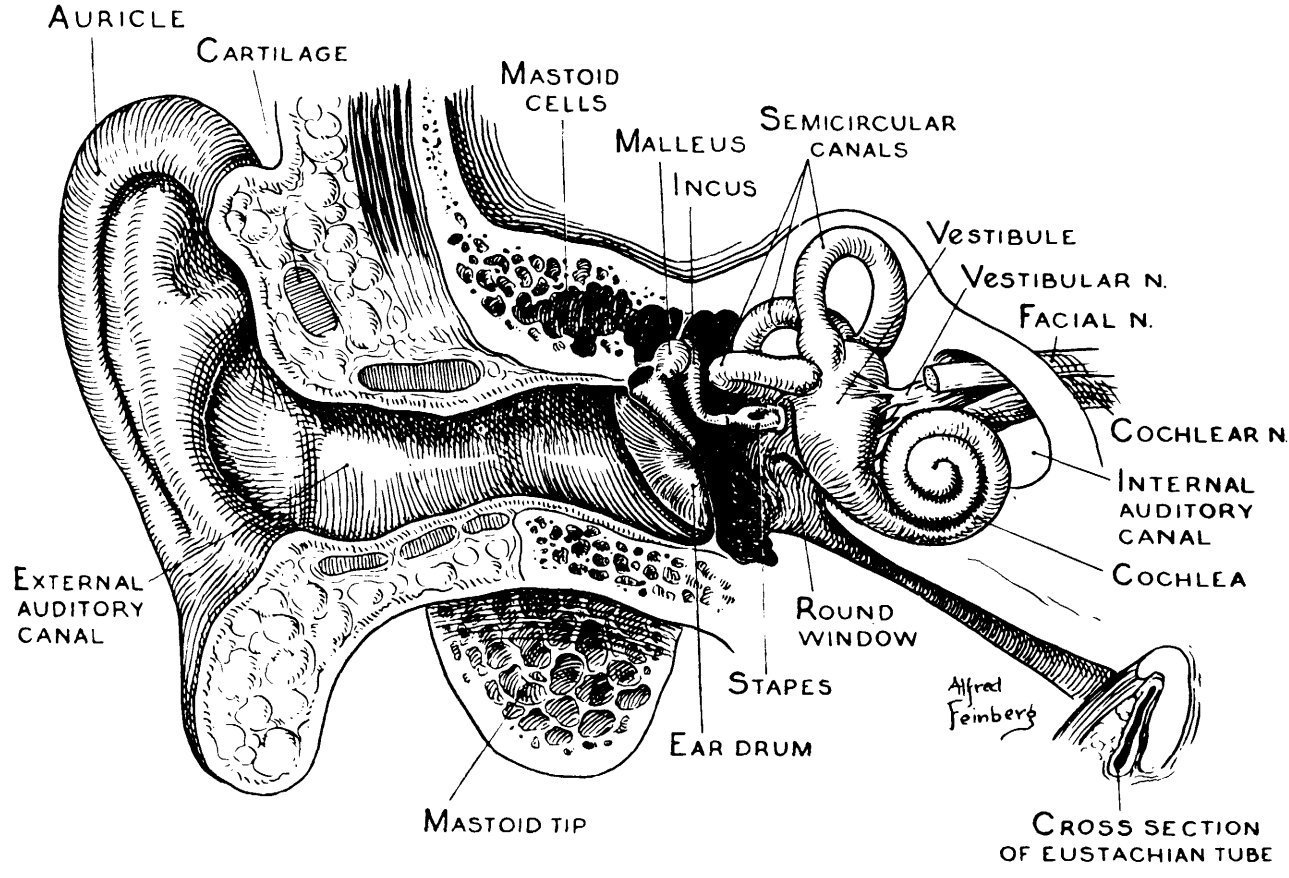

Fig. 2. Schematic diagram of the gross anatomy of the peripheral auditory system. (After H. Davis (ed.), Hearing and Deafness: A Guide for Laymen. New York, Rinehart, 1947.)

Fig. 3. A horizontal midmodiolar section through the cochlea of a cat. The turns of the cochlea of the cat are clearly discernible. The VIIIth nerve can be seen emerging from the various turns of the cochlea, forming a bundle that enters the cochlear nucleus (from Kiang et al.[36]).

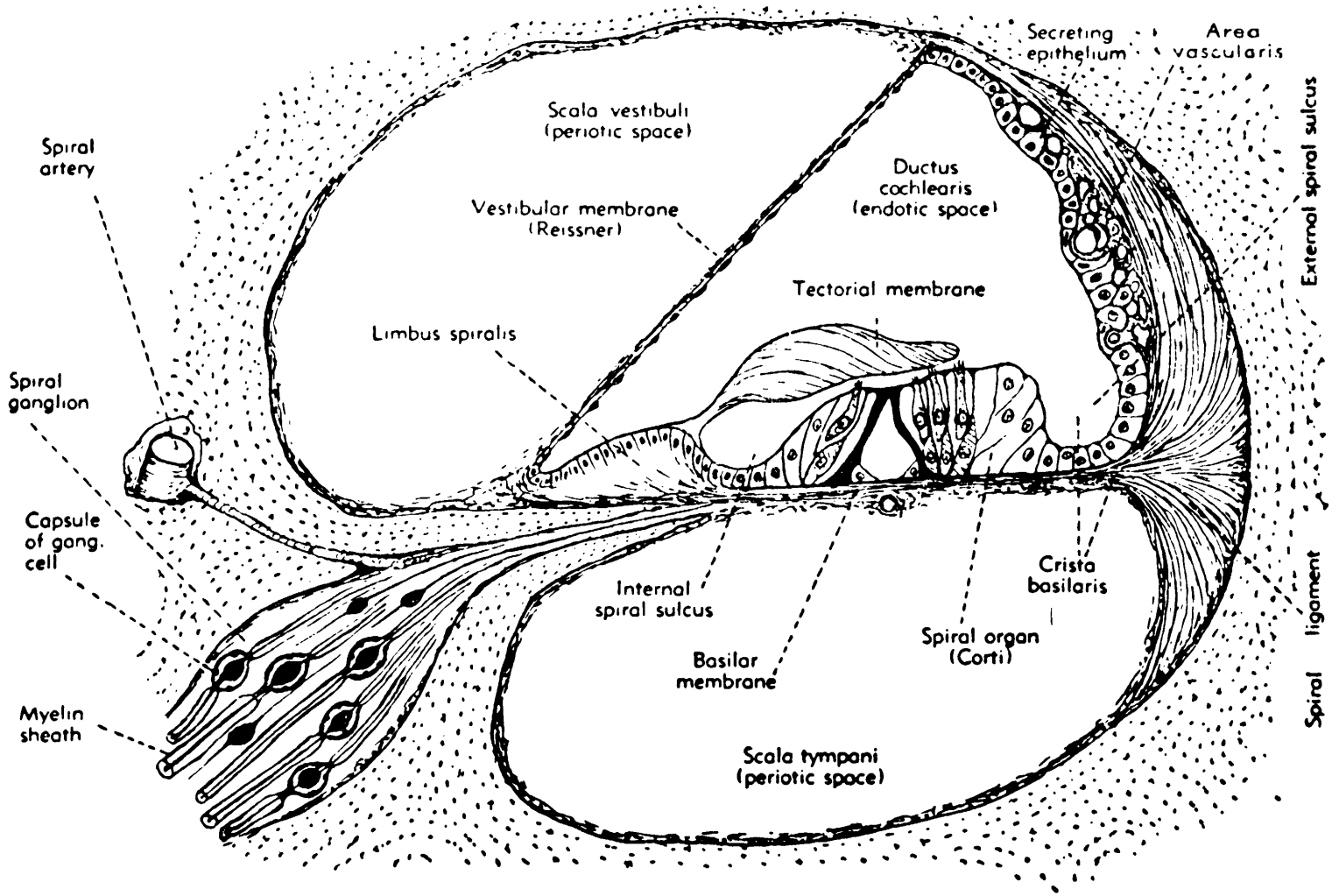

Fig. 4. Schematic diagram of a cross section of the cochlear canal (from A. T. Rasmussen, Outlines of Neuroanatomy. William C. Brown Company, Dubuque, Iowa, 3d edition, 1943).

The cochlear partition is bounded by and includes Reissner's membrane and the basilar membrane. The partition consists of the ductus cochlearis – a space filled with the endolymph fluid, the Organ of Corti (a detail of the Organ of Corti is shown in Fig. 5) – containing the auditory receptor cells and their innervation, and certain structural and trophic parts (such as the spiral ligament, stria vascularis, etc.). There are at least two types of auditory receptor cells: a single row of inner hair cells (approximately 3.5×10^3 cells, in man) and three or four rows of outer hair cells (approximately 20×10^3 cells, in man).[48a] These cells are supported on the basilar membrane and give off hairs at their apices that extend through the reticular lamina and into the tectorial membrane. The innervation of these hair cells is not entirely known. There appear, however, to be at least two kinds of innervation of these hair cells: a local innervation provided by the radial nerve fibers; and the more diffuse innervation of the spiral nerve fibers. The inner hair cells appear to be innervated preponderantly by the radial fibers,[13] one radial fiber innervating perhaps one or two inner hair cells, and a hair cell being innervated by one or two radial fibers. The outer hair cells seem to be innervated by radial fibers, as well as by spiral fibers that enter radially, and after making a right-angle turn, travel toward the round window along the base of the outer hair cells for as much as a half turn of the cochlea.[13] The spiral fibers appear to innervate several outer hair cells along their path.[13] In addition to these two groups of fibers, there is a smaller number of fibers that innervate both inner and outer hair cells.[13]

Electron-microscopic studies of the cochlea[9, 10, 57] have shown that a substantial morphological difference exists between inner and outer hair cells. (There also appear to be at least two morphologically different kinds of outer hair cells.[57]) Furthermore, the nerve fiber endings, adjacent to the hair cells, also show some differentiable features. Some of these endings show simple knoblike structures, while others form a large area of contact between hair cell and neuron. The latter junctions show enlarged membranes on the hair cell adjacent to the innervating fiber in addition to vesicles on the neural fiber side of the junction. The last properties are usually associated with synaptic endings; the vesicles appearing on the presynaptic side. These results have led to the speculation that the vesiculated endings are the endings of efferent fibers. Thus far, firm relationships between all three of these gross categorizations of innervation have not been conclusively demonstrated: (i) spiral vs radial, (ii) efferent vs afferent, and (iii) vesiculated ending vs nonvesiculated ending.

The afferent nerve fibers that innervate the hair cells have their cell bodies in the spiral ganglion and send their other processes through the modiolus to the cochlear nucleus in the medulla oblongota (a distance of approximately 5 mm). The cells (27×10^3, in man) of the spiral ganglion are bipolar cells, and no synaptic connections have been seen in the ganglion.[48b] Histology of a cross section

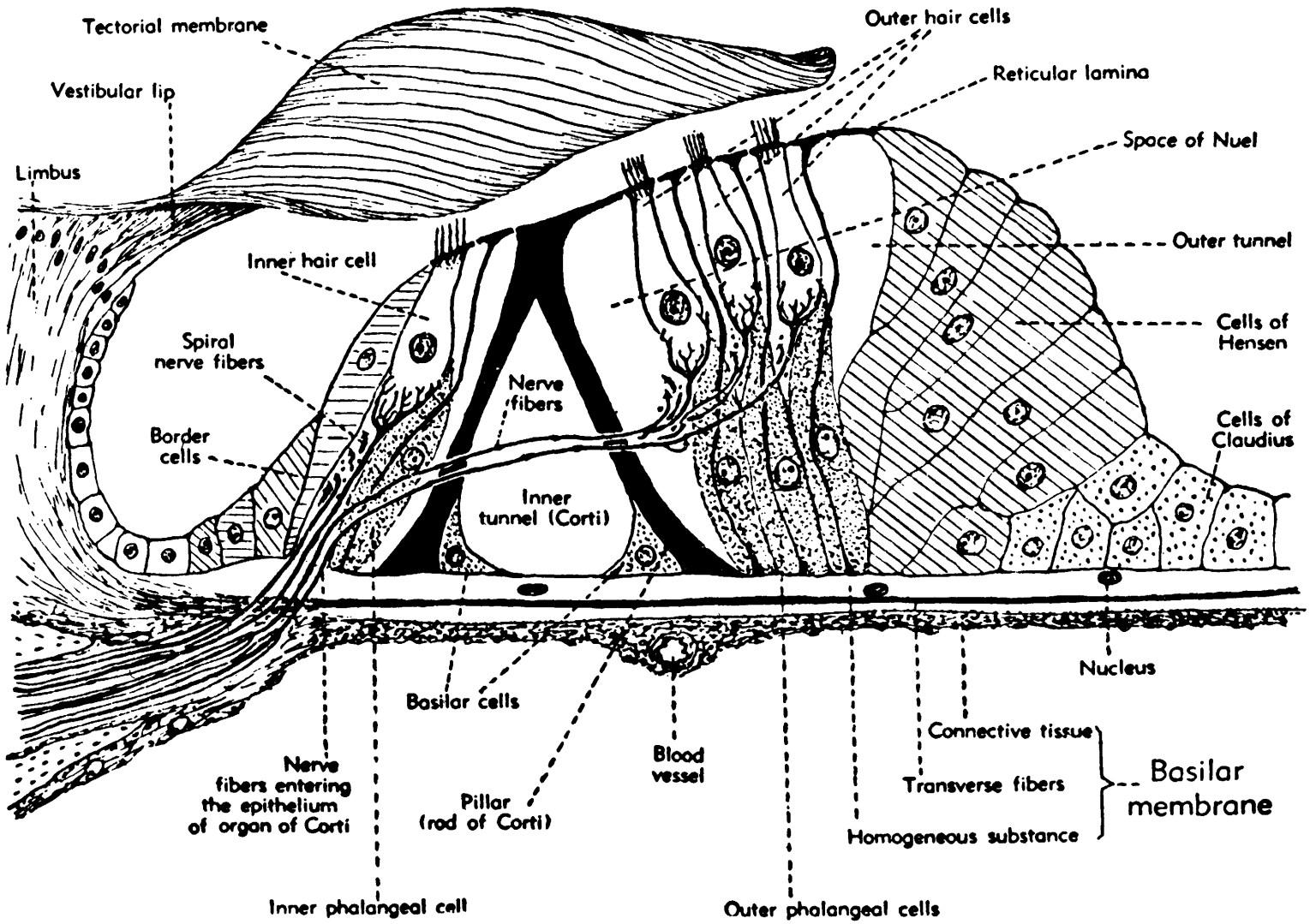

Fig. 5. Schematic diagram of the Organ of Corti (from A. T. Rasmussen, Outlines of Neuroanatomy. William C. Brown Company, Dubuque, Iowa, 3d edition, 1943).

of the VIIIth nerve reveals a remarkable uniformity of fiber diameters (between 3 μ and 5 μ).[21, 52]

A cross section of the VIIIth nerve exhibits another regularity. As the fibers exit the modiolus, the fibers originating in the more basal turns of the cochlea wrap around the central core of fibers originating in the more apical turns of the cochlea. The VIIIth nerve, therefore, is composed of a regular array of fibers. Spatial contiguity of the adjacent fibers in the cochlea is preserved in the auditory nerve.

There is evidence in published works for several efferent neural pathways to the peripheral auditory system. First, there is the innervation of the heretofore unmentioned middle-ear muscles. The stapedius muscle, connected to the stapes, is innervated by the facial (VIIth Cranial) nerve, and the tensor tympani, which exerts tension on the manubrium of the malleus, is innervated by the mandibular division of the trigeminal (Vth Cranial) nerve. Also, there is a number of efferent fiber bundles originating in several different areas of the central nervous system, and these fibers are thought to terminate in the Organ of Corti.[50]

III. SYSTEMS PHYSIOLOGY OF THE PERIPHERAL AUDITORY SYSTEM

We are primarily interested in the relation between the firing patterns of single fibers in the VIIIth nerve and acoustic stimuli delivered to the ear. Our approach takes into account the input-output relations of the major components of the peripheral system, rather than the detailed structure and function of each part.

3.1 DYNAMICS OF THE OUTER AND MIDDLE EAR

The detailed physiology of the outer and middle ear is well documented (see for instance Wever and Lawrence[71]) and thus in our description we shall concentrate on a systems approach. The role of these two structures is now quite clear. The specific acoustic impedance of air is 41.5 ohms/cm^2 (at 20°C), and the specific acoustic impedance for a fluid such as the perilymph has been estimated to be approximately 16×10^3 ohms/cm^2. Thus an impedance-matching device is needed in order to make the transmission loss of sound waves going from air to perilymph (the site of the receptor cells) tolerable. The middle ear provides this mechanism for transforming the relatively large displacements and small pressures in air into relatively small displacements and large pressures in the perilymph. Essentially, the transformer ratio is achieved by the difference in effective cross-section areas of the tympanic membrane and oval window (approximately 21, in man), but the ossicular chain provides an additional mechanical advantage (estimated to be 1.3, in man).[71a]

While these principles are quite simple, the realization of the transformation and the detailed motion of the middle-ear structures are quite complex. For instance, the tympanic membrane does not have a simple drumlike motion,[1a] nor is its characteristic motion the same for all frequencies of sinusoidal pressure stimulation.[1b] Similarly, the oval window seems to change its mode of vibration as a function of intensity.[1c] Also, the incudostapedial joint is loose and lowers the efficiency of sound transmission to the cochlea at high intensities.[71c] For high intensities of prolonged sound stimulation, a middle-ear muscle-contraction reflex is actuated that effectively decreases the efficiency of transmission through the middle ear.[71d]

Despite this complexity, there is a wide range of intensity of stimulation over which the operation of the mechanical part of the peripheral auditory system can be considered as linear. The transfer characteristic of the mechanical part of the system has been determined, albeit in an approximate way and over a limited range of frequencies.

Since none of the studies to which we shall make reference use free-field stimulation, we can ignore the effects of the auricle on sound transmission to the ear. The external meatus is a bony tube terminated by the tympanic membrane. Wiener and Ross[72] measured the pressure transformation from the outside of the ear to the tympanum in human subjects. Figure 6 shows their results. The relatively flat peak of the response occurs at the predicted resonance frequency (3.8 kc) of a closed tube approximately 2.5 cm long.

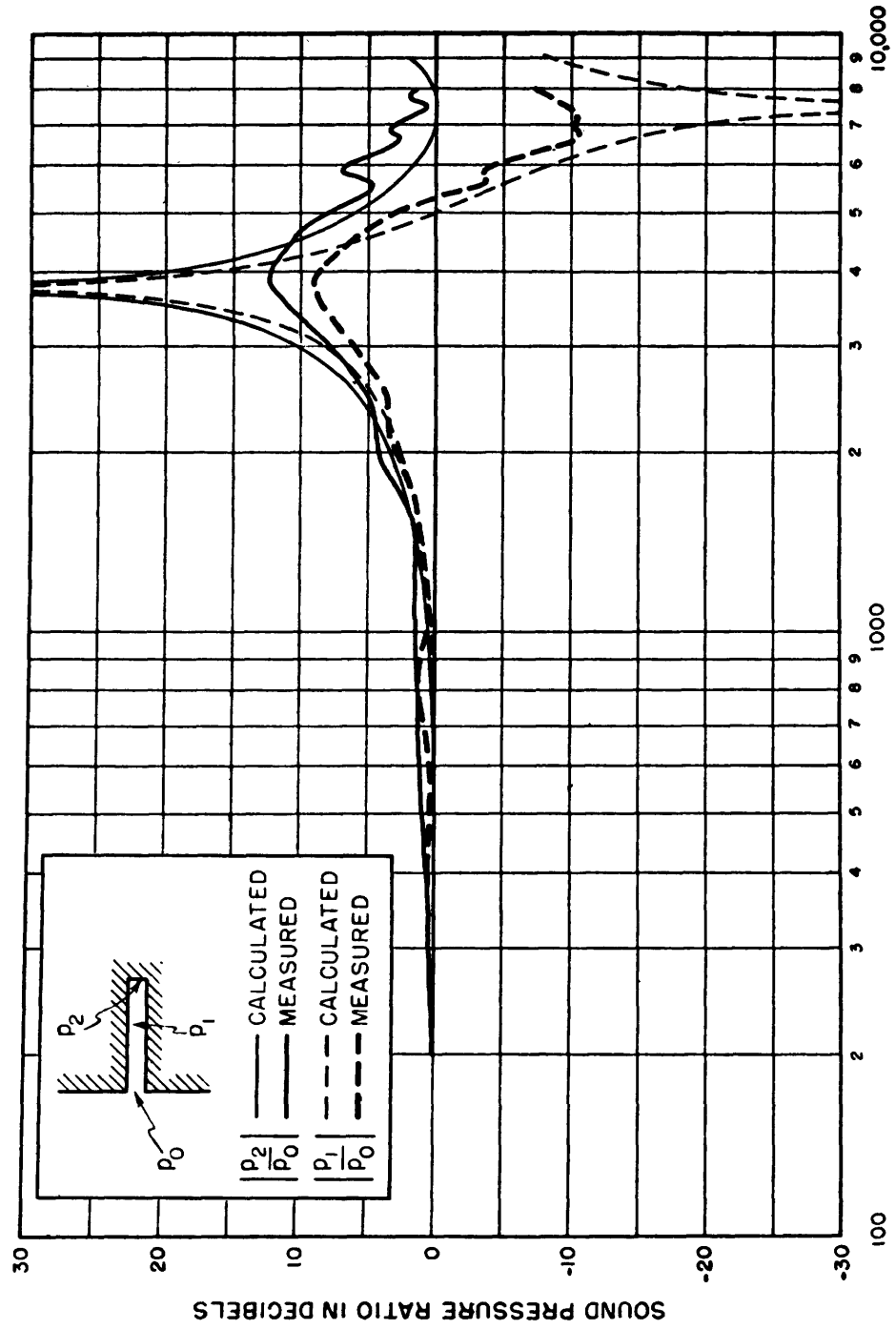

Fig. 6. Ratio of amplitude of pressure at tympanum to amplitude of sinusoidal pressure at entrance to the meatus (measured in man) (from Wiener and Ross[72]).

(v is the velocity of sound in air at 20°C, λ is the wavelength, and f the frequency. Then

$\lambda/4 = 0.025$ meter

$\lambda = 0.1$ meter

$f = v/\lambda = 340/0.1 = 3.4$ kc for a tube 2.5 cm long.)

Since the termination of the tube is a flexible membrane, the resonance is relatively flat. Note that the transfer function varies less than 10 db over the 8-kc range of the measurements.

Von Békésy has made a number of measurements that aid in revealing the transfer characteristic of the middle ear. This transfer characteristic is defined as the ratio of the amplitude of the displacement of the stapes to the amplitude of a sinusoidal pressure variation at the tympanum. The utility of such a function depends strictly on the linearity of the system. Von Békésy has reported that the middle ear is essentially linear up to the threshold of feeling.[1d]

In discussing the data on the middle ear it is useful to consider its circuit representation. In Fig. 7, p_d is the pressure at the ear drum, v_d is the velocity of displacement of the ear drum, p_o is the pressure at the oval window, v_o is the velocity of the displacement of the oval window (or stapes) and z_o is the mechanical input impedance of the cochlea as seen from the oval window. z_{11}, z_{12}, z_{22} are the mechanical impedances that characterize the middle ear.

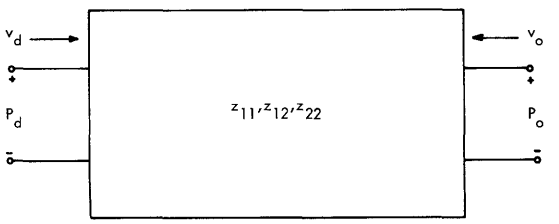

Fig. 7. Circuit representation of the middle ear.

$$p_d = z_{11}v_d + z_{12}v_o$$

$$p_o = z_{12}v_d + z_{22}v_o$$

Von Békésy[1d] has measured the pressure ratio (in human cadavers) from both the entrance of the meatus and the tympanum to the stapes by balancing the pressure at the stapes from inside the cochlea until the stapes was motionless. This corresponds in our framework to a measurement of the open circuit pressure ratio, $(p_o/p_d)_{v_o=0} = z_{12}/z_{11}$. Figure 8 shows these data. Note again that the variation over a 2-kc range is not greater than 10 db. Von Békésy[1e] has also measured the volume displacement of the round window to a known pressure at the ear drum

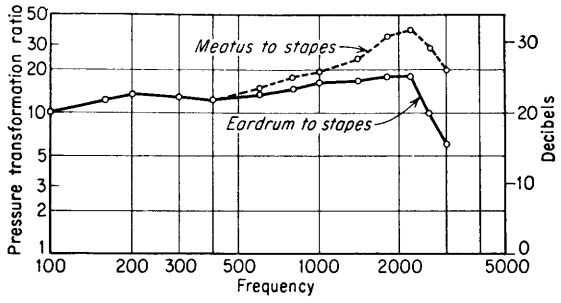

Fig. 8. Open-circuit pressure ratio from the entrance to the meatus (dashed) and the tympanum (solid) to the stapes. (From von Békésy[1d].)

as a function of frequency. His measurement corresponds to measuring $(q_o/p_d) = -(k/j\omega)(z_{12}/z_{11})\left(z_o+z_{22}-(z_{12}^2/z_{11})\right)^{-1}$, where q_o is the displacement of the oval window, under the assumption that the displacement of the oval window is equal to the displacement of the round window. (This assumption is valid under the assumptions that the walls of the cochlea are rigid and the cochlear fluids are incompressible.) Von Békésy's data are shown in Fig. 9. Again, the amplitude variation as a function of frequency is below 10 db.

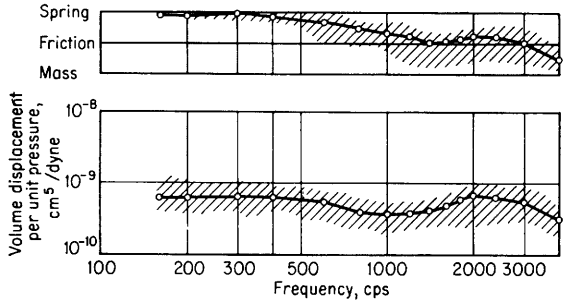

Fig. 9. Amplitude and phase of the volume displacement of the round window for a sinusoidal pressure variation at the tympanum. Upper curve shows the phase angle; lower curve, the volume displacement per unit of pressure. (From von Békésy[1e].)

Further data on the dynamics of the middle ear have been obtained from measurements of the input impedance of the ear in human subjects. In our terminology, $z_{in} = (p_d/v_d) = (z_{11}/z_{22}+z_o)(z_{22}+z_o-(z_{12}^2/z_{11}))$. On the basis of their measurements of the input impedance of the ear, both Møller[41, 42] and Zwislocki[75] have constructed equivalent electric circuits of the middle ear.

Transfer characteristics plotted from Møller's data are relatively flat in the region 100 cps-1 kc. A similar computation performed by Flanagan[17] on Zwislocki's data

yields results that, while not the same in detail as our results calculated from Møller's model, again indicate a flat amplitude response up to approximately 1 kc.

We have tried to summarize a wide variety of data concerning the mechanical transmission of displacements to the stapes. (A recent paper[78] indicated that gross postmortem changes occur in the acoustic impedance of the ear.) To our knowledge, there are no reliable data for frequencies above 2 kc, and we conclude from available data that the frequency response of the outer and middle ear is flat within 10 db for frequencies below 2 kc. This is probably true for the cat as well as for man.[43] The measurements on acoustic transmission and impedance of the ear show great variability for frequencies above 2 kc. At high frequencies the motion of the various middle-ear structures becomes quite complicated and this has complicated the measurement problem.

3.2 DYNAMICS OF THE COCHLEA

The direct observations and measurements of the dynamics of the cochlea are due entirely to von Békésy. In this section we shall consider von Békésy's measurements of various physical properties (such as viscosity, density, elasticity, etc.) of the cochlea. We shall then discuss his observations of the motion of the cochlear partition (in physiological preparations as well as in mechanical models) as a function of the displacement of the stapes.

The most important physical parameters that von Békésy measured were the properties of the cochlear partition. He showed[1f] that the cochlear partition was not in tension and, therefore, could not be considered as a stretched membrane. Von Békésy[1g] discovered that the elasticity of the cochlear partition varies from the basal to the apical end of the cochlea. Figure 10 shows a curve of the variation of the elasticity of the cochlear partition for human cadavers. The partition is relatively stiff at the basal end,

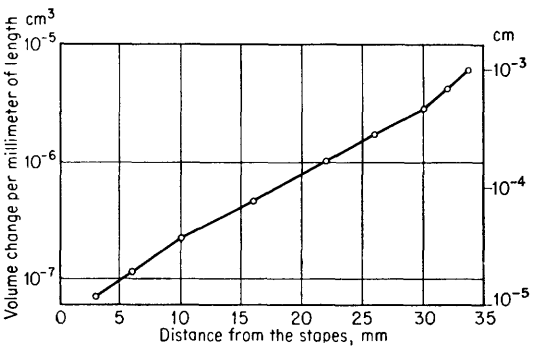

Fig. 10. Elasticity of the cochlear partition as a function of distance from the stapes. Volume displacement per millimeter of the cochlear duct (left-hand ordinate) and maximum displacement of the cochlear partition (right-hand ordinate) for a pressure of 1 cm of water. (From von Békésy[1g].)

while at the apical end the partition is relatively flaccid. Von Békésy[1h] was further able to demonstrate that it is the elasticity distribution of the basilar membrane that dominates this pattern. The elasticity of the other structures in the cochlear partition (tectorial membrane, Reissner's membrane and reticular lamina) is relatively constant over the length of the cochlea. Needless to say, the elastic characteristics of the partition are much more complex than as shown here. For instance, it is clear that the elastic properties must vary along the cross section of the cochlear partition, since the basilar membrane is supported on one side by bone, and on the other side by ligament. Nevertheless, it is the 100:1 variation in elasticity of the basilar membrane in its longitudinal direction that gives the cochlear partition its chief dynamic properties.

Von Békésy also estimated the density and viscosity of the perilymph[1i] and showed that the mass loading of this fluid[1j] on the cochlear partition was an important factor in the dynamics of the cochlea. In addition, he estimated[1k] the damping of the cochlear partition.

Observations on the motion of the cochlear partition in human cadavers were achieved by cutting away various portions of the cochlea and/or replacing these portions with transparent surfaces. The cochlea was stimulated mechanically through an artificial stapes usually located at the round window. Even for the relatively large stapedial displacements that he used, von Békésy found that the relation of the displacement of the cochlear partition to a stapes displacement was linear.[1ℓ] For a sinusoidal stimulus, the displacement of the cochlear partition was sinusoidal in time, and the envelope of the displacement exhibited a spatial pattern whose maximum moved as a function of frequency.[1m] Figure 11 is such a "cochlear map,"[1n] obtained by measuring the position of the maximum displacement of the cochlear partition as a function of frequency

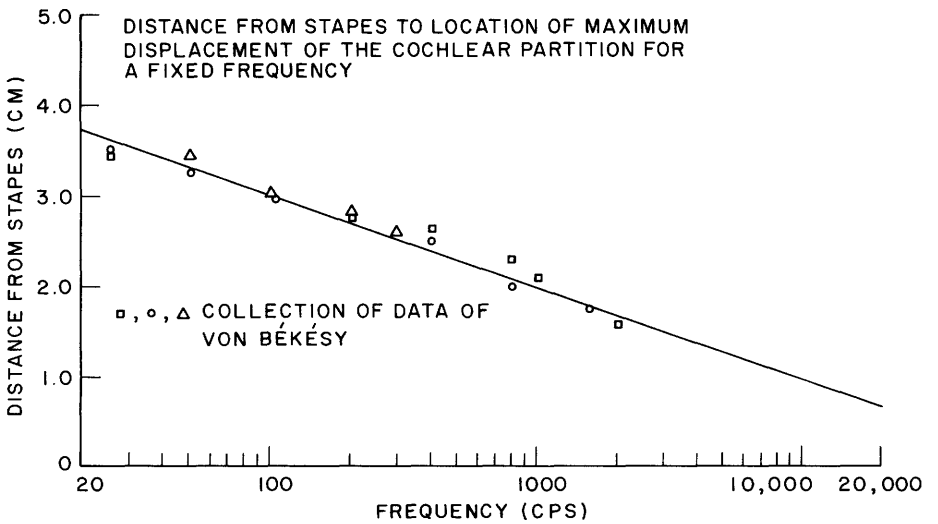

Fig. 11. Position of the maximum displacement of the cochlear partition as a function of the frequency of sinusoidal stapes displacements. (From Siebert[55].)

Von Békésy has stated that these measurements show "great stability" for different cochleas.

Figure 12 shows the amplitude of displacement at a point on the membrane as a function of frequency for several different points plotted on a normalized scale.[1p] Note that all curves have the same general shape when plotted in logarithmic coordinates. If the frequencies of their maxima are brought into coincidence on a logarithmic frequency scale, the curves are almost identical. These

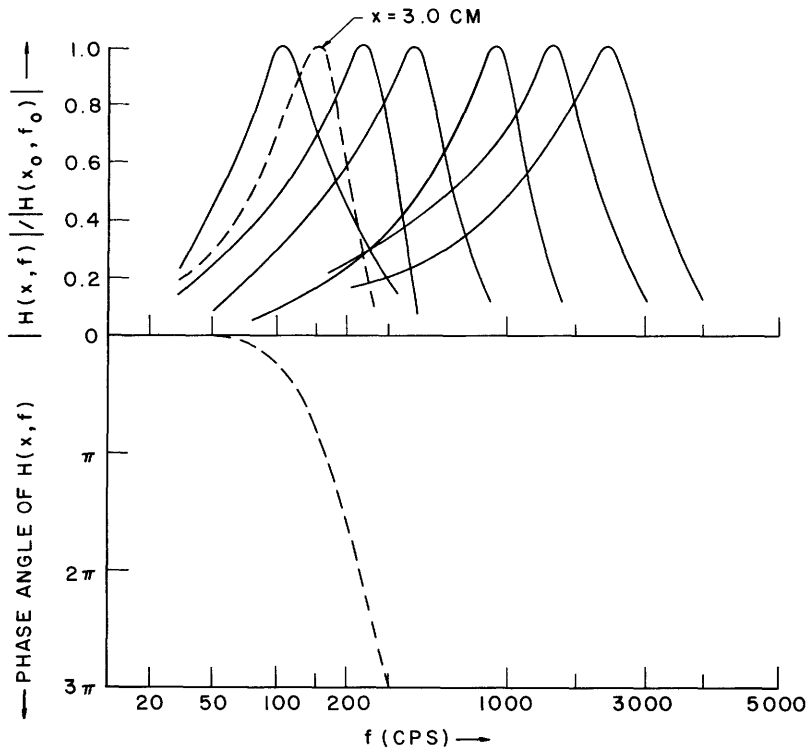

Fig. 12. Amplitude and phase of displacement of the cochlear partition as a function of frequency for several positions along the cochlear partition. H(x,f) is the transfer function of the cochlear partition for a sinusoidal displacement of the stapes. The scales of the amplitude and phase responses are the same. Solid curves, von Békésy (1943)[1p]; dashed curves, von Békésy (1947).[1q] (The figure is reproduced from Siebert[55].)

curves show a relatively broad resonance with a figure of merit, Q = 1.6 (when Q is defined as the ratio of the resonant frequency to the bandwidth measured at -3 db with respect to the maximum). The value of the maximum displacement of each point along the cochlear partition varies as a function of frequency as

shown in Fig. 13.[1r] The coordinates of a point on the curve are to be interpreted in the following manner: Suppose the frequency yielding a maximum displacement of the cochlear partition at point x_o is f_o. The maximum amplitude of displacement of the cochlear

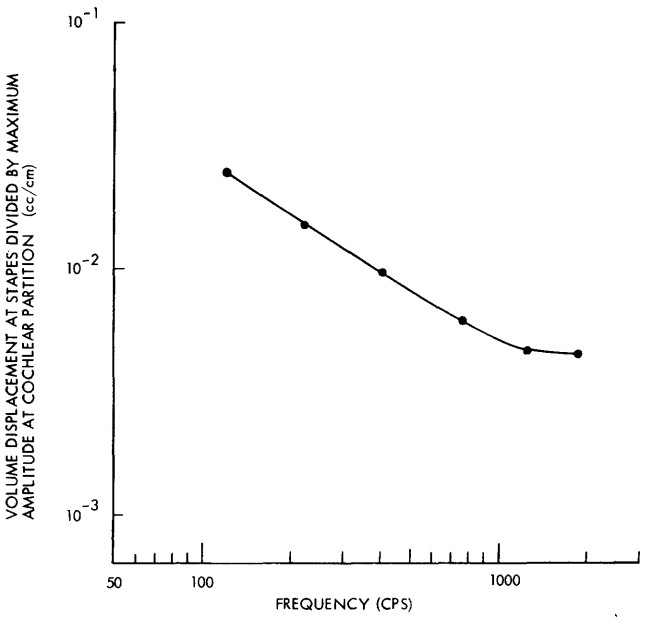

Fig. 13. Volume displacement at stapes divided by maximum amplitude at cochlear partition as a function of frequency. (From von Békésy[1r].)

partition at point x_o and at frequency f_o is $|H(x_o, f_o)|$ for a unit volume displacement of the stapes. The curve shown in Fig. 13 is a plot of $1/|H(x_o, f_o)|$ as a function of f_o in logarithmic coordinates.

Von Békésy has also obtained curves of the displacement pattern of the cochlear partition as a function of position for various frequencies of stapes displacement.[1s] He describes the motion of the cochlear partition[1q] as that of a traveling wave whose envelope has a maximum at some position (determined by the frequency of the stapes displacement) and whose wavelength decreases as a function of distance from the stapes.

This entire response pattern is reported to be independent of the point of excitation. That is, when the fluid displacements are initiated in the apical end of the cochlea through an artificial opening, the same pattern of traveling waves is seen from the base to the apex.[1t, 71b] This phenomenon was named the "paradoxical direction of propagation" by von Békésy.

The dynamics of the cochlea can now be understood, at least in a qualitative way. First, consider the propagation velocity of a compression or sound wave in a medium such as perilymph. Since the density of perilymph is approximately the same as that of water, the velocity of sound in perilymph can be assumed to be approximately equal to the velocity of sound in water. This velocity is 1.4×10^3 mm/msec. The cochlea of man is approximately 35 mm long; thus the propagation time of sound from one end of

the cochlea to the other is approximately 25 μsec. This is two orders of magnitude smaller than the propagation time of the traveling waves that von Békésy observed at the apical end of the cochlea. Therefore, the pressure wave generated by stapes displacements (or stimulation at any other point in the cochlea) can be assumed to reach the apical end of the cochlea almost instantaneously.

The response of a point on the cochlear partition to this pressure change depends upon the physical parameters of the membranes and fluids. The frequency of stimulation giving maximal response for that point, f_o, is determined largely by the elasticity of the cochlear partition at that point, and by the mass loading of the fluid in the neighborhood of that point, as well as friction, viscosity, and membrane coupling effects. Since the elasticity increases continuously as a function of distance from the stapes, we would intuitively expect that f_o will decrease. Furthermore, as the elasticity increases, the response time or lag time of a point on the cochlear partition also increases. Since the parameters of the cochlear partition vary continuously, this response time varies continuously and thus the response of the partition to a sudden displacement of the stapes appears as a progressive set of displacements, or as a wave that travels down the cochlea. This pattern is not a traveling wave in the ordinary sense, since all of the energy is not transferred from one element of the membrane to another. Von Békésy, using scaled models of the cochlea, has demonstrated that it is most likely that the energy for the motion of the membrane is transmitted to the membrane from the fluid. Thus, it is the change in elasticity of the basilar membrane as a function of distance that gives the cochlea its particular response characteristics. Unfortunately, the equations of motion of such a system are complicated both by the geometry and the interaction terms. That is, one can probably not reduce the mechanics of the cochlea to a simple lumped parameter system that includes mass, elasticity, and damping. The cochlea can best be regarded as a distributed parameter system whose parameters vary grossly with distance from the stapes.

Several workers have attempted to derive the equations of motion of the cochlear partition,[18,45,49,70,73,74] with varying degrees of success. Most of the analytic approaches that yield solutions ultimately arrive at a one-dimensional representation of the cochlea. The relevant equations that have been used are: the continuity equation for an incompressible fluid; the Navier-Stokes equation of motion for an incompressible fluid with irrotational, infinitesimal motion; and the beam equation, including elasticity, mass, and damping. Various authors have made further assumptions as to which terms in the equations dominate and therein lie the differences in the approaches.

One of the earlier and more interesting analytic approaches to the problem is that of Zwislocki,[73] who derived a closed-form expression (under a multitude of assumptions) for the displacement of the cochlear partition in response to a sinusoidal displacement of the stapes. The results that he plots seem to fit the von Békésy frequency-response curves rather well.

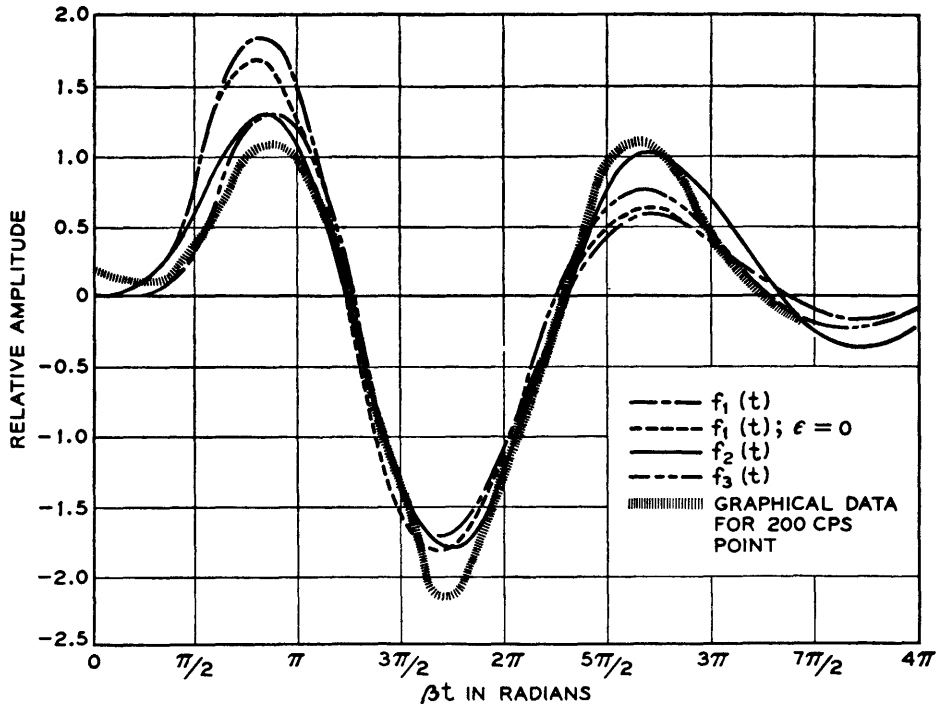

Fig. 14.

Impulse responses for several models of the displacement of the cochlear partition. (From Flanagan[16].)

$$f_3(t) = \frac{C_3\beta^{1+r}}{6}[\beta(t-T)]^2\,\epsilon^{-\beta(t-T)/1.7}\sin\beta(t-T) \quad \text{for } t \geq T$$

$$= 0 \quad \text{for } t < T$$

$\beta T = 3\pi/4$

$f_3(t)$ is the impulse response.

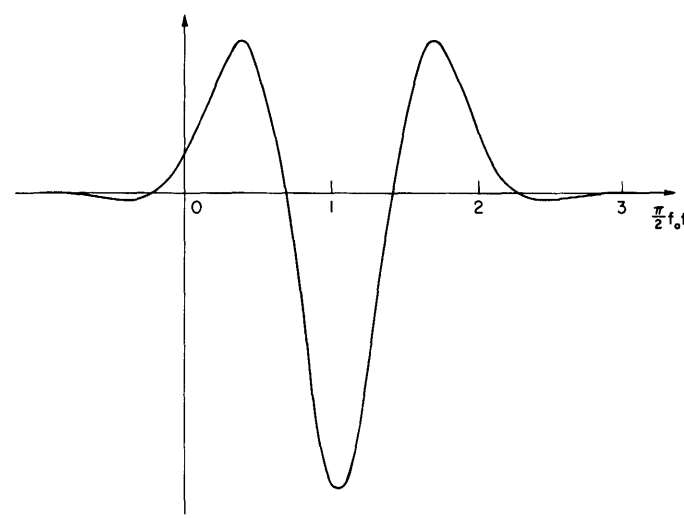

Fig. 15.

Impulse response of a model of the displacement of the cochlear partition. (From Siebert[55].)

$h(x,t) = -2.03 f_{max}(x)\,\epsilon^{-2\nu^2}(3/4\cos 3\nu - \nu\sin 3\nu)$,

where $h(x,t)$ is the impulse response,

$f_{max}(x) = 10^{5-x}$, and $\nu = \pi(1/3-(1/2)\,f_{max}(x)t)$.

In the past few years, with the participation of communication engineers in studies of the auditory system, interest has been aroused in the impulse response of the cochlear partition. At least two such studies have been undertaken. In the first of these studies, Flanagan[16,17] has approximated the frequency response data of von Békésy, by using rational functions of frequency. Flanagan has also derived impulse responses of the cochlear partition (shown in Fig. 14) that can be realized with lumped parameter electric circuit components. Siebert[55] also has empirically determined analytical expressions that approximate the frequency-response data. Siebert's functions are not rational functions and are not unlike Zwislocki's expressions, derived from fundamental considerations. Siebert's transfer functions yield the impulse response seen in Fig. 15. Neither of these empirically derived impulse responses can be entirely accurate. All of the impulse responses derived by Flanagan are based on lumped parameter models. Real delays are included to aid in the approximation of the phase data. The impulse response derived by Siebert is unrealizable and, therefore, cannot be entirely correct. These discrepancies may, however, be inconsequential in the study of the activity of VIIIth-nerve fibers resulting from displacements of the cochlear partition.

These impulse responses are plotted on normalized time scales. For a point at the basal end (a point tuned to relatively high frequencies) the impulse response is a relatively fast transient with an oscillation whose frequency is approximately the tuning frequency of that point on the basilar membrane. For an apical or low-frequency location the impulse response is a slow transient with correspondingly slow oscillations. It is well to point out that these impulse responses are all based upon the data of von Békésy. These data extend over a range of frequencies up to approximately 2 kc. Strictly speaking, the impulse responses can be considered valid only over this range of frequencies.

A word of caution concerning our interpretation of the mechanical system is in order. Many of the data on which these interpretations are based are the results of the work of one man, and many of these results have never been verified by other workers. Furthermore, many of the data are based on observations made on cadavers. The relevance of these data to the operations of the systems in the living organisms is always subject to question. Many of the data were obtained for intensity of stimuli that correspond to a very high intensity of acoustic stimulation. The relevance of these data is also subject to question. Nevertheless, were it not for the data of von Békésy, all attempts to formulate a model of the peripheral system would be futile at this time.

3.3 BRIEF ELECTROPHYSIOLOGY OF THE COCHLEA

Measurements of the electrical activity recorded with gross electrodes (electrodes with diameters that are large compared with the dimensions of the microstructures that are generating the electrical events recorded by the electrodes) placed on the round window or in the cochlear scalae indicate the presence of several distinguishable electrical

potentials. In the absence of stimulation the endolymph in scala media is reported to be at a potential of +50 millivolts (a potential referred to as the EP or endocochlear potential) with respect to the perilymph.[1w] If the ear is stimulated with sound, several other potentials may be observed at the same time. These are the cochlear microphonic potential (CM), the summation potential (SP), and the gross action potential (N_1). Stevens and Davis,[58] among others,[71e, 46] have shown that CM is linearly related to the acoustic signal over a range of at least 60 db SPL. Von Békésy[1x] has shown that CM is proportional to the displacement of the cochlear partition, rather than to the time derivative of the displacement. Davis[5-7] has constructed a consistent set of hypotheses concerning the function and origination of CM. In this scheme, the bending of the hair cells, which results from a displacement of the basilar membrane, changes the electrical milieu in the Organ of Corti. The electric currents that result from this change flow through and depolarize the nerve endings near the hair cells and thus initiate action potentials in the nerve fibers. Therefore, CM is viewed as a mechanism for the initiation of electrical activity in the VIIIth nerve. Local recordings of CM at the hair cells are, however, difficult to obtain. CM has been recorded intracochlearly (between scala vestibuli and scala tympani),[62, 63] and the results indicate that the time course of CM as a function of distance along the cochlea is similar in some qualitative respects to von Békésy's observations on the motion of the basilar membrane. These results are difficult to interpret, since one cannot be certain that the recordings are sufficiently local in origin. Nevertheless, it appears quite certain that CM represents a spatio-temporal summation of local generator potentials that are involved in some way in the process of initiation of action potentials in the VIIIth nerve.

Similarly, the SP[5, 8] (there is an SP+ and an SP-) is felt to be involved in the process of initiation of action potentials. It is also a cochlear potential and thought to be generated in some way by forces on, or by movements of, the hair cells. The SP is not linearly related to the acoustic stimulus.

Finally, N_1[19, 46, 58] is thought to represent a spatio-temporal summation of electrical activity in the fibers of the VIIIth nerve, and it can be recorded from a variety of locations, such as in, on or outside the cochlea and in the VIIIth nerve. We shall not now discuss the voluminous literature on N_1, since we are more concerned here with the all-or-none events in the nerve at the level of single fibers.

3.4 PATTERNS OF ACTION POTENTIALS IN THE AFFERENT FIBERS OF THE VIIIth NERVE

Although the recording of spike potentials in the VIIIth nerve has been reported elsewhere (only reports in which the locations of the electrode have been verified histologically as being in the VIIIth nerve are considered here),[32, 33, 53, 59] the recent work of Kiang and his co-workers[34-36] gives by far the most complete picture of unit fiber activity in the VIIIth nerve. Most of this work is still unpublished; since it is

germane to our problem, we shall discuss some of the major results.

All of the data were obtained by means of (3 M KCl-filled glass micropipette) microelectrodes from cats anaesthetized with Dial and urethane. These electrodes were placed in the VIIIth nerve peripheral to its entry into the cochlear nucleus. From the wave shape of the spike potentials, location of the electrodes, absence of injury discharges, and other indications, it appears that all of these data were obtained from fibers of the VIIIth nerve.

The fibers exhibit a number of interesting properties. First, all fibers studied thus far exhibit spontaneous firings, that is, action potentials can be observed to occur in the absence of acoustic stimulation. The average rate of firing varies from fiber to fiber, but generally lies in the range of a few spikes per second to as many as 150 spikes per second. Figure 16 shows a representative histogram of the time intervals between the occurrence of spikes for a typical fiber (plotted in semi-logarithmic coordinates).

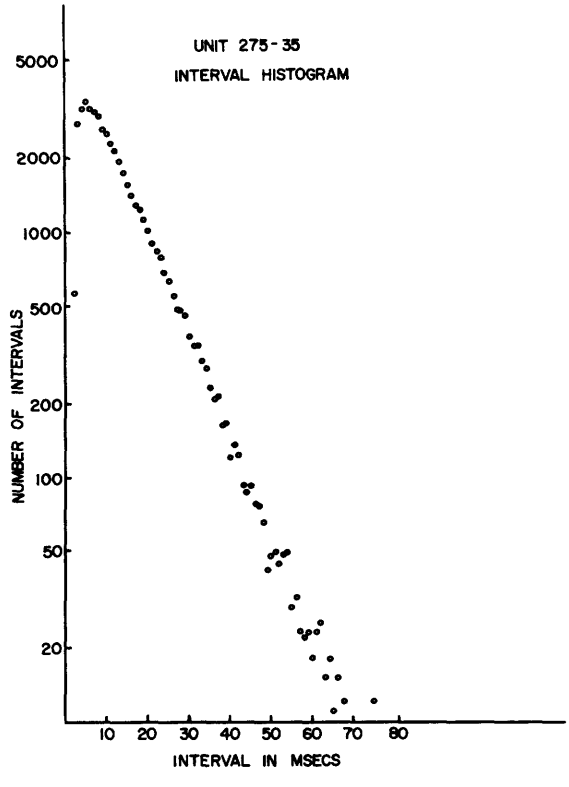

Fig. 16. Interval histogram of the spontaneous firings of a fiber in the auditory nerve (in cat) plotted in semi-logarithmic coordinates. (From Kiang et al.[36])

The distribution of intervals can be described adequately as exponential except for very short intervals.[34] Presumably, this is the range in which the refractoriness of the fiber affects the firing pattern.

Figure 17 shows tuning curves for several fibers observed in one cat. (Tuning curves are graphs of the threshold of firing of a unit as a function of the frequency of sinusoidal sound stimulation. In Section V there is a further discussion of both the tuning curves

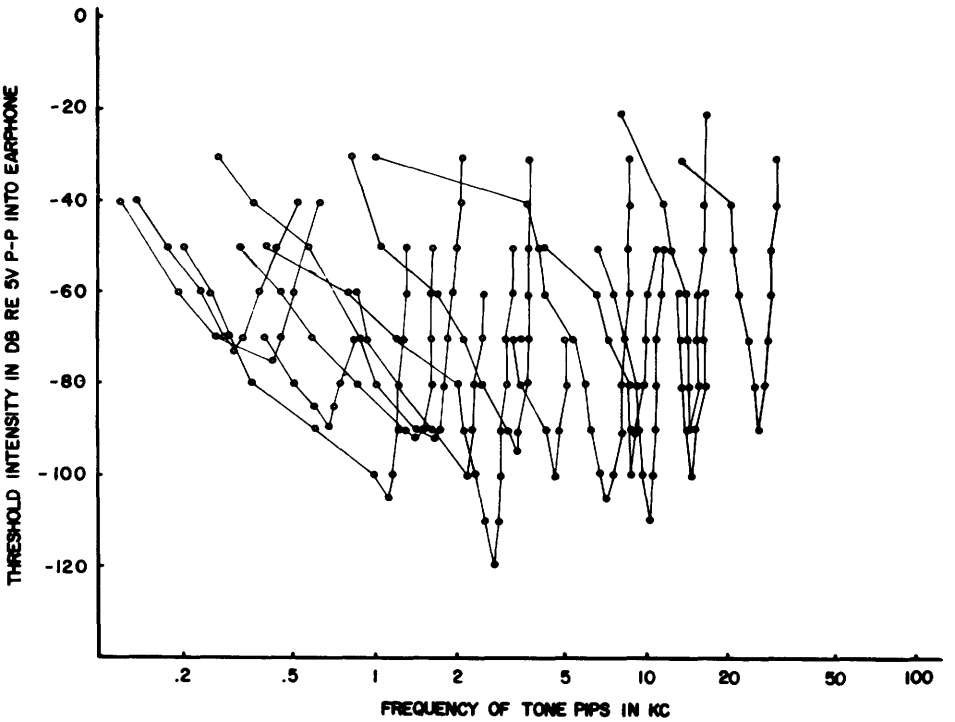

Fig. 17. Tuning curves for 16 different auditory nerve fibers in 9 cats. Each curve is obtained by setting the intensity of tone bursts and measuring the frequency range for which spike responses are obtained. The limits of this frequency range for a number of intensities are represented by points that have been joined to produce a "curve." The abscissa of the lowest point of each curve is defined as the characteristic frequency (CF or f_o) of that unit. The tone-burst stimuli had rise-fall times of 2.5 msec and a duration of 50 msec. (From Kiang et al.[35])

and the concept of threshold of firing.) Note that different cells seem to tune (that is, to be maximally sensitive) at different frequencies. The cells that tune to higher frequencies are found farther from the center of the VIIIth nerve than the cells that tune to low frequencies.

From further data of this kind, it can be seen that the relative width of tuning, Q, of these curves does not vary with frequency up to approximately 1 kc. Above 1 kc, the Q increases markedly as a function of frequency, that is, the tuning curves get narrower at high frequency. When wideband noise is added to the sinusoidal stimulation, the over-all sensitivity decreases but the general shape of these tuning curves remains the same.

Figure 18 shows the response to acoustic clicks (100-μsec electrical pulses applied to a condenser earphone) of units tuned to different characteristic frequencies f_o (frequency of lowest threshold of firing). The figure consists of post stimulus-time (PST) histograms[25] (histograms of the times of occurrence of spike potentials measured from

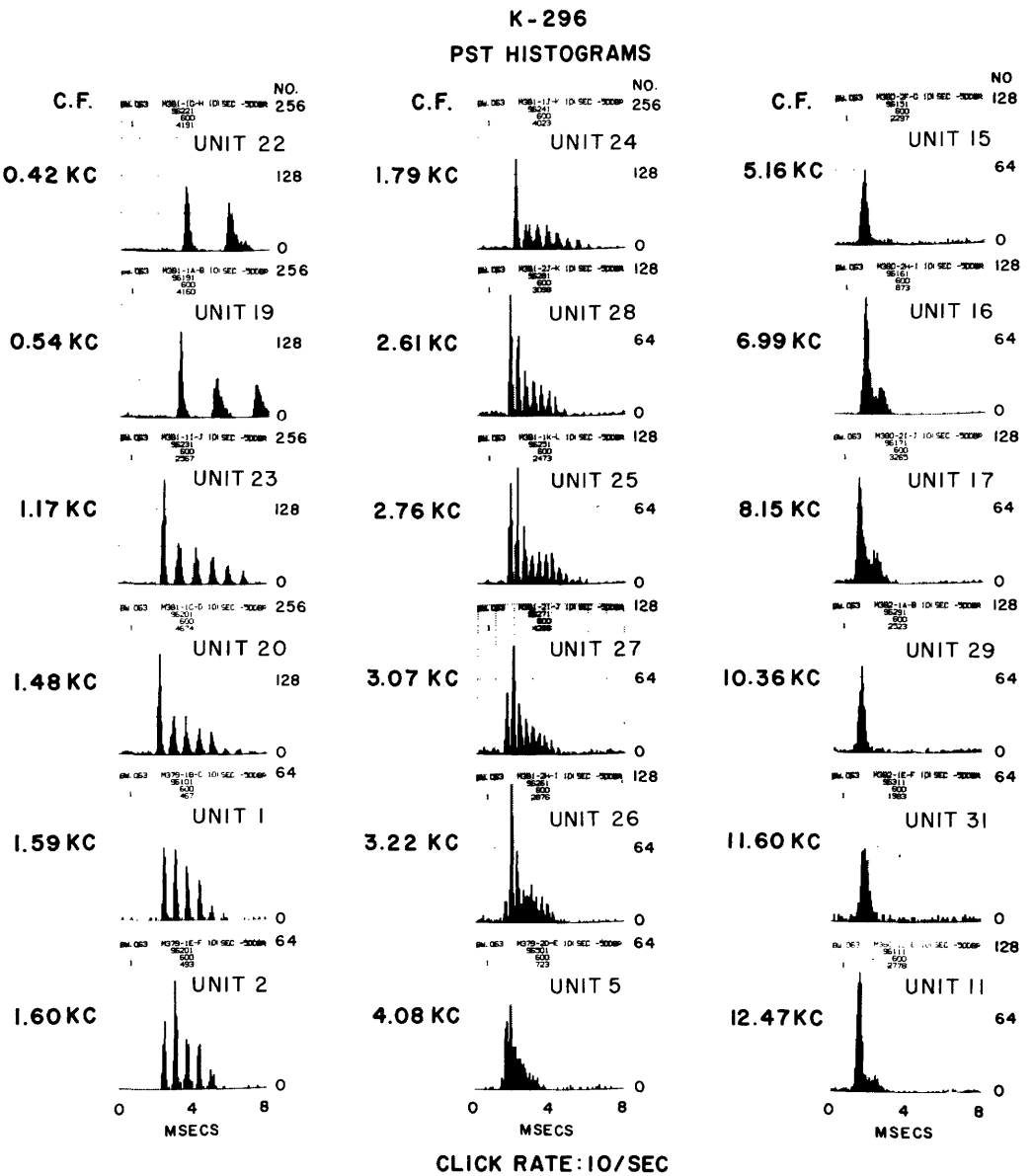

Fig. 18. Post stimulus time histograms of responses for fibers in the auditory nerve (cat) to click stimulation. Click intensity, +30 db (re VDL of N_1) at a rate of 10/sec. CF is the frequency for which the lowest intensity of sinusoidal acoustic stimulation is required in order to elicit synchronized firings in the fiber. (From Kiang et al.[36])

the onset of the stimulus). Note that the time of occurrence of the first peak is later for low-frequency tuning units than for high-frequency tuning units. Note also that the time between maxima in the PST histograms is inversely related to the tuning frequency (in fact this time can be shown to be $1/f_o$ within statistical variations).

Further data obtained by Kiang et al. indicate that the time of occurrence of the first peak in the PST histogram of a unit does not vary much (less than $1/(4f_o)$) with changes in intensity of stimulation. At high intensities an additional peak may appear to precede the first peak. This additional peak appears approximately $1/f_o$ seconds before the original first peak. Responses to clicks of different polarity (condensation clicks and rarefaction clicks) show differences in the times of occurrence of peaks in the PST histogram which correspond to $1/(2f_o)$. At high intensities, the first peak in the PST histogram in response to a rarefaction click leads the first peak in the PST histogram for the response to a condensation click.

For fibers with characteristic frequencies greater than approximately 4 kc, the PST histograms exhibit no such multiple peaks. This may be due to a number of causes: (a) the electronic equipment used to record and process the data has a resolution limit of 4 kc; (b) the fiber itself has a limit of resolution of 4 kc; or (c) the mechanism of excitation is different for frequencies above 4 kc.

Some studies[53] of the electrical activity of auditory nerve fibers have reported the presence of "inhibitory effects" on the firing patterns of these fibers. Two distinct inhibitory effects have been reported: diminution of the rate of spontaneous activity of an VIIIth-nerve fiber in the presence of tonal stimuli, and diminution of the response to an intense tone by the introduction of a second tone. The first of these inhibitory effects has not been seen by Kiang et al., although they have not studied the effect directly. The second inhibitory effect has been seen by them, although this effect has not been studied exhaustively.

IV. MODEL OF THE PERIPHERAL AUDITORY SYSTEM

This section is a discussion of a model of the peripheral auditory system relating the spike activity of fibers in the VIIIth nerve of cats to acoustic stimuli. An attempt has been made to include in the model the principal functional constituents of the peripheral system (see Fig. 19). The "Mechanical System" represents the functional relation between an acoustic pressure input to the ear and a displacement of the

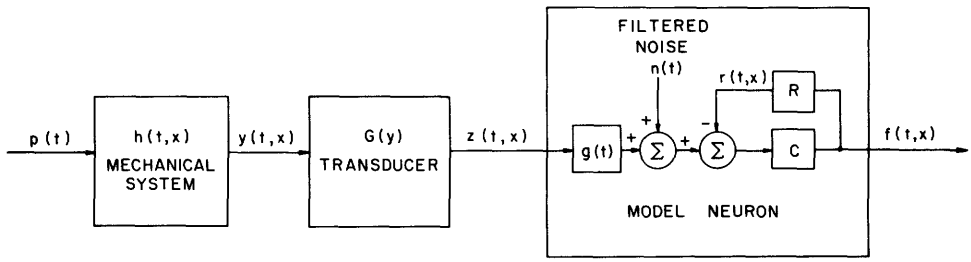

Fig. 19. Model relating the firing patterns of fibers in the auditory nerve to acoustic stimuli.
p(t), pressure at the ear
y(t, x), displacement of the cochlear partition
z(t, x), output of a sensory cell
f(t, x), sequence of spikes generated in an VIIIth-nerve fiber
r(t, x), threshold potential
h(t, x), impulse response of the mechanical system
G(y), transducer function
g(t), a linear filter
t, time
x, distance from the oval window to a point along the cochlear partition.

cochlear partition at a point x centimeters from the stapes. The excitatory process is interposed between the displacement of the cochlear partition and the firing of the VIIIth-nerve fiber. This process is not well understood, but undoubtedly involves the action of the hair cells. The "Transducer" is intended to represent the action of these hair cells and associated structures. The final block shows a "Model Neuron" – a formal and simplified model of excitable nerve membrane. [For simplicity, we shall refer to the whole model of the peripheral auditory system as the PAS model, or simply as the "model." The model of the mechanical system will be referred to as the M model, the model of the transducer as the T model, and the model neuron as the N model. The combination of transducer and model neuron will be referred to as the TN model, and so on.] The output of the transducer serves as the input to the "Model Neuron" and is filtered and then added to noise. Noise is included in order to account for both the spontaneous activity and the probabilistic response behavior characteristic of VIIIth-nerve fibers. The noisy membrane potential is next compared with a threshold in the box labelled "C". If the threshold is exceeded, then a spike occurs by definition and the threshold

is reset to some larger value by the box labelled "R". Figure 20 shows both the noisy membrane potential of the model neuron and the threshold as a function of time. The threshold is reset to some larger value (R_M) upon the occurrence of a spike and decays to its resting value (R_R) with an exponential decay (of time constant τ_R). The threshold change is intended to represent the refractoriness of neural fibers.

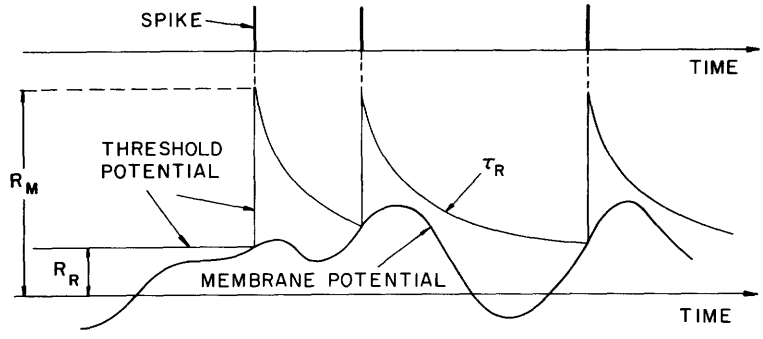

Fig. 20. Diagrammatic representation of membrane potential, threshold potential, and spike activity of the model neuron.
R_M, maximum threshold potential
R_R, resting threshold potential
τ_R, time constant of the exponential decay of the threshold from its maximum to its resting value.

4.1 SUMMARY OF ASSUMPTIONS OF THE MODEL

(i) The mechanical part of the peripheral auditory system is assumed to be representable as a linear system over an intensity range of 80 db. The mechanical system encompasses the outer, middle, and mechanical part of the inner ear and relates the displacement of the cochlear partition to acoustic pressure at the ear. Furthermore, the transfer function characterizing this mechanical system is assumed to be determined by the data of von Békésy. Implicit in this assumption is another assumption that the outer and middle ear have flat frequency responses over the range of validity of this model (from approximately 100 cps to 2 kc).

(ii) A point-to-point relation between the displacement of the cochlear partition and the neural excitation process is assumed. A particular neural fiber is assumed to be excited by a particular hair cell responding in turn to the displacement of the cochlear partition at a single point along its length.

(iii) The process of neural excitation is represented by a simple model neuron. This model is probabilistic and contains both threshold and refractory properties.

(iv) The effect of efferent fibers on the spike activity of the afferent fibers of the VIIIth nerve is ignored.

(v) A mechanism to account for active neural inhibition effects is not included in the model.

4.2 DISCUSSION OF THE ASSUMPTIONS OF THE MODEL

(i) Representation of the mechanical system. The validity of representing the mechanical part of the peripheral auditory system by a linear system was discussed in Section III. The outer and middle ear are assumed to have flat frequency responses (10-db fluctuations in the frequency responses are ignored) for frequencies up to 2 kc. The transfer function of the mechanical system has been assumed to be simply the transfer function relating the displacement of the stapes to the displacement of the cochlear partition. This transfer function is based upon the observations of von Békésy on the response of the cochlear partition to sinusoidal displacements of the stapes. These data comprise observations on human cadavers, guinea pigs, cows, and even elephants, but not on cats. There is, however, strong justification for inferring that the transfer function in cats is similar to that in the other species for which it has been measured. The experimentally determined tuning curves[1p, 1q, 1y] for all species (including the chicken, which has a very crude cochlea) are very similar. For instance, the sharpness of tuning, Q, varies very little across species. The cochlear maps[1z] (distributions of maxima of displacement of the cochlear partition versus frequency of stimulation), and the elasticity of the cochlear partition as a function of distance along the partition[1g, 26] are all similar in these different species. It seems reasonable, therefore, to assume that the data of von Békésy are valid for the cat. This assumption is strengthened because we are not concerned so much with the details of the tuning curves as with their first-order properties, such as width and asymmetry.

(ii) Representation of the sensory cells and their innervation. The point-to-point relation between the displacement of the cochlear partition and the excitation of an adjacent neural fiber assumed in the model is the most parsimonious assumption that is possible. Anatomically, this assumption appears to be consistent with the pattern of radial fiber innervation. A radial fiber is connected at most to two or three hair cells.[13] The hair cell spacing is estimated to be approximately 2.5 μ for outer hair cells, and 8.5 μ for inner hair cells. (These values are obtained by dividing the length of the cochlear partition by the number of hair cells. The density of hair cells is assumed to be constant.[54]) In either case, these distance are negligible compared with the widths of von Békésy's tuning curves (when they are plotted against position along the cochlear partition).[1a] Therefore, a single radial fiber is essentially sensitive to the pattern of displacement of the cochlear partition over a relatively short length of the partition. The spiral-fiber innervation does not appear to be as simply structured. Spiral fibers are thought to innervate the hair cells more diffusely (although there appears to be some difference of opinion about this in published works).[13,48c] It is not clear which of these two major groups of fibers contributes predominantly to the VIIIth-nerve afferent fibers. The point-to-point relation assumed in the model leads to results that appear to be qualitatively consistent with some of the electrophysiological data of Kiang and his co-workers; this assumption also

appears to be consistent with the radial-fiber innervation.

Initially, the relation between the excitation of a fiber and the displacement of the cochlear partition is assumed to be linear with no energy storage elements. Thus a hair cell is assumed to generate a current that is proportional to the displacement of the cochlear partition at a point, and this current flows through and depolarizes a fiber adjacent to the hair cell. The excitatory process is the subject of a considerable amount of investigation at the present time,[7] but the process is not understood in detail. We are forced to make some rather simple assumptions in the model. The consequences of these assumptions will be given in Section V.

(iii) Representation of the nerve excitation process. The representation of the initiation of action potentials in the fibers of the VIIIth nerve is the most phenomenological part of the model. It would perhaps be possible to include a more complete model of a nerve fiber (such as the Hodgkin-Huxley model[30]) in the representation. These membrane models are too detailed and cumbersome, however, for our purpose, and are generally based on empirical evidence obtained from nonmammalian and relatively large fibers. These fibers show no spontaneous activity and their response to stimulation can be adequately described by deterministic models. (A number of simplified models of nerve membrane have been proposed.[28, 37, 64, 65, 69]) This is not the case for VIIIth-nerve fibers in the cat, and as a result the more detailed models of the initiation of action potentials are inadequate for our purposes.

(a) The need for a probabilistic neuron model: The work of Kiang et al. suggests rather strongly that a probabilistic description of the spike activity of VIIIth-nerve fibers is necessary. There are two reasons: these fibers exhibit spontaneous spike activity whose origin cannot be related to any controllable stimulus to the cat; and the response of a fiber is not the same to each presentation of the acoustic stimulus; but averages of the spike activity appear to be stable. With our current understanding of the peripheral auditory system, it is difficult to account for the origin of the apparent random behavior of the spike activity of the fibers. The cause might be Brownian motion in any of the acoustic or mechanical parts of the system; fluctuations in osmotic pressure caused by blood pulsation in the surrounding capillaries in the cochlea; fluctuations of ionic potentials across the hair cell and nerve membranes; fluctuations in the amount of the chemical activating substance at the hair cell-neuron junction; and/or a number of other possibilities.

At this point we wish to digress from the main discussion to present a possible explanation of the probabilistic behavior of the spike activity in the VIIIth nerve. The seemingly random behavior of single neural fibers in response to stimuli has been reported by a number of workers. The early work of Monnier,[44] Blair and Erlanger[3] and others indicated clearly that the responses of neural fibers exhibited intrinsically random components.

The first comprehensive study devoted to the problem of characterizing the random behavior of single neural fibers is due to Pecher.[47] The work of Pecher and the more

recent work of Verveen[66-68] will be considered in more detail below.

Since the time of Pecher, a number of probabilistic models of electrophysiological data have been proposed. Some of these models have been reviewed by Frishkopf and Rosenblith.[20] In particular, the models of McGill[40] and Frishkopf[19] are both concerned with the ensemble responses of populations of fibers in the VIIIth nerve to acoustic clicks. In each case, a population of units with randomly fluctuating thresholds for firing was defined, and statistics of the population response to click stimuli were predicted.

In the experiments of Pecher and Verveen, the sciatic nerves of frog were stimulated directly by short pulses of electric current. When the amplitude of these pulses was sufficiently small these single fibers rarely responded. For sufficiently large amplitude pulses the fiber responded to almost every current pulse. The fiber responded to pulses of an intermediate range of amplitude in seemingly random fashion. Upon more careful investigation it was found that the set of spike responses to a periodic pulse train (when the period of the train was large compared with the refractory period of the fiber) could be characterized as a set of Bernoulli trials in which the probability of a response to a pulse was a sigmoid function of the amplitude of the pulse. This phenomenon was referred to as the fluctuation of excitability of nerve fibers. Typically, the standard deviation (σ) of the threshold potential (difference in potential between threshold for firing and resting value) normalized by the mean threshold (R_R) potential is 0.01 in sciatic nerve fibers of frogs.

Further evidence,[11, 68] including data obtained from nerve fibers of other species, indicates that the normalized standard deviation of the threshold potential (σ/R_R) is a function of the diameter of the fiber. Small-diameter fibers have large values of σ/R_R – an intuitively appealing result. In terms of fluctuations in ionic concentrations, this result implies that for large fibers containing a large number of ions, the fluctuation in ionic concentration is small (Law of Large Numbers). The relation that Verveen[68] infers from his data is

$$\sigma/R_R = 0.03d^{-0.8},$$

where d is the diameter of the fiber in microns. The data of Verveen were obtained from fibers with diameters in the range of a few microns up to a few hundred microns. If the relation is extrapolated to smaller values of fiber diameter, then σ/R_R becomes appreciably large. For d = 0.1, σ/R_R = 0.26. Therefore, for diameters of fibers approaching those of the terminal endings of the VIIIth-nerve fibers near the base of the hair cells,[9] σ/R_R approaches 1/3. This implies that the fluctuations in membrane potential are occasionally large enough to exceed threshold. This argument thus leads to the prediction of the existence of spontaneous activity in fibers as large as VIIIth-nerve fibers.

Although this explanation may have some merit, it has not been verified empirically.

Nevertheless, the need for a probabilistic mechanism in the model is patent and such a mechanism has been included as a Gaussian noise, added to the input of the neuron.

(b) Threshold and refractory properties of the model neuron: The neuron model contains two other major properties that are intended to represent properties of nerve membrane. (A linear filter is provided at the input to the neuron to include the effect of membrane capacitance. The time constant of this filter is assumed to be approximately 0.5 msec.[60,65]) These properties are: (i) There is a threshold for firing and a spike is defined to occur when the sum of the output of the transducer and the noise exceeds this threshold potential. (ii) Refractory effects are included in the model through the mechanism of having this threshold depend upon the time of occurrence of the previous spike. The refractoriness of the model can be summarized by stating that the probability of the occurrence of a spike immediately after a spike has occurred is low because the threshold is very high. This probability increases (to an asymptote) as the time intervals between spikes increase and is a function of both the stimulus and the time of occurrence of the last spike. The refractory effect is assumed to last one or perhaps a few milliseconds.

This representation of the excitation of a nerve membrane is considerably simplified and does not account for some of the details of the initiation of action potentials, such as the shape of the spike potential or the detailed recovery properties of a fiber. Nevertheless, some of the first-order properties of the excitability of nerve fibers are included, and perhaps the coding of information about acoustic events in the VIIIth nerve does not depend upon the details of the initiation of action potentials. This conjecture can only be validated by the descriptive and predictive capabilities of the model.

(iv) Efferent systems. The schematic representation of the auditory system (Fig. 1) suggests that there are at least two efferent neural pathways to the periphery. The dotted line from the central nervous system to the middle ear represents the two tracts innervating the middle-ear muscles. We have mentioned that the primary purpose of the middle-ear muscles appears to be the protection of the ear from sustained high-intensity sounds. This is accomplished by a reduction of the transformer ratio provided by the middle ear. It is clear that this action of the middle-ear muscles is inconsequential in both the von Békésy data and the VIIIth-nerve data of Kiang and his co-workers. In the latter case, the barbiturate anaesthesia used during the experiments effectively blocks this action.

The figure shows the efferent fibers that enter the cochlea through the VIIIth nerve as a dotted line going to the inner ear. Several distinct tracts have been identified by Rasmussen.[50] One of these – the crossed olivocochlear tract – has been shown to originate in the neighborhood of the contralateral accessory nucleus of the superior olivary complex. Suggestions that these fibers terminate near the hair cells have been put forward, but the fineness of the fibers has prevented any direct verification of this hypothesis.

There has been considerable speculation concerning the role of these efferent tracts

on the processing of sensory information. Galambos[22] and Fex[15] have demonstrated that electrical stimulation of this tract (at the floor of IVth ventricle) inhibits both N_1 and single-unit activity of the VIIIth-nerve afferent fibers. Fex[14] has also shown that CM is augmented slightly when these fibers are stimulated electrically. He has demonstrated that these efferent fibers (this time the recording electrodes were located in fibers just before their entry into the cochlea) respond to acoustic stimulation of the contralateral ear. It is difficult to interpret the effect of these fibers on the coding of acoustic information in the VIIIth nerve, particularly in the light of some of the results of Galambos.[23] Despite many attempts to interfere with this pathway, Galambos has not found any systematic changes in behavioral thresholds or discriminations. The effect of the efferent fibers on the coding of acoustic information in the VIIIth nerve remains equivocal; therefore, we choose to ignore these fibers in our model.

(v) Neural inhibition. No clear picture of inhibitory effects on the activity of VIIIth-nerve fibers has emerged. We have chosen to ignore these effects. We fully understand that such an omission might very well lead to a model of the peripheral system that ignores an essential feature.

V. RESULTS OF TESTING THE MODEL

The model of the peripheral auditory system presented in Section IV is based on a number of assumptions. These assumptions in turn are based on inferences derived from physiological data. The model that has resulted from these inferences is analytically unwieldy and the mathematical derivation of even the simplest statistics of the behavior of the model appears to be quite difficult. For instance, the distribution of intervals between spikes generated spontaneously by the model is equivalent to the distribution of successive crossings of a Gaussian noise process with a function of time (in this case the threshold function). A special case of this problem is the distribution of intervals between successive axis crossings of a Gaussian noise process – a problem for which no general solution exists.[31,39,51,56]

The complexity of the analytic problems involved in testing the model and the desirability for determining its response to a number of stimuli have made machine computation essential. [Appendix A gives a short discussion of the problem of finding the distribution of successive intervals between spikes generated by the model for a simple case.] The structure of the equations (multidimensional integral equations) governing the behavior of the model appears to make a direct solution of the problem more complex than a Monte Carlo scheme. For these reasons, and for reasons of personal bias, a general-purpose digital computer (the TX-2 computer of Lincoln Laboratory, M.I.T.)[4] was used to simulate the peripheral auditory system. Appendix C includes a discussion of the programs written for the TX-2 computer. The programs were written to generate the firing patterns of the model and to compute statistics of these firing patterns. Certain of these statistics were chosen to make possible direct comparisons of data obtained from the model with data obtained from VIIIth-nerve fibers.

In order to avoid confusing the activity of VIIIth-nerve fibers with activity generated by the model, we shall refer here to the former simply as "spikes," while the latter will be referred to as "events." Furthermore, in the results of the simulation and in any analytic arguments to be presented in this work a model that generates events at discrete intervals of time is assumed. Events, E_k, are defined to occur when signal, s_k, plus noise, n_k, exceeds the threshold, r_k, at time $k(\Delta t)$, where k ranges over the integers, and Δt is the fundamental sampling interval. We define $r_k = a_{k-j}$ if the last event occurred at time j, that is, the value of the threshold is reset upon the occurrence of an event. Moreover, $a_i = R_R + (R_M - R_R)\gamma_R^i$, where $\gamma_R = \exp(-\Delta t/\tau_R)$. The refractory period of a nerve fiber is assumed to be represented by an exponential decay of the threshold from its maximum value (R_M) to its resting value (R_R) after the occurrence of an event. The noise n_k has a Gaussian distribution with zero mean, standard deviation σ, and $E[n_j n_k] = \sigma^2 \rho_{j-k}$, with $\rho_i = \gamma_N^i$ and $\gamma_N = \exp(-\Delta t/\tau_N)$. [The noise is also filtered by a highpass filter so that the correlation function of the noise is actually given by

$$\rho_i = C_1 \gamma_N^i + C_2 \gamma_M^i$$

where

$\gamma_N = \exp(-\Delta t/\tau_N)$, $\quad \tau_N \ll \tau_M$

$\gamma_M = \exp(-\Delta t/\tau_M)$

$f_h = 1/\tau_N$ is the high-frequency 3-db point

$f_\ell = 1/\tau_M$ is the low-frequency 3-db point.]

5.1 RESPONSE OF THE MODEL NEURON TO "SHORT" PULSES

The response of the model neuron to short pulses is discussed (similarly to a discussion by Verveen[67a]) in order to present a rationale for the assumptions of the nature of the neural noise. This discussion is also intended to verify the results of the model of the fluctuation of excitability of neural fibers as described by Ten Hoopen and Verveen.[65]

Suppose the membrane potential of the model, $m_k = s_k + n_k$ and $\sigma/R_R \ll 1$. For this case the number of spontaneous events per unit time is vanishingly small. Assume that $\{s_k\}$ is a "short" pulse signal that is introduced at $k = 0$. A "short" pulse is defined as a pulse whose duration is short compared with all of the other important time constants in the model. That is, if $\delta(\Delta t)$ is the duration of the pulse, then $\delta(\Delta t) \ll \tau_R$, $\delta(\Delta t) \ll \tau_N$. The pulse is short compared with both the time over which the noise is correlated and the refractory time constant. These assumptions are equivalent to assuming that: (i) there can be at most one event in response to a pulse; and (ii) the noise is a constant over the duration of the pulse.

The event E is defined to occur when there is an event E_k for $0 \leq k \leq \delta$ or $E = E_o \cup E_1 \cup \ldots \cup E_\delta$. But for $\Pr[E] = 1 - \Pr[\overline{E}]$, where $\overline{E}$ is the complementary event, no firing occurs during the interval of the pulse.

$$\Pr[\overline{E}] = \Pr[n_k + s_k < R_R] \qquad k = 0, 1, 2, \ldots, \delta.$$

By assumption, the noise is a constant for $k = 0, 1, 2, \ldots, \delta$ and

$$\Pr[\overline{E}] = \Pr[n + s_k < R_R] \qquad k = 0, 1, 2, \ldots, \delta$$

$$= \Pr[\max(n + s_k) < R_R] \qquad [\max(x) \text{ is the largest value attained by the variable } x]$$

$$= \Pr[n < R_R - \max(s_k)]$$

$$p = \Pr[E] = 1 - \Pr[\overline{E}]$$

$$= 1 - \int_{-\infty}^{R_R - \max(s_k)} (1/\sqrt{2\pi}\sigma) \exp(-n^2/2\sigma^2)\, dn.$$

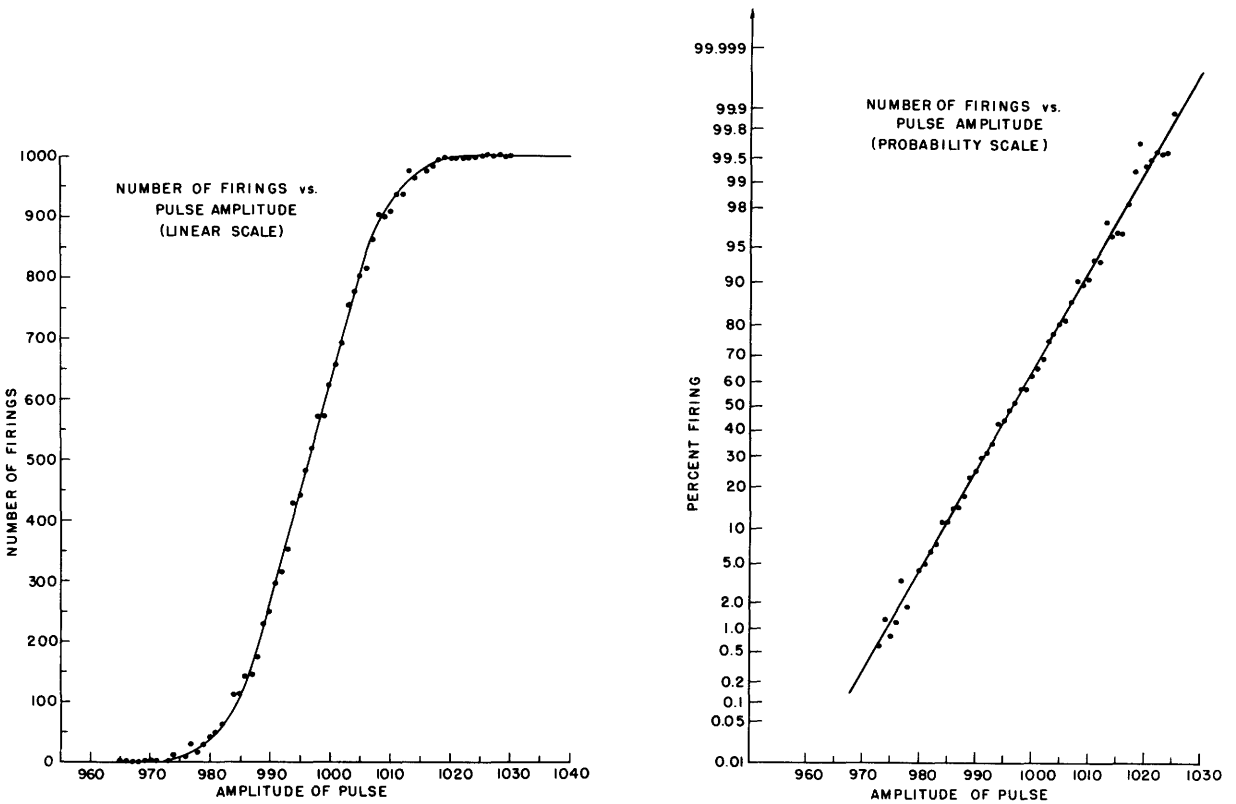

Fig. 21. Number of events generated by the model in response to a periodic train of short pulses as a function of the amplitude of the pulses.

$R_R = 1000$ $\quad f_\ell \doteq 20$ cps

$R_M = 1200$ $\quad f_h \doteq 2$ kc

$\tau_R \doteq 1$ msec $\quad \sigma \doteq 10$

Number of pulses, 1000; pulse duration, 0.3 msec; pulse period, 5.0 msec.

By further manipulation this can be put into the form

$$p = \int_{-\infty}^{\max(s_k)} (1/\sqrt{2\pi}\,\sigma)\, \exp(-(n-R_R)^2/2\sigma^2)\, dn.$$

Therefore, the probability p of a response to a pulse $\{s_k\}$ as a function of the amplitude of $\{s_k\}$ is an integrated Gaussian function with mean R_R (resting threshold) and standard deviation σ. The response of the model neuron to a periodic train of identical pulses of amplitude $\max\{s_k\}$ forms a set of Bernoulli trials with probability of success p. This result is valid under the assumption that the period of the train is large compared with both the refractory period of the model neuron and the correlation time of the noise. This description is consistent with the empirical findings of Verveen on the response of sciatic-nerve fibers. Figure 21 shows the results of the response of the computer-simulated model neuron. The number of responses of the model to a train of 1000 stimuli is plotted as a function of the amplitude of the pulses. Figure 21 also shows the same function plotted on Gaussian distribution coordinate paper.

A histogram of the distribution of intervals I between events E in response to a train of short pulses is given in Fig. 22. The number of intervals that is equal to an integral number of periods (T) of the stimulus, that is, the number of intervals of length T, 2T, 3T, ..., where T is the period of the train of pulses, forms the distribution of

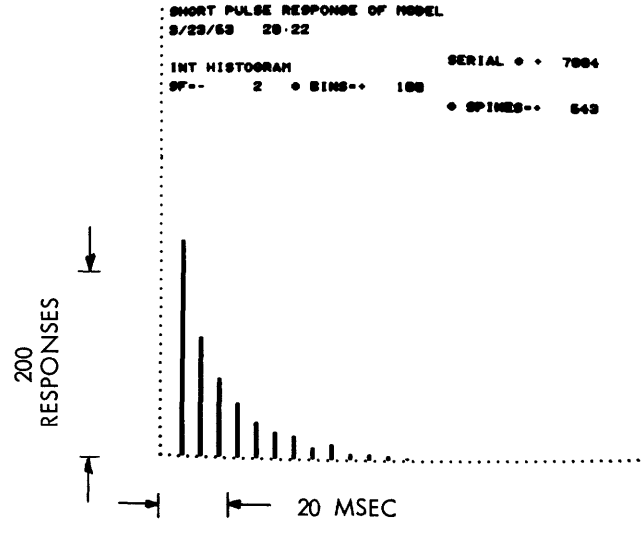

Fig. 22. Histogram of intervals of time between responses of the model to a periodic train of short pulses.

$R_R = 10,000$ $\quad f_h \doteq 5$ kc
$R_M = 100,000$ $\quad f_\ell \doteq 5$ cps
$\tau_R \doteq 0.3$ msec $\quad \sigma \doteq 100$

Pulse duration, 0.1 msec; pulse period, 5.0 msec; pulse amplitude, 9950; number of pulses, 2000; number of responses, 643.

successful runs in a set of Bernoulli trials. This distribution is the geometric distribution and the predicted interval distribution is $Pr[I=kT] = p(1-p)^{k-1}$; $k = 1, 2, \ldots$. Table 1 shows both the predicted set of intervals as well as the set of intervals generated by the computer for the distribution shown in Fig. 22. The predicted set of intervals was obtained by estimating p from the data computed in the same run.

Table 1. Predicted set of intervals and set of intervals generated by the computer.

k	I_k	$\hat{I}_k$	σ_k
1	232	207	11.8
2	129	140	10.5
3	84	95.2	9.0
4	58	64.3	7.6
5	38	43.8	6.4
6	28	29.7	5.3
7	24	20.1	4.4
8	12	13.7	3.7
9	16	9.3	3.3
10	7	6.3	2.5
11	7	4.3	2.1
12	4	2.9	1.7

Number of pulses, 2000
Number of events, N, 643
Estimated value of p, 0.322
I_k, number of intervals of length k
$\hat{I}_k = Np_k = Np(1-p)^{k-1}$, estimated mean number of intervals of length k
$\sigma_k = \sqrt{Np_k(1-p_k)}$, estimated standard deviation of the number of intervals of length k

Figure 23 shows the distribution of intervals between events as a function of the amplitude of the pulse. For large pulse amplitudes the probability of the occurrence of a long interval approaches zero, that is, events occur in response to almost every pulse.

5.2 SPONTANEOUS ACTIVITY OF THE MODEL

As the ratio of the standard deviation of the noise to the resting threshold, σ/R_R, increases, the probability that the model neuron will exhibit spontaneous events in the absence of an input increases. For small values of σ/R_R, the probability of a spontaneous event E_k at time $k\Delta t$ is given approximately by

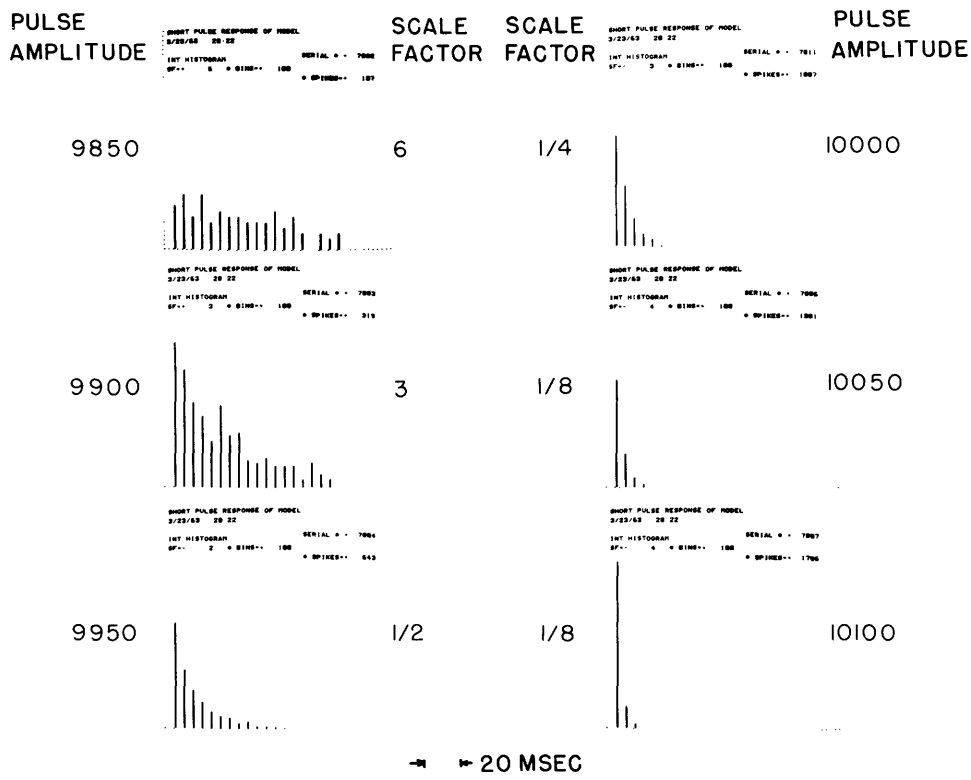

Fig. 23. Histograms of intervals of time between responses of the model to periodic trains of short pulses as a function of pulse amplitude.

$R_R = 10{,}000$ $\quad f_h \doteq 5$ kc

$R_M = 100{,}000$ $\quad f_\ell \doteq 5$ cps

$\tau_R \doteq 0.3$ msec $\quad \sigma \doteq 100$

Pulse duration, 0.1 msec; pulse period, 5.0 msec; number of pulses, 2000.
(The spacing between dots on the ordinate represents a number of entries in the histogram equal to 5/(scale factor).)

$$\Pr[E_k] = p[n_k \geq r_k] \leq p[n_k \geq R_R]$$

$$\Pr[E_k] \leq \int_{R_R}^{\infty} (1/\sqrt{2\pi}\sigma) \exp(-n^2/2\sigma^2)\, dn$$

$$\leq \int_{R_R/\sigma}^{\infty} (1/\sqrt{2\pi}) \exp(-n^2/2)\, dn.$$

The equality holds in the limit as σ/R_R goes to zero, that is, when the probability of an event is small and the threshold r_k decays essentially to the resting value R_R between events.

We are interested in a statistical description of the set of events $\{E_k\}$. First, it is clear that the events can not be described as "recurrent events"[12] in the general case. By a "recurrent-event" process we mean a statistical process that generates events for which the probability of an event at time $k(\Delta t)$ is dependent only on the time of occurrence of the last event, that is, after an event has occurred the statistics are reset. Figure 24 shows the spontaneous activity of the model for different noise spectra. For values of the bandwidth of the noise which are large compared with $1/\tau_R$ the noise appears uncorrelated between events, while for small values of noise bandwidth several events may occur on one large excursion of the noise.

A short interval occurring between events implies that the noise has assumed a relatively large value at the end of the interval because such a large value of noise was needed to exceed the relatively large value of the threshold. But if the noise is varying slowly with respect to the decay time of the threshold function, then a relatively short interval will tend to occur again. In other words, successive interevent intervals are so correlated that short intervals tend to be followed by short intervals. The existence of this statistical dependence is due to the fact that while the threshold is reset upon the occurrence of an event, the value of the noise is not reset.

To a first-order approximation, the parameters determining the degree of statistical dependence between successive interevent intervals are the time constant of the threshold decay, τ_R, and the bandwidth of the noise, $1/\tau_N$. If $\tau_R \gg \tau_N$, then the correlation of the noise between events approaches zero. Consider the expected value of the noise k units of time after an event has occurred. The value of the noise was n_o at the time of occurrence of the event.

$$E[n_k/n_o] = n_o \rho_k = n_o(\exp(-\Delta t/\tau_N))^k = n_o \exp(-k\Delta t/\tau_N).$$

For $k\Delta t > \tau_R$,

$$E[n_k/n_o] < n_o \exp(-\tau_R/\tau_N)$$

$$\lim_{(\tau_R/\tau_N)\to\infty} E[n_k/n_o] = 0.$$

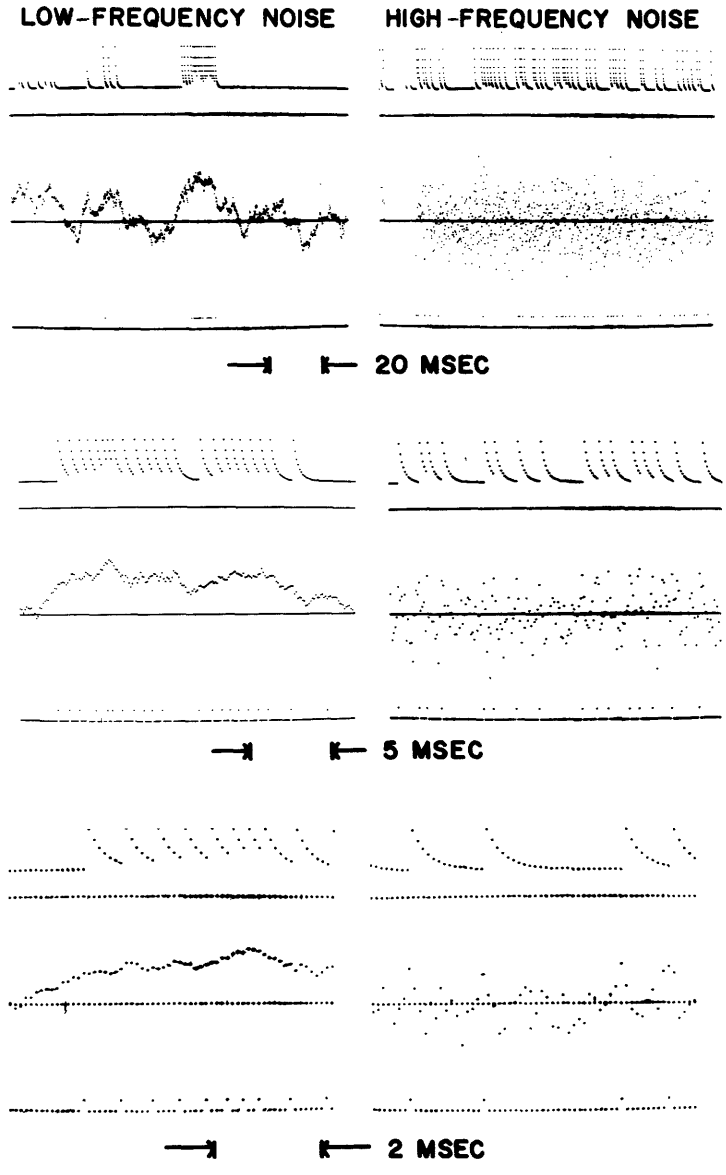

Fig. 24. Membrane potential and threshold potential of the model. The same data are shown on three time scales for each of two values of f_h. Upper traces show the threshold potential; middle traces, the membrane potential; lower traces, the times of occurrence of events. Threshold potential and membrane potential are on the same amplitude scale.

$R_R = 40$ $\quad f_h \doteq 100$ cps (left-hand)

$R_M = 100$ $\quad f_h \doteq 10$ kc (right-hand)

$\tau_R \doteq 0.3$ msec $\quad f_\ell \doteq 10$ cps

$\sigma \doteq 30$

$\Delta t = 100$ μsec

Therefore successive intervals between events become uncorrelated for noise whose correlation time, τ_N, is short relative to the time constant of the threshold decay, τ_R. Figure 25 shows the mean interevent interval, given the previous interval I_1, $(\bar{I}_2)_{I_1}$, as a function of I_1, for different values of $f_h = 1/\tau_N$. Note that the degree of correlation between successive intervals (as indicated by the estimate of the conditional mean interval given in Fig. 25) decreases as f_h increases. For an f_h approximately 2 kc, successive intervals are only slightly correlated. Similar statistics computed from the firing patterns of VIIIth-nerve fibers (in the absence of acoustic stimuli) indicate only a slight amount of correlation between successive interspike intervals. When present, this correlation is of the same form as the correlation of successive intervals shown by the model, that is, short intervals tend to be followed by short intervals. Therefore, the bandwidth of the noise in the model has been chosen to be approximately 2-5 kc. This value is consistent with the findings of a number of workers who have attempted to estimate such a figure.[19a, 65]

Figure 26 shows interval histograms calculated for the same data that were used to obtain the results of Fig. 25. As f_h decreases, not only does the statistical dependence between successive intervals increase, but a larger proportion of short intervals occurs (as Fig. 26 indicates). Figure 27 shows some of the same interval histograms plotted in semi-logarithmic coordinates. For values of the bandwidth of noise greater than 2 kc the tails of the distributions of intervals are clearly linear in these coordinates or exponential in linear coordinates. Figure 28 shows the rate of spontaneous events generated by the model as a function of the bandwidth of the noise.

Figure 29 shows interval histograms of the spontaneous activity of the model as a function of the standard deviation of the noise. These histograms all approach exponential functions for large time intervals. Figure 30 shows the rate of spontaneous firing of the model as a function of σ/R_R. The rate of firing is strongly dependent on the value of σ/R_R. A 50 per cent change in σ/R_R is seen to change the rate of firing by as much as 500 per cent.

Further investigations have shown that the general features of these interval histograms are attained under a large variety of parameter values of the model. The histograms approach exponential functions for large, interevent intervals and these histograms exhibit a "dead time" for very short intervals, with a smooth transition between these limits. For values of $\tau_R \doteq 1$ msec and $\tau_N \doteq 1/5$ msec, the histograms appear quite similar to interval histograms computed from VIIIth-nerve data.

5.3 RESPONSE OF THE MODEL TO SINUSOIDAL STIMULI

The fibers of the VIIIth nerve respond selectively to different frequencies of sinusoidal stimuli. Each fiber is tuned (that is, is maximally sensitive) to a particular frequency, which will be referred to as the characteristic frequency (CF) of the fiber. "Neural tuning curves" for a representative group of VIIIth-nerve fibers were presented

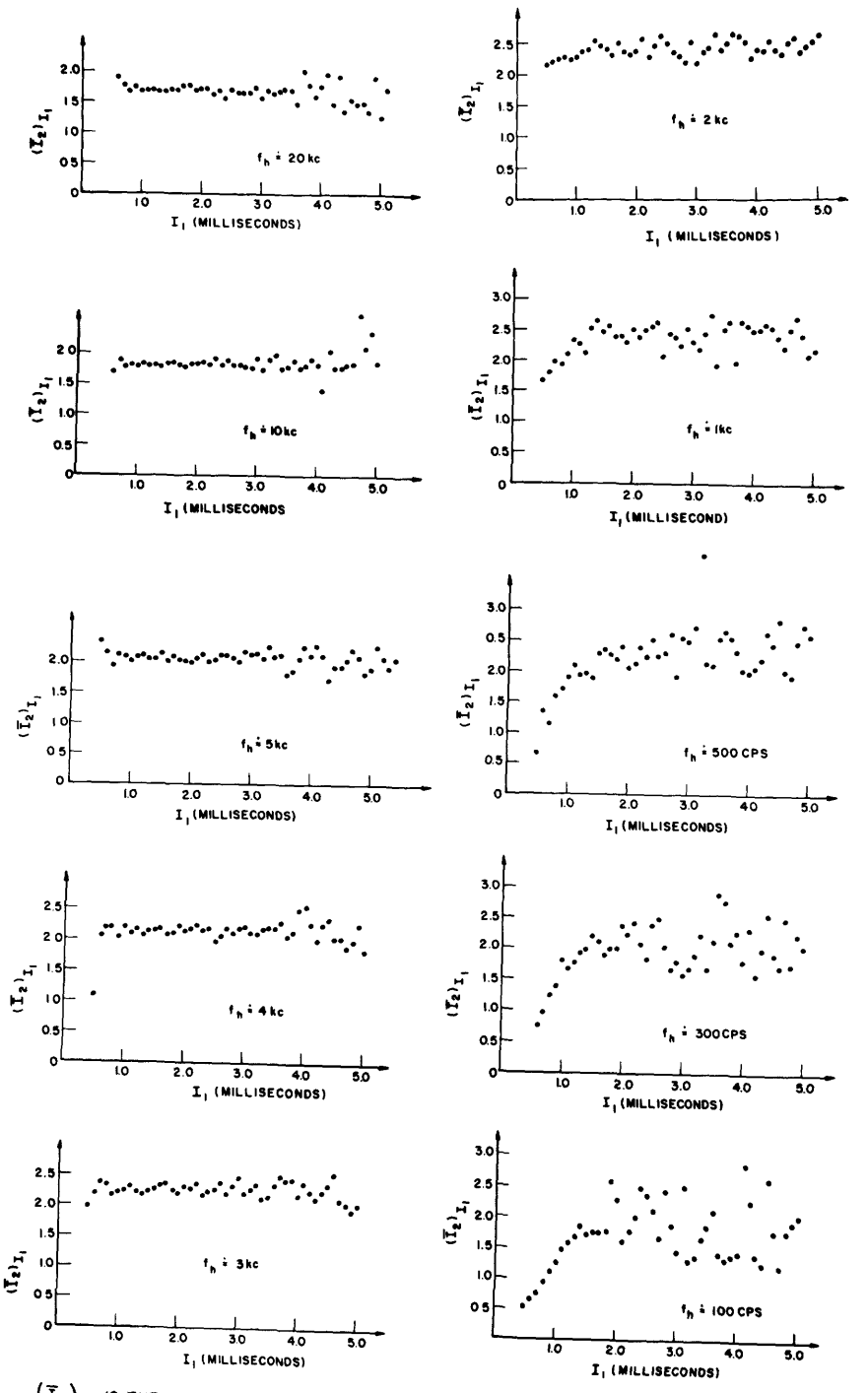

$(\bar{I}_2)_{I_1}$ IS THE AVERAGE INTERSPIKE INTERVAL I_2 GIVEN THE PREVIOUS INTERVAL IS I_1

f_h IS THE HIGH FREQUENCY LIMIT OF THE NOISE SPECTRUM

Fig. 25. Conditional average interspike intervals of the spontaneous activity generated by the model as a function of noise spectrum.

R_R = 10,000 $\quad \tau_R \doteq 0.3$ msec

R_M = 100,000 $\quad \sigma \doteq 10{,}000$

$f_\ell \doteq 5$ cps

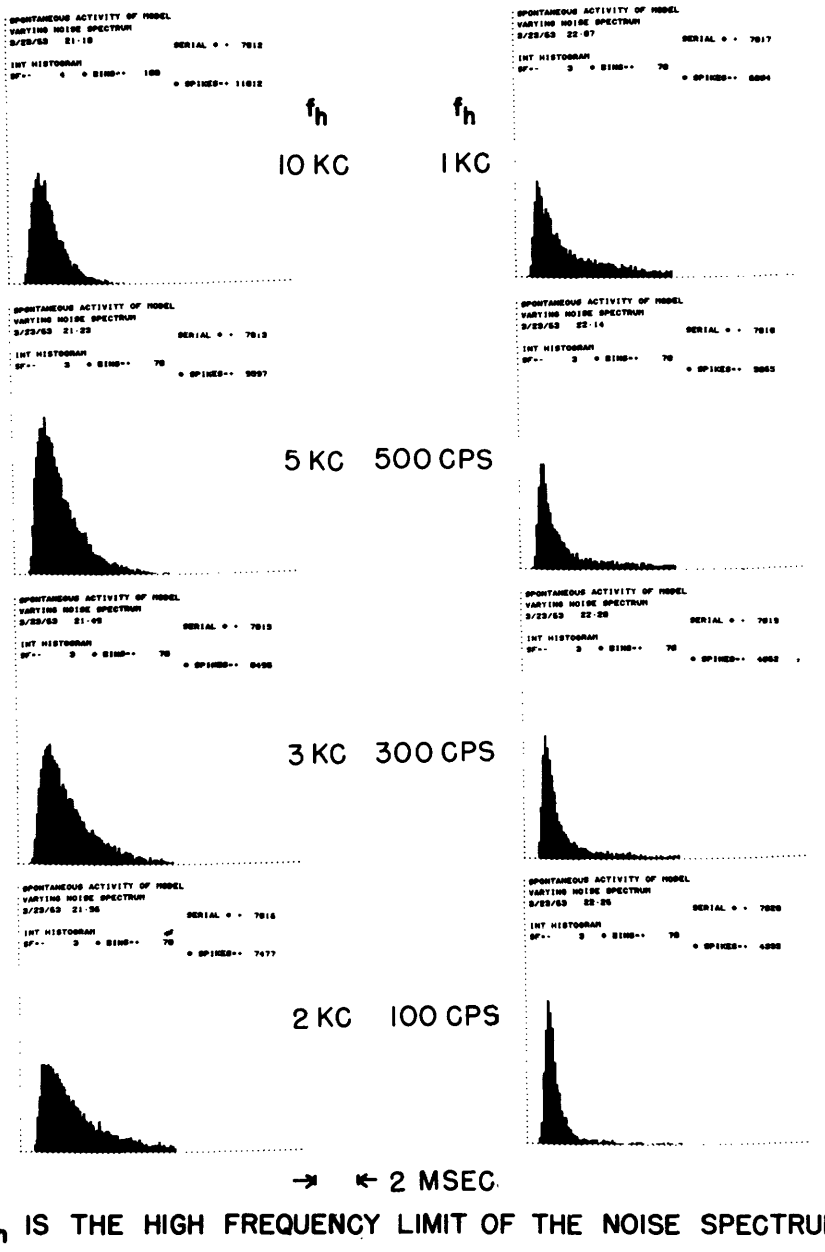

Fig. 26. Interval histograms of the spontaneous activity generated by the model as a function of noise spectrum.

$R_R = 10{,}000$ $\quad \tau_R \doteq 0.3$ msec

$R_M = 100{,}000$ $\quad \sigma \doteq 10{,}000$

$f_\ell \doteq 5$ cps

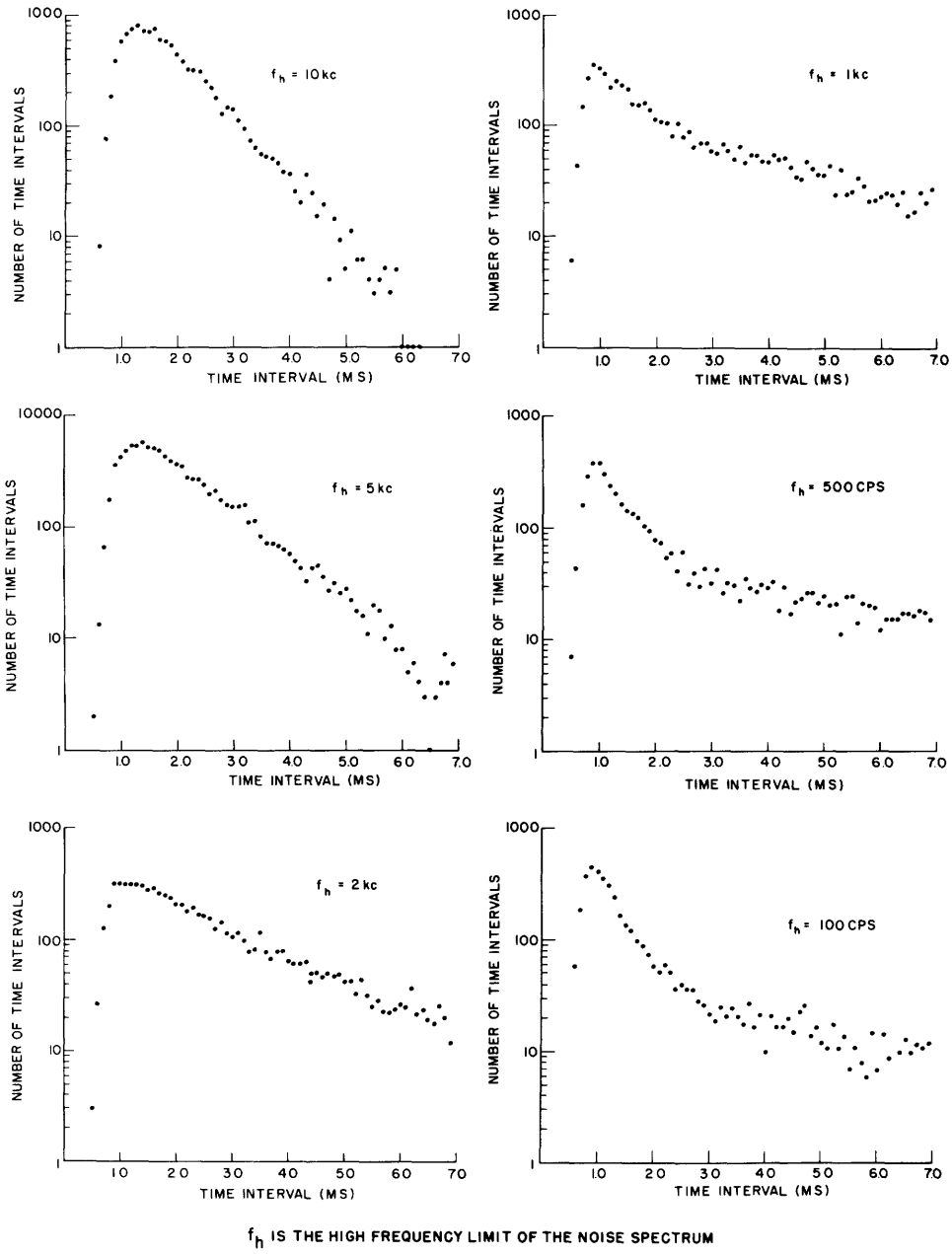

Fig. 27. Interval histograms of the spontaneous activity generated by the model as a function of noise spectrum (plotted in semi-logarithmic coordinates).

R_R = 10,000 $\quad \tau_R \doteq 0.3$ msec

R_M = 100,000 $\quad \sigma \doteq 10{,}000$

$f_\ell \doteq 5$ cps

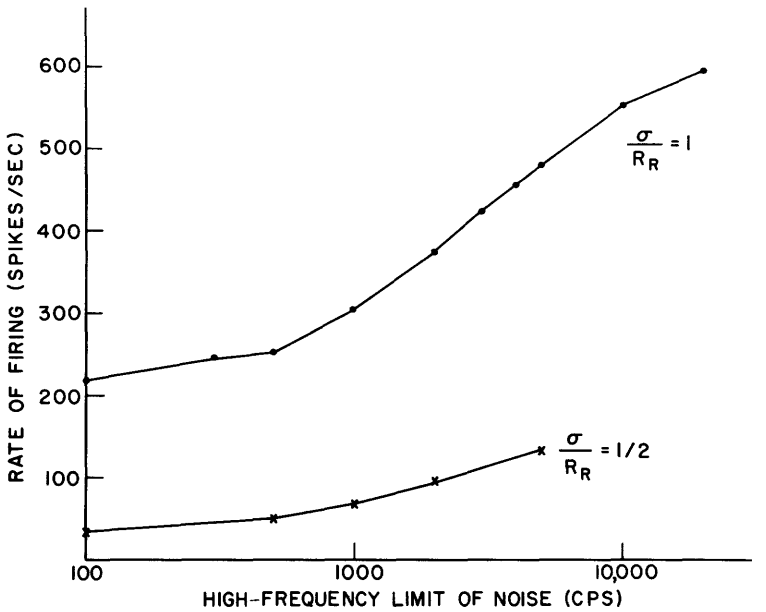

Fig. 28. Spontaneous rate of firing of the model versus the high-frequency limit of the noise.

R_R = 10,000 $\sigma \doteq 10{,}000$ (for $\sigma/R_R \doteq 1$)

R_M = 100,000 $\sigma \doteq 5000$ (for $\sigma/R_R \doteq 1/2$)

$\tau_R \doteq 0.3$ msec $f_\ell \doteq 5$ cps

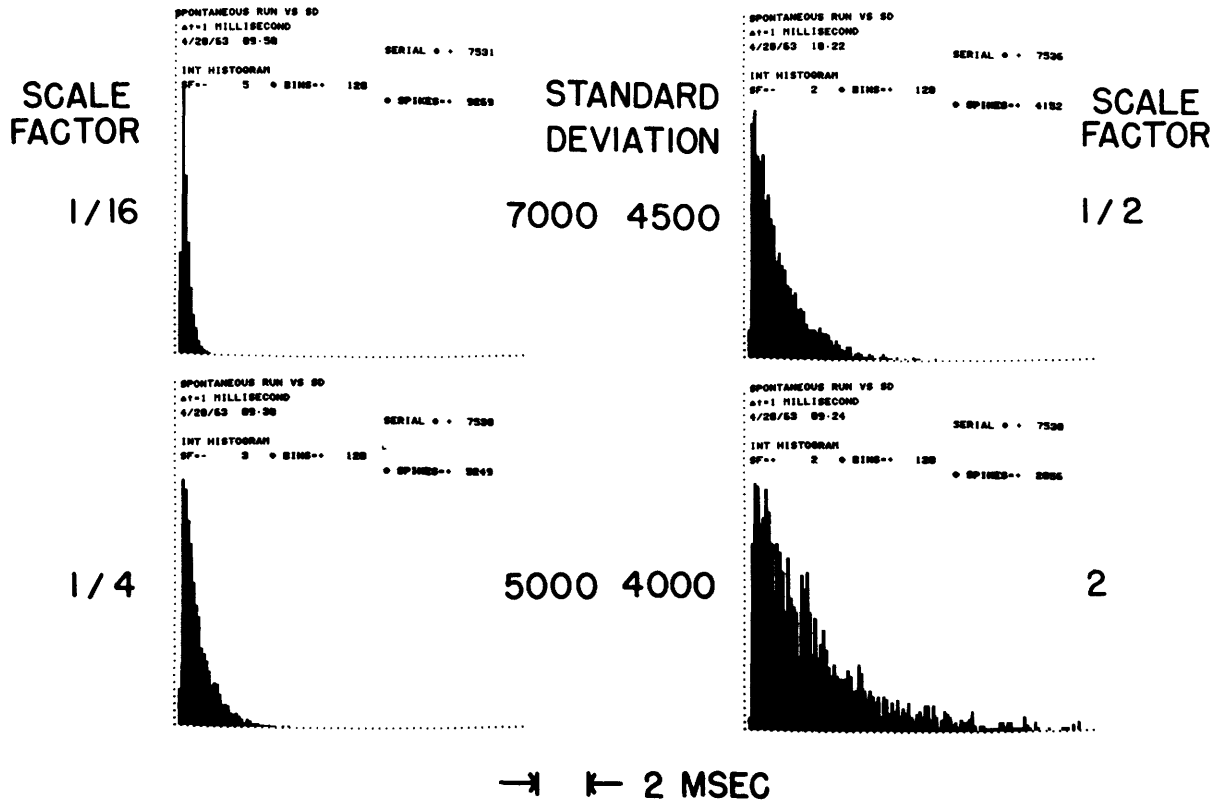

Fig. 29. Interval histograms of the spontaneous activity generated by the model versus the standard deviation of the noise.

$R_R = 10{,}000$ $\tau_R \doteq 0.3$ msec

$R_M = 100{,}000$ $f_h \doteq 5$ kc

$f_\ell \doteq 5$ cps

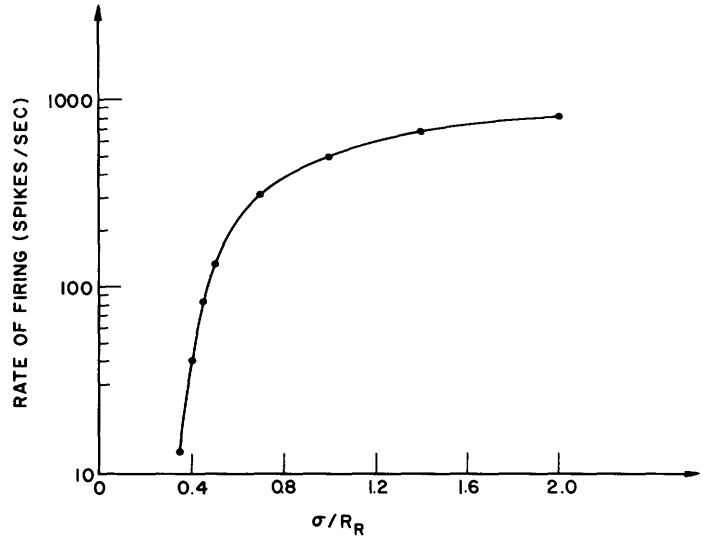

Fig. 30. Spontaneous rate of firing of the model versus the ratio of the standard deviation of the noise to the resting threshold (σ/R_R).

R_R = 10,000 $\quad \tau_R \doteq 0.3$ msec

R_M = 100,000 $\quad f_h \doteq 5$ kc

$f_\ell \doteq 5$ cps

in Fig. 17. These tuning curves are graphs of the threshold of firing of a fiber in response to a sinusoidal stimulus as a function of the frequency of the stimulus. The threshold of firing of a fiber has been defined by Kiang and others: It is (a) the intensity of the stimulus required to increase the rate of firing of the fiber 20 per cent above the spontaneous rate of firing for a fiber exhibiting a large spontaneous rate, and (b) the intensity of the stimulus required to elicit a time-locked response (determined visually) for a fiber exhibiting a low spontaneous rate of firing.

There is a second aspect to the frequency response of VIIIth-nerve fibers. Figure 17 indicates that the threshold of firing of VIIIth-nerve fibers in response to sinusoids whose frequencies are equal to the CF varies as a function of CF. The most sensitive points in the tuning curves of the most sensitive fibers shown in Fig. 17 constitute what we shall refer to as a "neural sensitivity curve." The neural sensitivity curve for the data represented in Fig. 17 shows a minimum at a frequency of ~2 kc. For frequencies below 2 kc, the "neural sensitivity curve" shows a decrease of sensitivity of approximately 30 db/decade. At frequencies above 2 kc, the sensitivity also decreases. A qualitatively similar change in sensitivity as a function of frequency can be noted in the response of cells in higher centers of the auditory system,[29] as well as in the over-all behavior of an organism, as indicated, for instance, by the human audiogram.[38]

It is perhaps already clear that we assume that a relation exists between the frequency-response curves of the cochlear partition (as shown in Fig. 12) and the tuning curves of VIIIth-nerve fibers (as shown in Fig. 17). A particular neural fiber with a CF equal to f_o is assumed to be stimulated by the displacement of the cochlear partition at a point x_o that responds maximally to the frequency f_o of sinusoidal stimulation presented to the ear. Furthermore, we are assuming the existence of a correspondence between the "neural sensitivity curve" and the "mechanical sensitivity curve" (shown in Fig. 13). The mechanical sensitivity curve relates the amplitude of the displacement of the stapes required to achieve some fixed maximum amplitude of displacement of a point on the cochlear partition as a function of frequency.

In this section we shall consider, first, the sensitivity curves generated by the model vis-à-vis the neural sensitivity curve. We shall then discuss the tuning curves of VIIIth-nerve fibers.

a. Sensitivity of the Model at Low Frequencies

The empirical data of Kiang and his co-workers on the response of VIIIth-nerve fibers to sinusoidal stimuli depend upon a determination of the "threshold of firing" of a fiber to a stimulus. Before we can discuss the data generated by the model, we feel that it is essential to discuss the concept of a threshold of firing in response to a stimulus.

The "threshold of firing" of a neuron to a stimulus is an old concept in neurophysiology. Pecher[47] was one of the first to recognize that the response to electrical stimulation of a sciatic-nerve fiber in a frog could not be described by a simple threshold below which the fiber never fired and above which the fiber always fired. Pecher

was able to demonstrate that a probabilistic description of the firing of a fiber was a more accurate description. For the sciatic-nerve fibers, a threshold can be defined arbitrarily as the intensity of stimulation producing a response to 50 per cent (or any other per cent) of the number of stimuli. With such a definition of threshold, equal-response curves can be determined, under a variety of physiological conditions.

For fibers that exhibit spontaneous activity (such as VIIIth-nerve fibers) the problem of defining a threshold of firing to a stimulus is more complicated and perhaps irrelevant. It appears to be unreasonable to identify some spikes with the response to a stimulus and other spikes as spontaneous activity. Results obtained from the model indicate that there is time-locked activity present in the response for every intensity of stimulus. For any particular intensity of stimulation there is a resultant perturbation of the average rate of firing of the model. In a sufficiently long record this time-locked activity can be seen as a perturbation in the PST histogram. Sufficiently long and stable records of data cannot be obtained from neural fibers and therefore such behavior cannot be demonstrated in a physiological preparation.

Despite the difficulty in defining the concept of "threshold," one still opts for a metric of the spike activity of fibers which permits equal response or relative sensitivity curves, if not absolute sensitivity curves, to be obtained. Clearly, if a sufficiently accurate and manipulatable model of the system were available, metrics of the spike activity might be derived that would be appropriate in some sense.

A somewhat arbitrary choice of metrics must be made, in the absence of more appropriate metrics. Kiang et al. have used arbitrary criteria for defining the threshold of firing of VIIIth-nerve fibers to sinusoidal stimuli. They chose the intensity required to increase the rate of firing by 20 per cent over the spontaneous firing rate as the definition of threshold for fibers having a relatively high spontaneous rate. For fibers exhibiting a low spontaneous rate, the threshold was defined as the intensity at which the fiber fired in a time-locked manner (determined visually) to the stimulus.

In order to compare results obtained from the model with data obtained from VIIIth-nerve fibers, we shall adopt the same criteria for threshold to tonal stimuli. In addition to investigating the rate of firing of the model as a function of stimulus parameters, we shall also investigate a metric that is closely related to the amount of time-locked activity. This same metric can be used to define a threshold and, as is discussed below, the thresholds obtained by using this criterion are lower than those obtained by using the 20 per cent change of rate as a criterion for threshold.

In order to define this metric, first consider the PST histogram obtained from an experiment (on model or fiber) as consisting of η_i firings in the i^{th} bin at time $i(\Delta t)$ following the onset of a stimulus, where Δt is the width of a bin in the PST histogram. Suppose that this record contains a total of N firings distributed in the n bins, that is, $i = 1, \ldots, n$. D^2 is defined as

$$D^2 = (1/n) \sum_{i=1}^{n} (\eta_i - E[\eta_i])^2,$$

where $E[\eta_i]$ is the average number of firings per bin.

The expected value of D^2 for the case of N firings placed at random in n bins is given by

$$E[D^2] = (N/n)(1-(1/n)) = \text{var}[\eta_i].$$

One can further determine that

$$\text{var}[D^2] = 2N(N-1)(n-1)/n^4 = [2(N-1)/n^2]\, E[D^2].$$

A full discussion of these and other derivations is given in Appendix B. D_n is defined as

$$D_n = \left[\frac{(1/n) \sum_{i=1}^{n} (\eta_i - (N/n))^2}{(N/n)(1-(1/n))} \right]^{1/2}.$$

The expected value of this function is 1 when there is no time-locked activity, and the value increases as the amount of time-locked activity increases. The expression for the variance of D_n yields an estimate of the significant variations of D_n from the value $D_n = 1$ for different values of N and n. Both of the definitions of threshold, the 20 per cent change of rate of firing and the D_n criterion, will be utilized in the discussion of the sensitivity of the model to sinusoidal stimuli.

To continue the discussion of the sensitivity curves generated by the model as compared with the results obtained from VIIIth-nerve fibers: A graph showing the intensity required to achieve the "threshold of firing" at the CF as a function of the CF for a number of VIIIth-nerve fibers is shown in Fig. 31. A curve composed of the lowest points in the figure shows an approximate change in sensitivity of 30 db/decade at low frequencies.

Figure 13 shows that the mechanical system exhibits a decrease of sensitivity of between 10 db/decade and 15 db/decade in the same range of frequencies. Therefore, if the model is assumed to be a valid representation of the peripheral auditory system then it must account for a change in sensitivity in excess of the 10 db/decade or 15 db/decade change in sensitivity exhibited by the mechanical part of the system. More specifically, in the frequency range 200 cps-2 kc, the transducer and model neuron (TN-model) must account for a change in sensitivity of approximately 15 db/decade or 20 db/decade.

We shall consider two properties of the response of the TN-model to a sinusoidal stimulus: (i) the amount of time-locked activity as given by the value of D_n; and

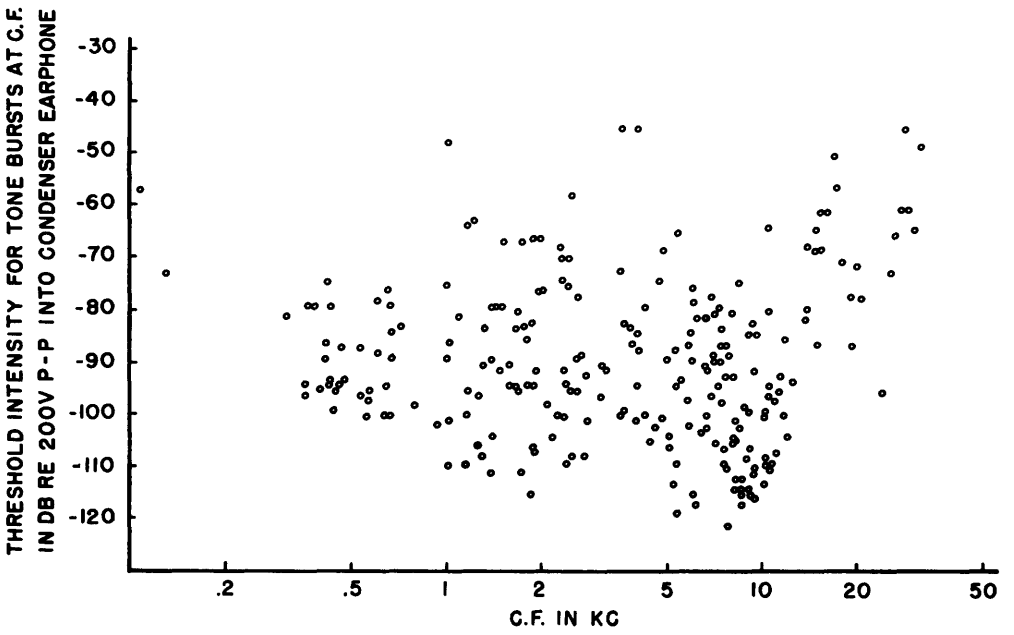

Fig. 31. Threshold of firing of VIIIth-nerve fibers (of cats) to tone bursts (delivered at the CF of the fiber) as a function of CF (from Kiang et al.[36]).

(ii) the rate of firing of the TN-model.

The response of the TN-model to sinusoidal stimuli for two different values of frequency is shown in Fig. 32. The response is displayed in the form of a post zero-crossing (PZC) histogram. This histogram is essentially a PST histogram in which the onset of the stimulus is assumed to occur at the positive-going zero crossing of the input sinusoid. The PZC histogram shows the number of firings that occur at time t after the positive-going zero crossing of the sinusoid as a function of t.

The histogram for a frequency of 208 cps and an intensity of -12 db shows an increase in the rate of firing of less than 8 per cent over the spontaneous rate, yet a considerable amount of time-locked activity can easily be seen in the histogram. The value of D_n is equal to 3.05 for this run. This value of D_n indicates that the rms value of the histogram is three times the value that would be expected for a spontaneous run, given the same number of firings. This value is highly significant and it can be shown that the probability of getting a value of $D_n = 3.05$ in the spontaneous case is vanishingly small (the 3σ level of significance in the variation of the sample standard deviation can be shown to yield values of D_n between 0.885 and 1.09 for this run). We mention in passing that using the criterion $D_n = 3.05$ to define threshold yields a lower threshold than the one attained by defining the threshold as the intensity required to increase the rate of firing 20 per cent over the spontaneous level.

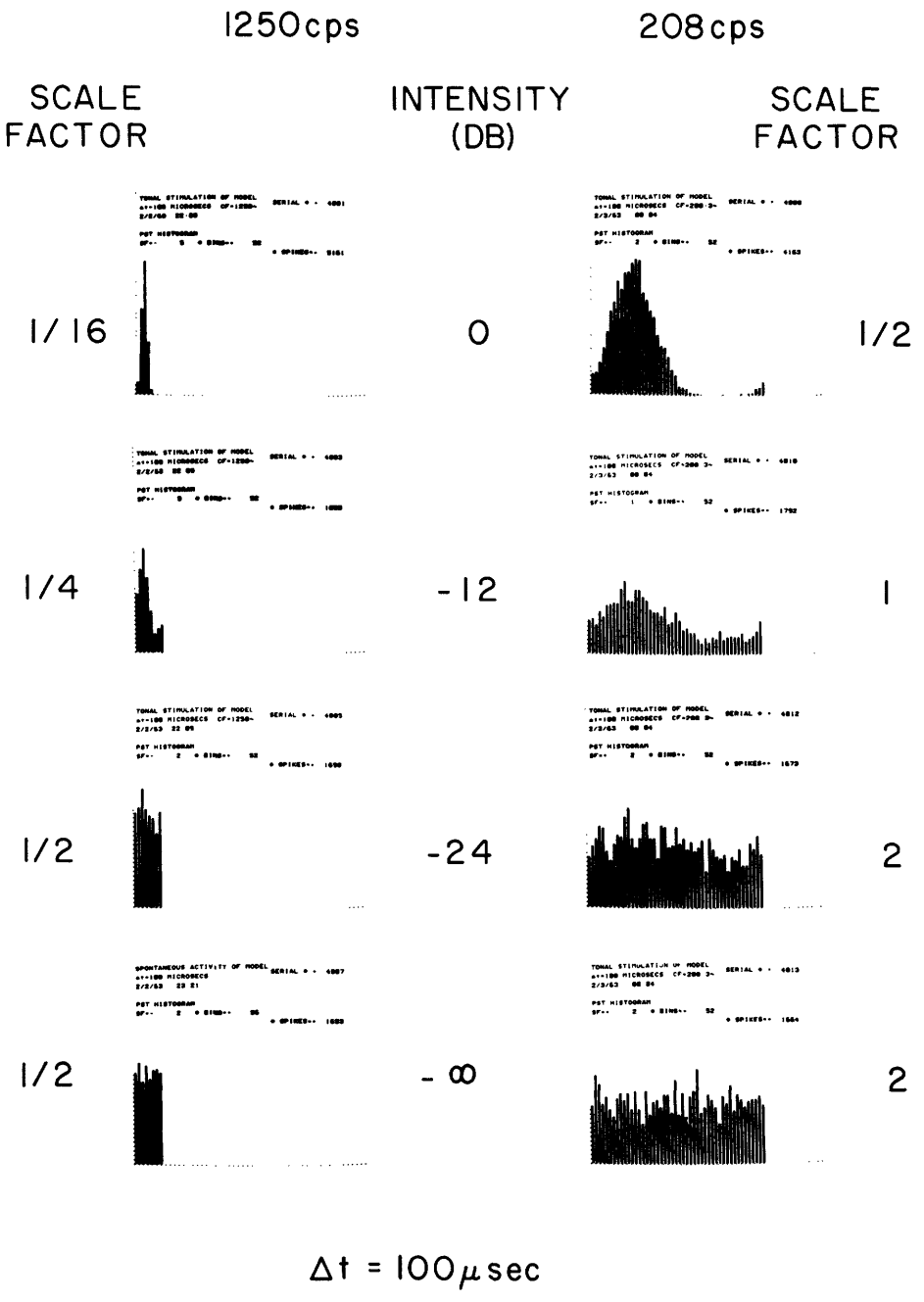

Fig. 32. Response of the TN model to sinusoidal stimuli as a function of intensity.

R_R = 25,000 $\sigma \doteq$ 10,000

R_M = 100,000 $f_h \doteq$ 5 kc

$\tau_R \doteq$ 0.3 msec $f_\ell \doteq$ 5 cps

Δt = 100 μsec

Rate of spontaneous events ≐ 40 events/sec; 0 db corresponds to a sinusoid whose amplitude is 10,000 units.

Figure 33 shows the rate of firing of the TN model as a function of the intensity of sinusoidal stimulation for six different frequencies. For any given intensity the rate increases with increasing frequency. For a fixed rate of firing, a higher intensity

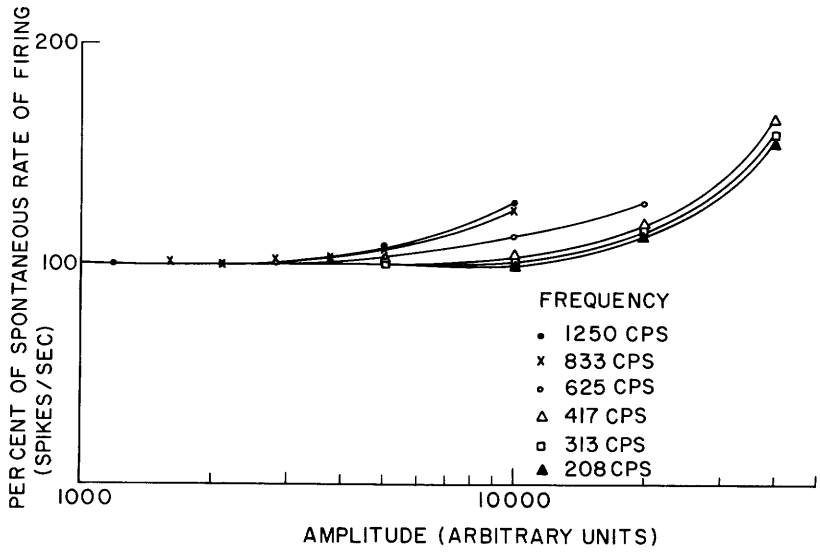

Fig. 33. Rate of firing of the TN model vs amplitude of sinusoidal stimulation.

$R_R = 10,000$ $\quad \sigma \doteq 10,000$

$R_M = 100,000$ $\quad f_h \doteq 5$ kc

$\tau_R \doteq 0.3$ msec $\quad f_\ell \doteq 5$ cps

Rate of spontaneous events $\doteq 490$ events/second.

is required at low frequencies than at high frequencies of sinusoidal stimulation. Similarly, Fig. 34 shows that the same trend holds if D_n is plotted as a function of intensity for different frequencies. D_n is a measure of the amount of time-locked activity, and it can be seen that a higher intensity is required at low frequencies to achieve some fixed value of D_n.

Figure 35 summarizes these data in a set of sensitivity functions generated by the TN model. The ordinate is the amplitude of the sinusoidal stimulus required to achieve the threshold criterion. The abscissa is the frequency of the sinusoid. The three definitions of threshold, or rather the three equal-response criteria, are: (i) a 20 per cent increase in the rate of firing above the spontaneous level; (ii) $D_n = 2$; and (iii) $D_n = 5$. In each case the sensitivity of the TN model is higher for higher frequencies. Furthermore, the sensitivity decreases at low frequencies at a rate of from approximately 12 db/decade to 20 db/decade, the rate depending on which criterion for threshold is utilized.

It is perhaps a little difficult to see why the TN model should exhibit such a frequency

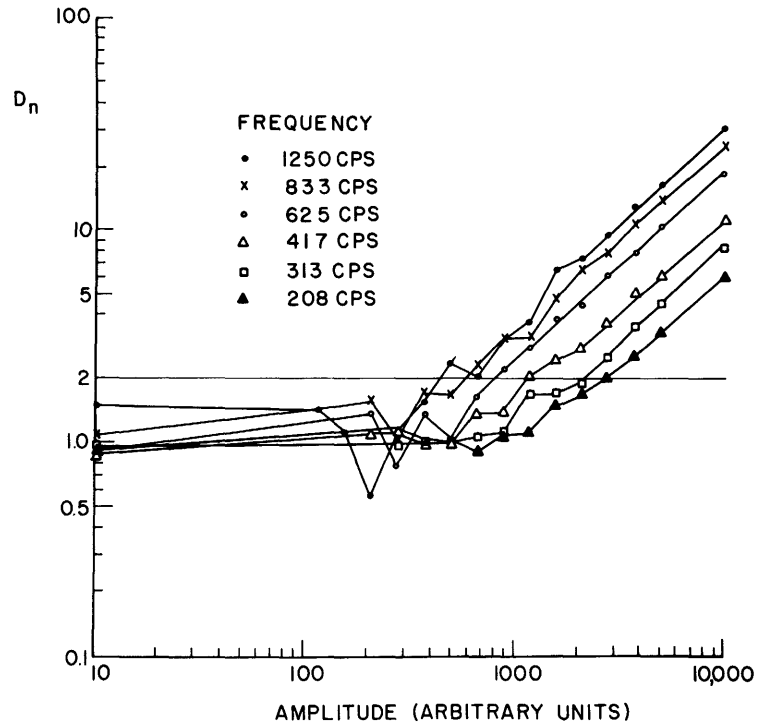

Fig. 34.

D_n vs amplitude of sinusoidal stimulation of the TN model.

R_R = 10,000 $\quad\quad$ $\sigma \doteq$ 10,000
R_M = 100,000 $\quad\quad$ $f_h \doteq$ 5 kc
$\tau_R \doteq$ 0.3 msec $\quad\quad$ $f_\ell \doteq$ 5 cps

Rate of spontaneous events $\doteq$ 490 events/second.

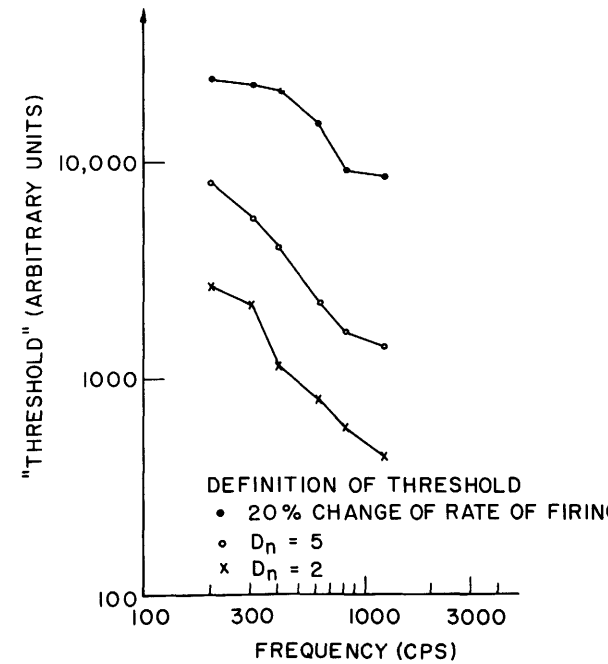

Fig. 35.

"Threshold" of firing of the TN model vs frequency of sinusoidal stimulation.

R_R = 10,000 $\quad\quad$ $\sigma \doteq$ 10,000
R_M = 100,000 $\quad\quad$ $f_h \doteq$ 5 kc
$\tau_R \doteq$ 0.3 msec $\quad\quad$ $f_\ell \doteq$ 5 cps

Rate of spontaneous events $\doteq$ 490 events/second.

sensitivity. In order to gain some insight into the reasons for this result, consider the case for which the TN model exhibits no spontaneous activity. [We are indebted to Professor W. M. Siebert for suggesting this particular discussion of the frequency sensitivity of the model.] Assume that the intensity of the sinusoid is large enough to exceed the value of the resting threshold, R_R. Then in the limit of high frequencies, the TN model fires at a rate determined entirely by the properties of the refractory period and the amplitude of the sinusoid. The sinusoid acts effectively as an increase in the average value of the membrane potential. The TN model fires, therefore, as soon as the threshold r_k has decayed to a sufficiently small value. In the limit of low frequencies, the sinusoidal input effectively acts as a square wave. In half of this cycle the TN model fires at a rate determined almost entirely by the refractory period and by the amplitude of the sinusoid; in the other half-cycle the TN model does not fire. Therefore the TN model fires at approximately twice the rate in response to the high-frequency sinusoid as it does in response to the low-frequency sinusoid. The frequency sensitivity of the TN model is more difficult to depict when spontaneous activity is present.

Figure 36 indicates that this decrease of sensitivity of the TN model for low frequencies exists for a large range of rates of spontaneous firing. The figure shows the rate of firing of the TN model as a function of the amplitude of sinusoidal stimulation for two frequencies and three different rates of spontaneous firing. The different rates of spontaneous firing have been achieved by varying σ/R_R. The TN model is seen to respond at a higher rate to high-frequency sinusoids than to low-frequency sinusoids for each rate of spontaneous firing.

Further investigations of a similar nature indicate that the TN model always exhibits a higher sensitivity at high frequencies than at low frequencies. This trend is independent of the definitions of the equal-response criteria which we have used. These results are also valid for all values of the rate of spontaneous firing which we have investigated (the range 500-10 events/second). The rate of change of sensitivity over the frequency range 100-1250 cps is, however, a function of all of these variables. In general, the slope of the sensitivity curve decreases as the rate of spontaneous firing of the model is decreased, that is, as σ/R_R is decreased. For rates of spontaneous firing comparable to the largest values seen in VIIIth-nerve fibers (approximately 150 spikes/second) the change in sensitivity produced by the TN model is not large enough to account for the additional 20 db/decade change in sensitivity.

Although the sensitivity of the model to sinusoidal stimuli is qualitatively in agreement with comparable results obtained from VIIIth-nerve fibers, the quantitative agreement is poor. Thus far we have assumed that the transducer element of the model serves no essential functional purpose except to convert the output of the mechanical system into the input to the model neuron, without distorting this signal in any way. Now suppose that the transducer could be characterized by a nonlinear memoryless function. Suppose, furthermore, that this function increased monotonically

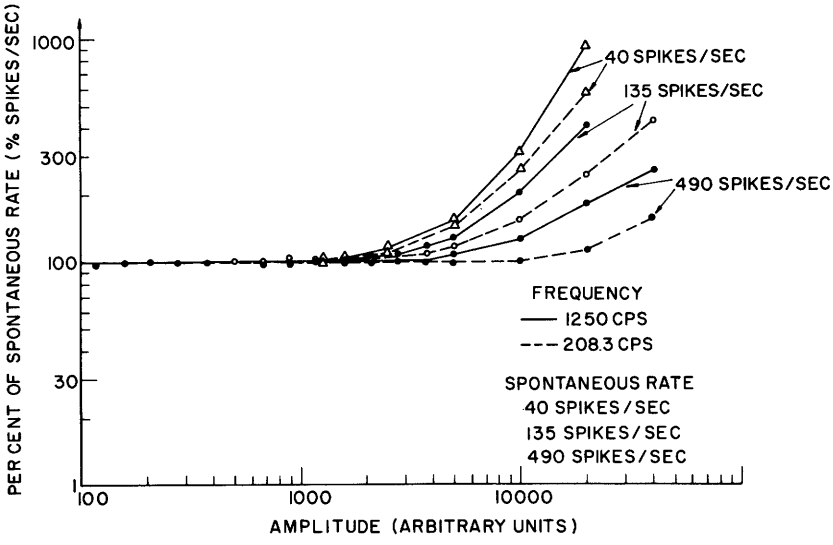

Fig. 36. Rate of firing of the TN model vs amplitude of sinusoidal stimulation for different rates of spontaneous firing.

R_R = 10,000 (for 490 spikes/sec curves)
R_R = 20,000 (for 135 spikes/sec curves)
R_R = 25,000 (for 40 spikes/sec curves)
R_M = 100,000
$\tau_R \doteq 0.3$ msec
$\sigma \doteq 10,000$
$f_h \doteq 5$ kc
$f_\ell \doteq 5$ cps.

with a slope that was positive but monotonically decreasing. For instance, $G(y) = (k_1 y)(k_2/(k_2+|y|))$ for $y \geq 0$ is such a function. To a first-order approximation, the effect of the introduction of such a function upon the sensitivity curves shown in Fig. 35 can be thought of as an expansion of the ordinate (threshold) scale. Therefore, given complete freedom to choose a nonlinear transducer function, the slope of the sensitivity curves shown in Fig. 35 can be adjusted to any desired value. This is clearly too much freedom and we shall defer a discussion of the transducer to the section on the acoustic-click response of the model.

b. The Shape of the Tuning Curves

Figure 37 shows the frequency response curves of the cochlear partition (Fig. 12) plotted as tuning curves. A representative set of neural tuning curves is also shown in Fig. 37. The absolute sensitivities of the neural curves have been normalized to make the thresholds of the fibers at their CF equal.

Both sets of tuning curves are very steep at high frequencies. Both sets of tuning curves are less steep at low frequencies, but the neural tuning curves are steeper than

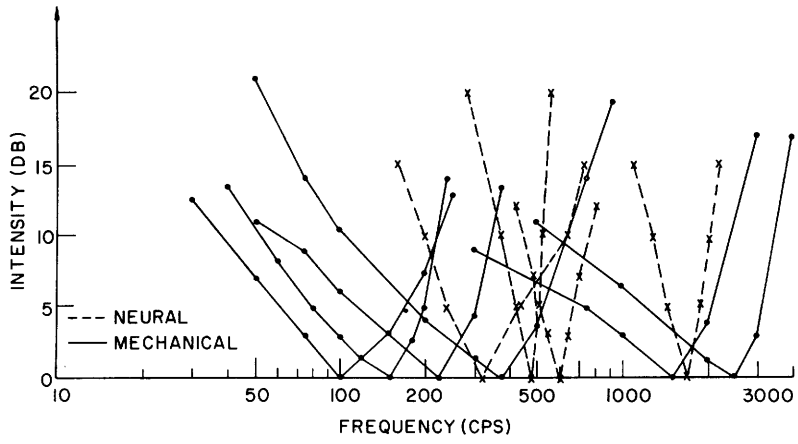

Fig. 37. Mechanical and neural tuning curves. The mechanical tuning curves are derived from the curves shown in Fig. 12, which are based on data obtained from human cadavers. The curves shown in Fig. 12 can be represented as $|H(f,x_o)|/|H(f_o,x_o)|$ for different values of x_o. The mechanical tuning curves are defined as $-20 \log (|H(f,x_o)|/|H(f_o,x_o)|)$. f_o is the CF for a point x_o cm from the stapes. The neural tuning curves were obtained from data on the VIIIth-nerve fibers of cats by Kiang et al.[36]

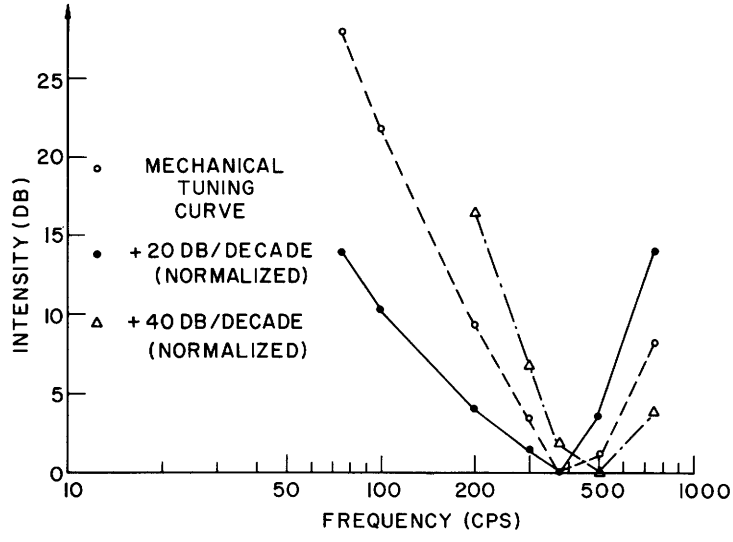

Fig. 38. Mechanical tuning curves. The augmented mechanical tuning curves were obtained by adding a 20 db/decade and a 40 db/decade change in sensitivity to a typical mechanical tuning curve.

the mechanical tuning curves at low frequencies. The mechanical tuning curves are wider than the neural tuning curves. Both sets of curves can be shown to be essentially constant-Q curves (to a first-order approximation) for the range of frequencies shown in the figure.

We have shown that the TN model exhibits a decrease in sensitivity at low frequencies. We have not been able to demonstrate that the TN model accounts entirely for the additional 20 db/decade change in sensitivity which is needed to approximate the VIIIth-nerve data. We have indicated that this discrepancy may be due to ignorance of the nature of the proper transducer function of the hair cells.

In order to discuss the shape of the tuning curves, we shall assume that the transducer and model neuron exhibit a rate of change of sensitivity of 20 db/decade of frequency. Figure 38 shows tuning curves constructed by adding both a 20 db/decade and a 40 db/decade change in sensitivity to a typical mechanical tuning curve. The results have been normalized to make the minima of the curves equal. Note that although the resultant curves are still slightly wider than the neural tuning curves, they are in closer agreement with them. Furthermore, the slopes of these augmented mechanical tuning curves are steeper at low frequencies than the slopes of the mechanical curves. We think it reasonable to say that the augmented mechanical tuning curves correspond more closely to the neural tuning curves than do the mechanical tuning curves. Any further discrepancies between mechanical and neural tuning curves may be attributed to the differences in species and preparations used to obtain the two sets of data, as well as to the degree of approximation of the argument presented here. (We have also assumed that the mechanical tuning curves reported by von Békésy (as shown in Fig. 12) represent the mechanical tuning curves of the cochlear partition of the cat.)

We have attempted to show that the tuning curves generated by the model are similar to the tuning curves of VIIIth-nerve fibers, although we have not demonstrated these results directly.

5.4 RESPONSE OF THE MODEL TO ACOUSTIC CLICKS

Responses of a number of VIIIth-nerve fibers to periodic trains of acoustic clicks (100-μsec pulses applied to a condenser earphone) were shown in Fig. 18. The responses are depicted in the form of poststimulus-time (PST) histograms (histograms of the times of occurrence of spike potentials following the onset of the stimulus). The PST histograms shown in Fig. 18 have been ordered according to the characteristic frequencies of the fibers. All histograms of fibers whose CF are less than approximately 4 kc exhibit multiple peaks. The intervals between the peaks are equal to 1/CF. Figure 39 shows the displacement of the cochlear partition (as computed by Flanagan[16]) and the PST histogram for two polarities of acoustic clicks as generated by the model. [The conditions for obtaining the PST histograms shown in Fig. 39 are discussed below. The click response of the cochlear partition corresponds to the impulse response ($F_3(t)$) shown in Fig. 14.]

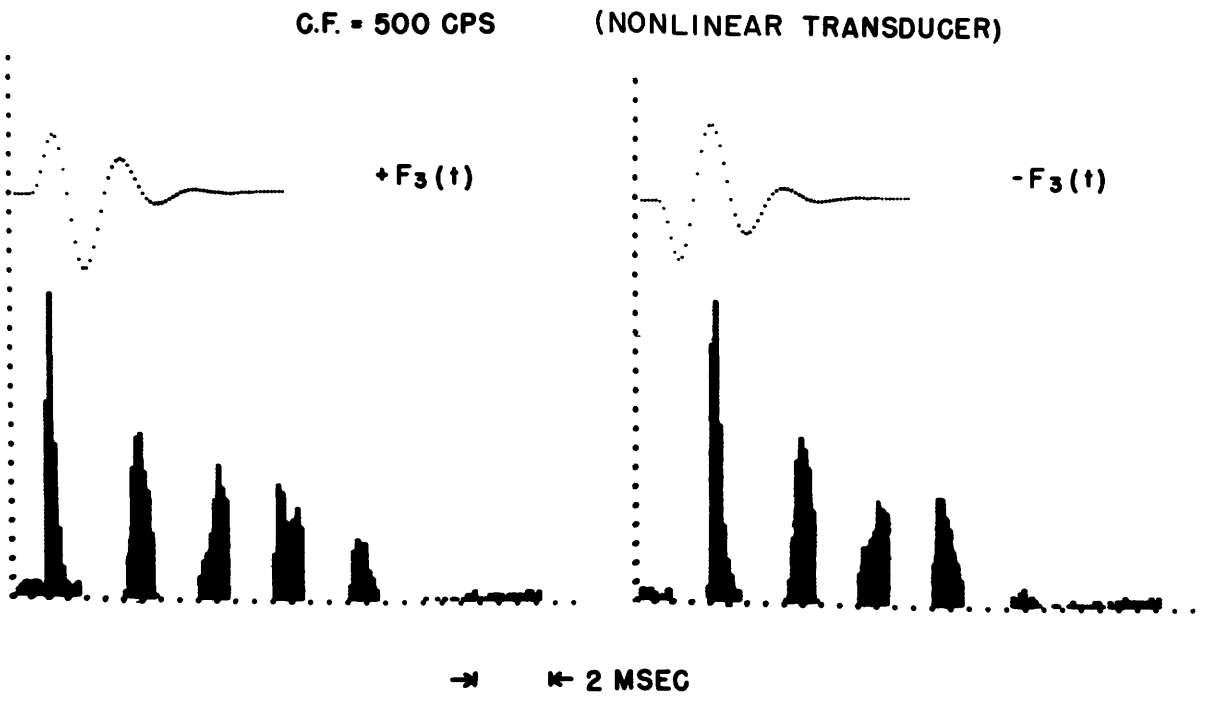

Fig. 39. Response of the cochlear partition and model neuron for two different polarities of acoustic clicks. Dotted curves are the response of the cochlear partition to positive (left) and negative (right) polarities of clicks. The impulse responses are equal to $F_3(t)$ (after Flanagan[16]) for a point along the partition with CF = 500 cps. The transducer function is $G(y) = (k_1 y)[k_2/(k_2+|y|)]$.

$k_1 = 1$	$\tau_R \doteq 1$ msec
$k_2 = 20{,}000$	$f_h \doteq 5$ kc
$R_R = 10{,}000$	$f_\ell \doteq 5$ cps
$R_M = 100{,}000$	$\sigma \doteq 5000$

Spontaneous rate of firing $\doteq$ 90 events/second.

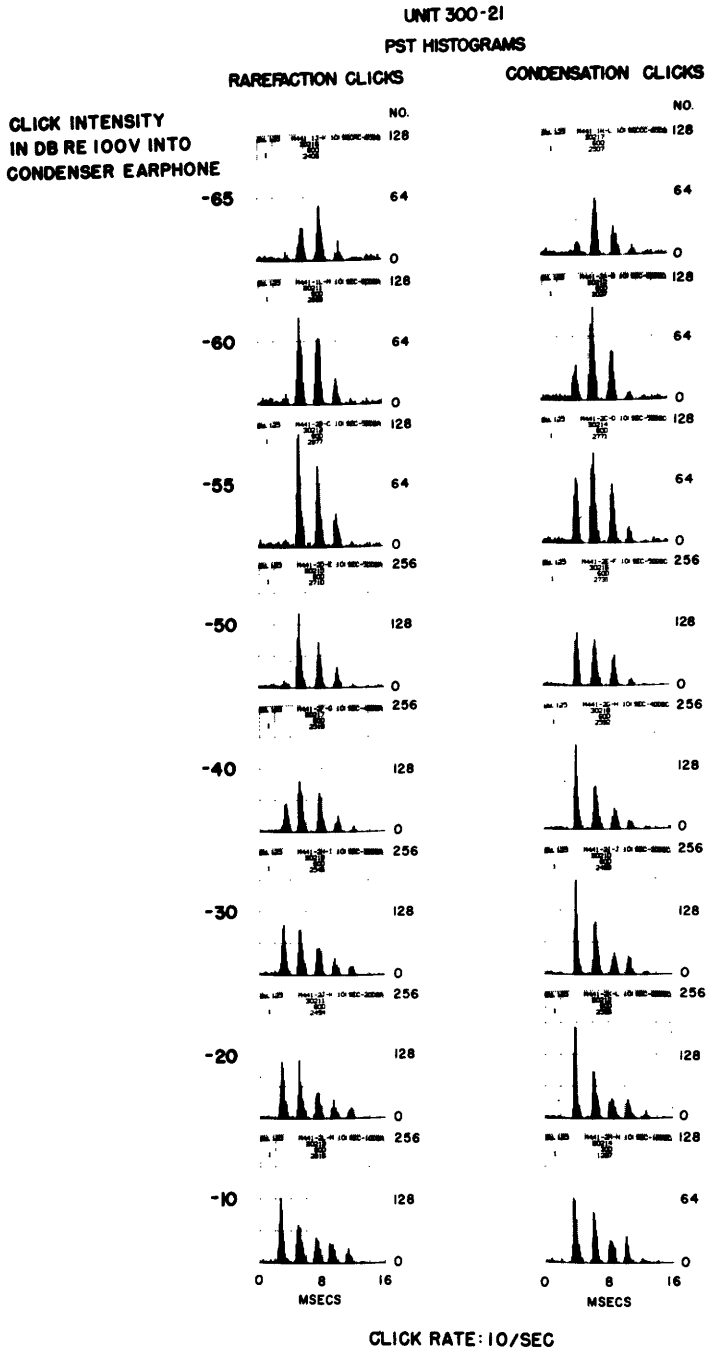

Fig. 40. Response of an VIIIth-nerve fiber to condensation and rarefaction clicks as a function of intensity (from Kiang et al.[36]). CF = 472 cps; rate of spontaneous firing, 52.5 spikes/sec; rate of presentation of clicks, 10/sec.

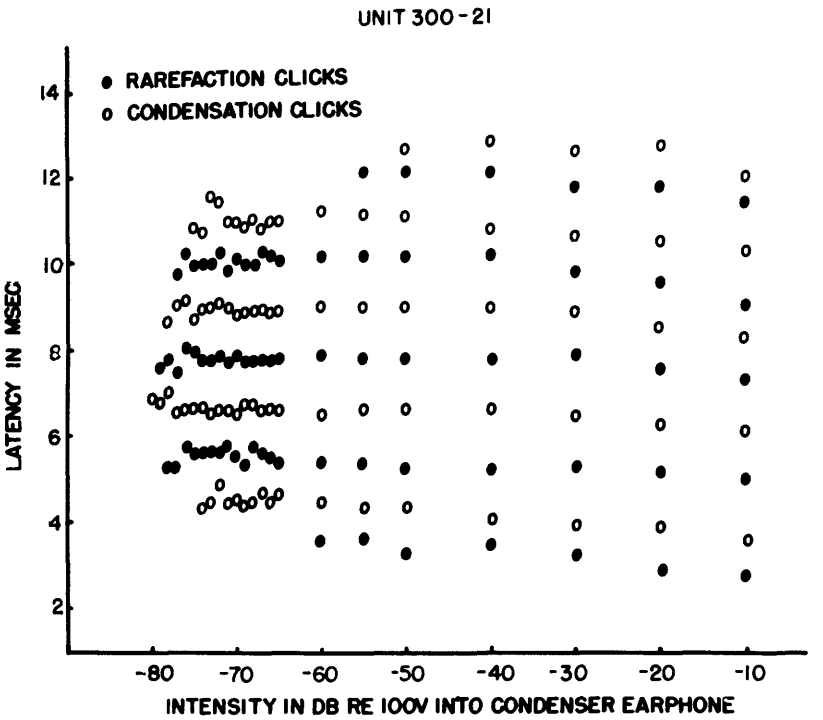

Fig. 41. Times of occurrence of peaks in the PST histogram of the response of an VIIIth-nerve fiber to condensation and rarefaction clicks as a function of intensity (from Kiang et al.[36]). CF = 472 cps; rate of spontaneous firing, 52.5 spikes/sec; rate of presentation of clicks, 10/sec.

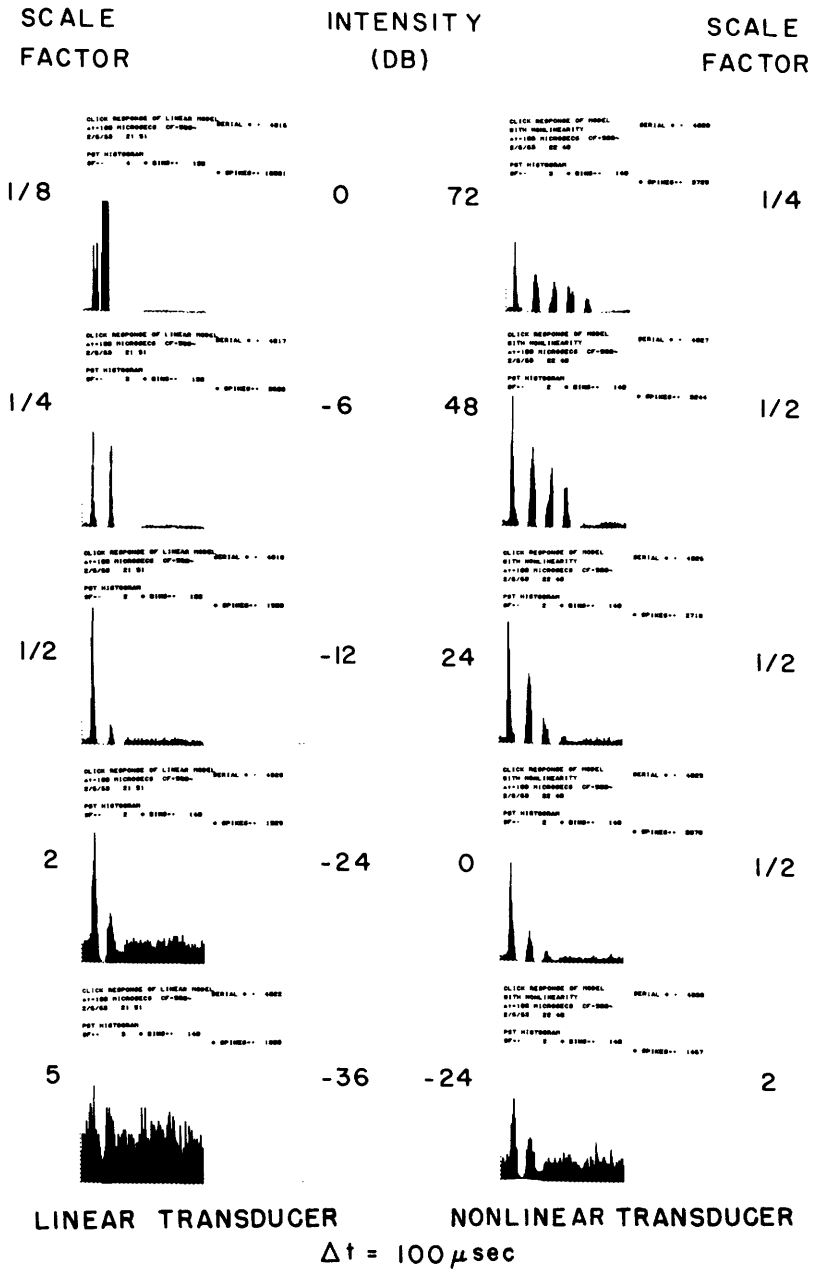

Fig. 42. Acoustic-click response of the model for a linear (left) and nonlinear (right) transducer as a function of intensity.

CF = 500 cps
G(y) = y (for linear transducer)
G(y) = y[20,000/(20,000+|y|)] (for nonlinear transducer)

R_R = 10,000 $\quad\quad$ $\sigma \doteq 5000$
R_M = 100,000 $\quad\quad$ $f_h \doteq 5$ kc
$\tau_R \doteq 1$ msec $\quad\quad$ $f_\ell \doteq 5$ cps

Rate of spontaneous firing ≐ 90 events/second.

The results shown in Fig. 39 correspond to a point along the partition whose CF = 500 cps. Note that in each case shown the PST histograms exhibit peaks at intervals of 2 msec, and these peaks occur at the positive deflections of the impulse response of the cochlear partition. Several peaks can be seen in the PST histograms, while only a few are discernible in the response of the cochlear partition. The amplitudes of successive peaks of the response of the cochlear partition decrease at a rate of not less than 20 db/cycle of oscillation. As a result, the fourth, fifth and later peaks are too small to be seen in Fig. 39.

Figure 40 shows the response of a typical VIIIth-nerve fiber to rarefaction and condensation clicks as a function of intensity. [The two polarities of clicks used in the VIIIth-nerve data are referred to as "condensation and rarefaction clicks." The two polarities of clicks used to test the model are referred to as "positive and negative clicks." This distinction is drawn in order to avoid a discussion of which direction of displacement of the cochlear partition is effective in depolarizing the nerve fibers. A correspondence between positive and negative clicks versus rarefaction and condensation has been avoided.] The interval between peaks equals 1/CF and these intervals remain relatively constant as a function of intensity. Furthermore, the peaks of the response to a rarefaction click occur at the troughs of the response to a condensation click and vice versa. The times of occurrence of the peaks in the PST histogram for condensation and rarefaction clicks as a function of intensity for the VIIIth-nerve fiber are shown in Fig. 41. The almost perfect interleaving of peaks is readily apparent.

Figure 42 shows the response of the model to acoustic clicks as a function of intensity (the intensity scale has an arbitrary reference level and only relative intensities should be considered meaningful). The PST histograms in the left-hand column were obtained by using a linear transducer function. Note that there is a 36-db range between the intensity at which a response is first visible in the PST histogram and the intensity at which the response of the model becomes stereotyped (that is, the model responds to the largest positive deflection of the cochlear partition every time a stimulus is presented in a manner unlike the response of VIIIth-nerve fibers). Since the envelope of the impulse response of the cochlear partition decays at a rate exceeding 20 db per cycle of oscillation, there can be at most two or three peaks in the PST histogram when a linear transducer is used. These results are clearly at variance with the empirical data of Kiang et al.[36]

It is clear that the peaks of the PST histogram increase too rapidly as a function of intensity. The right side of Fig. 42 shows the PST histograms of the click response of the model for a nonlinear transducer function. The function chosen in this case is $G(y) = k_1 y(k_2/(k_2+|y|))$. This function (shown in Fig. 43) has the following limiting behavior:

$G(y) \sim k_1 y$ for small values of y and

$G(y) \sim k_1 k_2 (y/|y|)$ for large values of y.

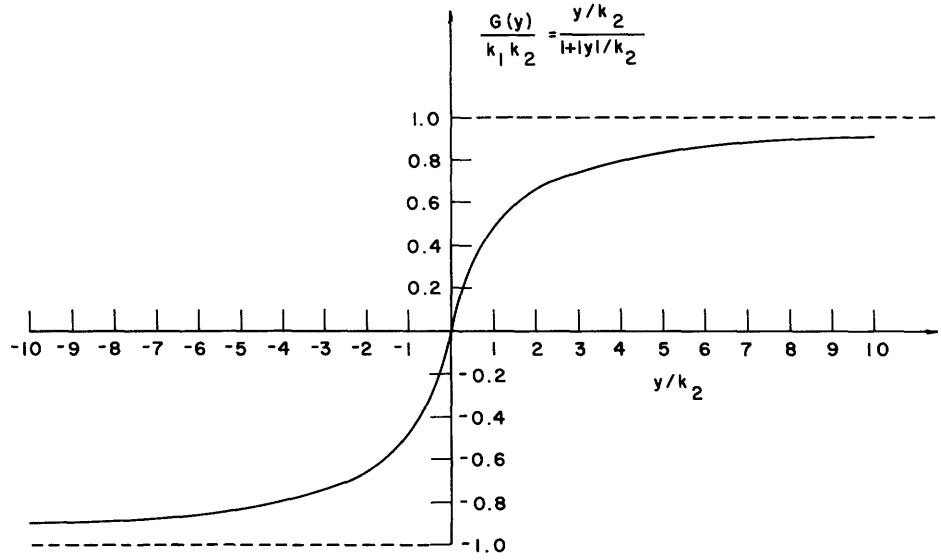

Fig. 43. A nonlinear transducer function.

The effect of this function is to prevent the increase of amplitude of the large peaks in the deflections of the cochlear partition and to allow the smaller peaks to increase as a function of intensity.

Figure 44 shows the click response of the model for both positive and negative clicks. The same nonlinear function was used to obtain the results shown in Fig. 44 as on the right side of Fig. 42. Figure 45 shows the time of occurrence of the peaks in the PST histogram in response to clicks of opposite polarity as a function of intensity. The intervals between peaks (for each polarity of click) are 2 msec. The peaks resulting from the responses to positive and negative clicks are seen to interleave.

Figure 46 shows PST histograms generated by the model for four different values of CF. The intervals between peaks correspond to 1/CF in each case. The data for values of CF equal to 4 kc and 8 kc were computed at a resolution of 12.5 μsec. The large statistical fluctuations shown in Fig. 46 result from the limited sample size used for the high-resolution runs.

Figures 47 and 48 are included to demonstrate the results obtained when a different nonlinear transducer function is used; $G(y) = k_1(y/|y|) \log|y|$ in these two cases. Both figures show the PST histograms of the click response of the model as a function of intensity. Figure 47 shows these results for CF = 500 cps, and Fig. 48 for CF = 1 kc. The results obtained by using the logarithmic nonlinearity are similar to the results obtained by using the previously mentioned nonlinearity. The general features of the PST histograms are in close agreement with the VIIIth-nerve data. The peaks in the PST histogram occur at intervals of time separated by 1/CF. These peaks interleave for the response to positive and negative clicks. The intervals of time between peaks remain constant as a function of intensity. The intervals of time between the onset of

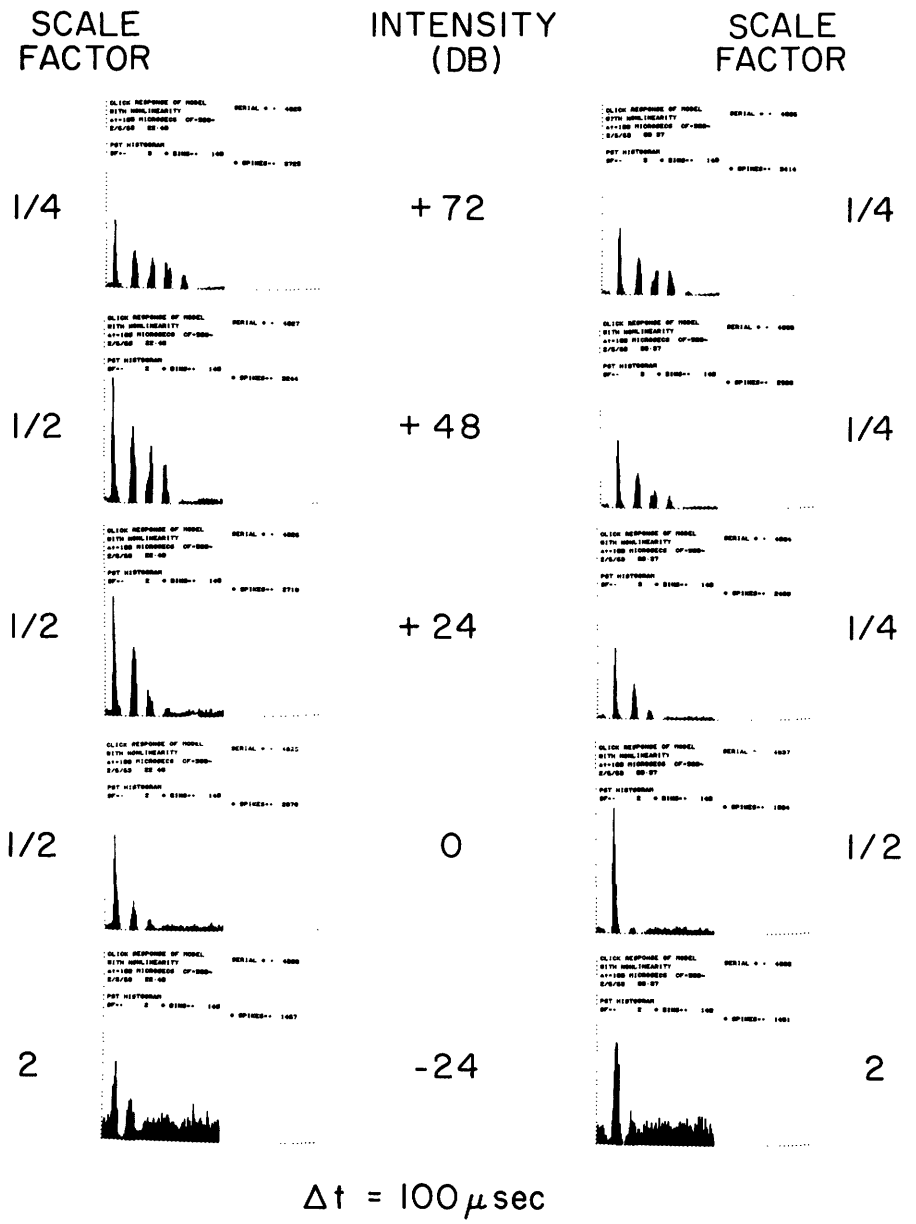

Fig. 44. Response of the model to positive and negative clicks as a function of the intensity of click stimulation (the reference level is arbitrary). The response to positive (left) and negative (right) clicks is shown.

CF = 500 cps
$G(y) = y[20{,}000/(20{,}000+|y|)]$

R_R = 10,000	$\sigma \doteq 5000$
R_M = 100,000	$f_h \doteq 5$ kc
$\tau_R \doteq 1$ msec	$f_\ell \doteq 5$ cps

Rate of spontaneous firing ≐ 90 events/second.

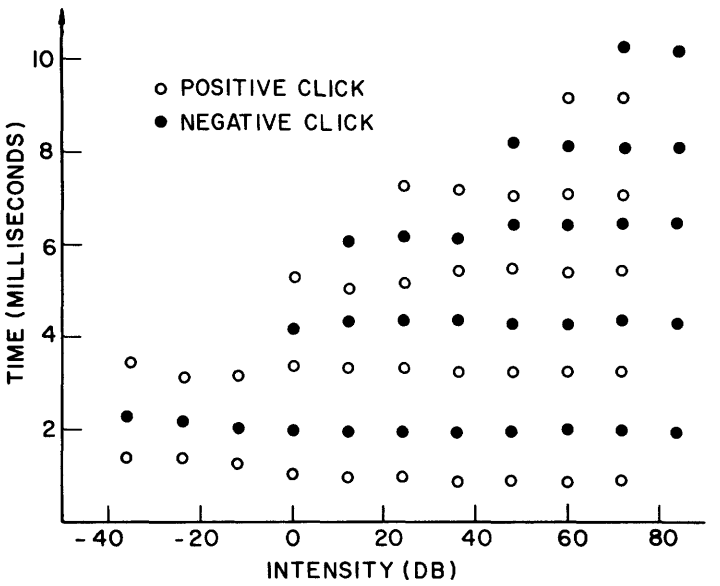

Fig. 45. Times of occurrence of peaks in the PST histograms of the response of the model to acoustic clicks.

CF = 500 cps
$G(y) = y[20{,}000/(20{,}000+|y|)]$

$R_R = 10{,}000$	$\sigma \doteq 5000$
$R_M = 100{,}000$	$f_h \doteq 5$ kc
$\tau_R \doteq 1$ msec	$f_\ell \doteq 5$ cps

Rate of spontaneous firing = 90 events/second.

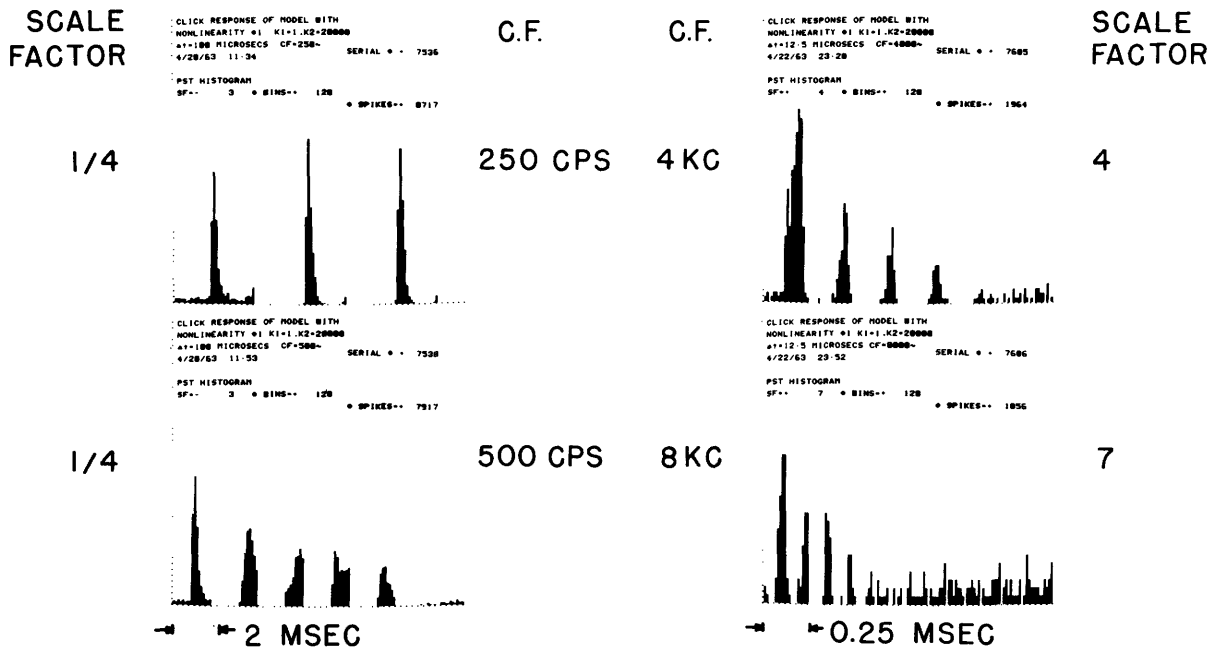

Fig. 46. Acoustic click response of the model for different values of CF.

$G(y) = y[20{,}000/(20{,}000+|y|)]$

$R_R = 10{,}000$ $\quad \sigma \doteq 5000$

$R_M = 100{,}000$ $\quad f_h \doteq 5$ kc

$\tau_R \doteq 1$ msec $\quad f_\ell \doteq 5$ cps

Rate of spontaneous firing $\doteq$ 90 events/second.

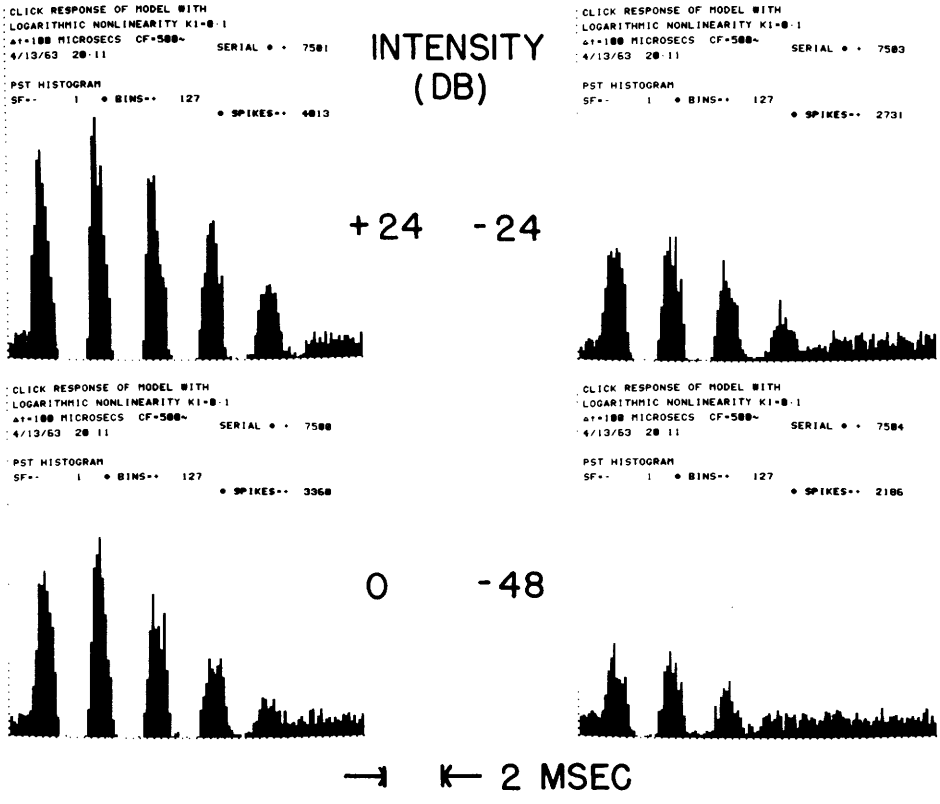

Fig. 47. Acoustic-click response of the model as a function of intensity.

CF = 500 cps

$G(y) = 0.1(y/|y|) \log_2 |y|$

$R_R = 10{,}000$	$\sigma \doteq 5000$
$R_M = 100{,}000$	$f_h \doteq 5$ kc
$\tau_R \doteq 0.3$ msec	$f_\ell \doteq 5$ cps

Rate of spontaneous firing $\doteq$ 135 events/second.

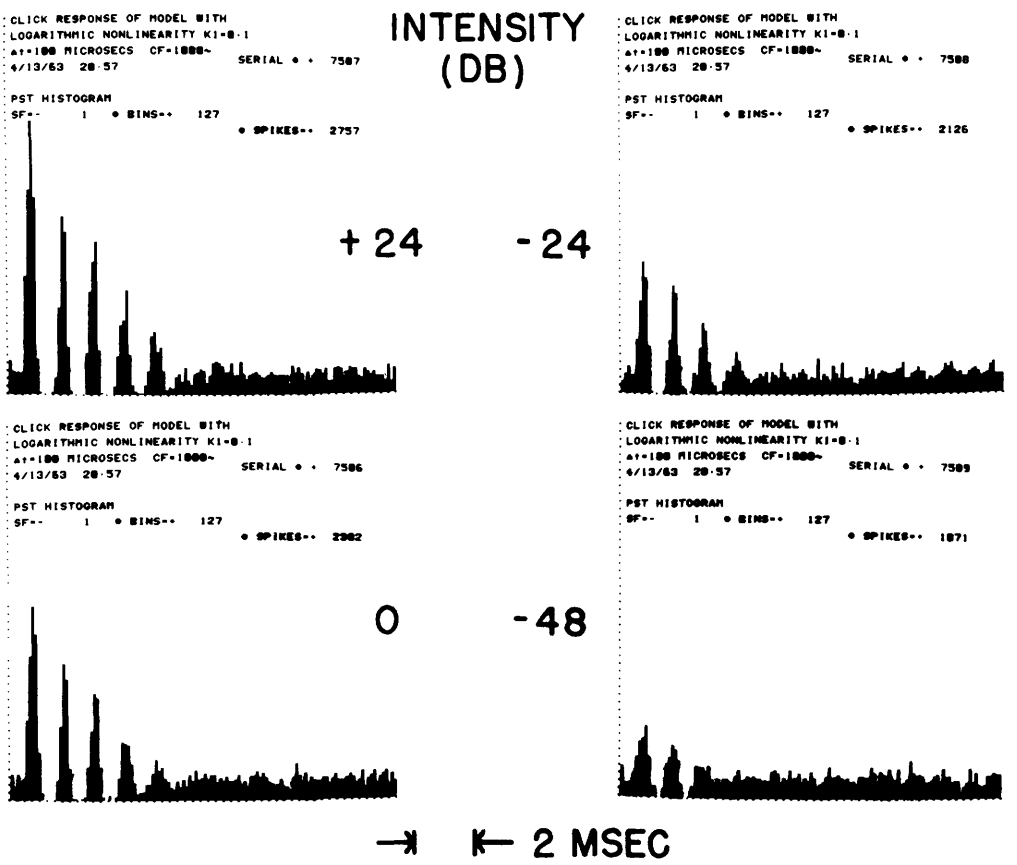

Fig. 48. Acoustic-click response of the model as a function of intensity.

CF = 1000 cps

$G(y) = 0.1(y/|y|) \log_2 |y|$

$R_R = 10{,}000$	$\sigma \doteq 5000$
$R_M = 100{,}000$	$f_h \doteq 5$ kc
$\tau_R \doteq 0.3$ msec	$f_\ell \doteq 5$ cps

Rate of spontaneous firing $\doteq$ 135 events/second.

the stimulus and each peak decrease slightly as the intensity of stimulation is increased.

There are, however, at least two discrepancies between results obtained with the model and data obtained from VIIIth-nerve fibers responding to acoustic clicks. The first one is somewhat trivial: A careful study of the response of VIIIth-nerve fibers to rarefaction clicks of high intensity reveals that a new peak appears early in the PST histogram. Similarly, a new trough appears early in the PST histogram of the response to condensation clicks of high intensity. For instance, the early peak can be clearly seen to appear at -40 db in Fig. 40. This peak appears at an interval of time equal to 1/CF with respect to the next peak (or what was previously the first peak). This early peak is never seen in data generated by the model. The peaks in the PST histograms generated by the model correspond to the positive displacements of the impulse response of the cochlear partition. Since the impulse response (Flanagan[16]) that we have utilized in this model exhibits no such early peak, neither does the PST histogram of the model. We conclude that the particular approximation to the impulse response of the cochlear partition is probably responsible for the discrepancy.

There is, however, a more serious difficulty with the model. Too large a dynamic range of intensity is required to obtain results from the model similar to those generated by VIIIth-nerve fibers. For instance, a 70-db range of intensity is required to obtain the results shown in Fig. 41. Further data indicate that the patterns of firing of VIIIth-nerve fibers require a range of intensity of approximately 50-70 db from threshold to an intensity at which the PST histograms no longer change greatly (that is, no new peaks appear). For the nonlinearities tested thus far, the comparable range of intensity for the model appears to be approximately 100 db. Furthermore, additional peaks appear at uniform intervals of intensity in this 100-db range (that is, the peaks appear at approximately 24-db intervals in Fig. 44). A smaller range of intensities is required to obtain a full complement of peaks for the VIIIth-nerve data.

These facts suggest that either a fundamental assumption of the model may be invalid or the nonlinear characteristics employed are not correct. The latter alternative, together with the results obtained thus far, suggests a class of nonlinear functions that have a sigmoid shape. $G(y) = k\left[\left(\int_{-\infty}^{y} \exp(-ax^2)\,dx\right) - 1/2\right]$ is such a function.

In conclusion, the model predicts a number of features of the response of VIIIth-nerve fibers to clicks. The peaks in the PST histograms appear at the proper intervals of time. These intervals remain fixed as a function of intensity. The times of occurrence of these peaks interleave for positive and negative clicks and these times of occurrence decrease slightly (less than 1/4 CF) as the intensity of click stimulation is increased. The dynamic range of intensity required to achieve these results in the model is larger than a comparable range for VIIIth-nerve fibers. A knowledge of the transducer function of the sensory cells would perhaps aid in eliminating this discrepancy.

5.5 REMARKS ON THE RESPONSE OF THE MODEL NEURON TO HIGH-FREQUENCY TONES AND TONE BURSTS

By purely heuristic reasoning, it would appear that the response of the model neuron to a high-frequency sinusoidal stimulus approaches the response to the envelope of the stimulus alone. Thus the response to a high-frequency continuous tone can be approximated by the response to a constant shift of the membrane potential toward the threshold potential. Similarly, the response to a tone burst can be approximated by the response to a rectangular pulse. These approximations appear to hold when the period of the sinusoidal stimulus is short compared with the refractory period.

These two stimulus paradigms have been investigated in a preliminary manner. First, the response of the model neuron to a constant shift in membrane potential was investigated and the results were compared with the response of VIIIth-nerve fibers stimulated with continuous high-frequency tones presented at the characteristic frequency of each fiber. The histograms of interevent and interspike intervals qualitatively resemble the histograms of the spontaneous activity for both model and fiber. For large values of the intervals the histograms appear to follow an exponential function, and for small values of the intervals both model and fiber show a diminution of the number of intervals. The exponential decrement of the histogram is a function of intensity for both model and fiber, and this trend indicates that the rate of firing increases as the intensity of stimulation is increased.

The response of the model neuron to rectangular or "long" pulses has also been investigated, albeit in a very preliminary manner. In this case, the "long" pulse response is to be compared with data obtained from a fiber responding to a high-frequency tone burst delivered at the characteristic frequency of the fiber. The PST histograms for both model and fiber data were compared for these stimuli. Once again there were many qualitative similarities.

There are some collaterally interesting properties of the "long" pulse response of the neuron model. For large amplitudes of stimulation (when the height of the rectangular pulse is much larger than the value of the resting threshold), the PST histograms exhibit a damped oscillatory behavior whose period is a function of intensity of stimulation. The period decreases as the intensity is increased. This response pattern is evident both in the presence and absence of spontaneous activity. Plausible heuristic explanations for this phenomenon are patent. This phenomenon is not evident in the VIIIth-nerve data, perhaps because it appears at a relatively high intensity of stimulation.

VI. CONCLUDING REMARKS

6.1 COMPARISON OF THE "DATA" GENERATED BY THE MODEL WITH DATA OBTAINED FROM VIIIth-NERVE FIBERS

We have considered three experimental conditions in order to compare results produced by the model with data obtained from VIIIth-nerve fibers. [We refer here to the electrophysiological data of Kiang and his co-workers.[34-36] In most, but not all, respects these data are in agreement with results obtained by other investigators.] These conditions are: (i) spontaneous activity; (ii) responses to sinusoidal stimuli; and (iii) responses to clicks.

Both qualitatively and quantitatively the model generates spontaneous activity that is in substantial agreement with the data obtained from fibers. The interval histograms of the spontaneous activity for both model and fibers can be described as exponential functions in the limit of large intervals; for short intervals the interval histograms exhibit a refractory effect with a smooth transition between the two regions. The model and some fiber data show a small amount of statistical dependence between successive interspike intervals: short intervals tend to be followed by short intervals, while successive intervals of time between events are uncorrelated if the preceding interval is long. The critical parameters for determining this dependence are the time course of the refractory period and the passband of the noise. The present results obtain for a time constant of the refractory period of approximately 1 msec and a noise passband of from 2 kc to 5 kc. The duration of the refractory effects of neural fibers is 1 msec, or perhaps a few milliseconds, and the value of the bandwidth of the noise used here is consistent with estimates obtained by others.[19, 64]

The response of the model to sinusoidal stimuli is qualitatively similar to data obtained from VIIIth-nerve fibers. Arguments have been presented to show that the tuning curves generated by the model approximate the tuning curves of VIIIth-nerve fibers. The post zero-crossing histograms (histograms of the times of occurrence of spikes after each positive-going zero crossing of the sinusoid) of the response of model and fiber to sinusoidal stimuli appear to be similar in some rather gross respects. The sensitivity curves generated by the model and by a population of fibers in response to sinusoidal stimuli (delivered at the characteristic frequencies) show the same trend as a function of frequency. For frequencies below 2 kc both model and fibers exhibit a decrease of sensitivity. The fibers of the VIIIth-nerve exhibit a change of sensitivity of approximately 30 db/decade of frequency. The model can exhibit a change of sensitivity of approximately 20-25 db/decade in the same range of frequency. The part of the model that represents the mechanical parts of the ear accounts for approximately a 10-15 db/decade change in sensitivity. The remaining 10 db/decade or 15 db/decade change in sensitivity must be due to the part of the model that represents the transducer and neuron. We have presented arguments suggesting that the differences between the

sensitivity curves derived from model and fiber data may be attributed to our ignorance of the actual transducer function of the sensory cells.

We have shown that using a linear, memoryless function to represent the transducer action of the sensory cells yields responses of the model to simulated acoustic clicks that are at variance with the VIIIth-nerve data of Kiang, et al. For instance, the PST histograms (histograms of the times of occurrence of spikes after the onset of a stimulus) generated by the model do not show the multiple-peak structure that is evident in the fiber data. A nonlinear transducer function can be shown to improve the agreement between model and fiber data. For the nonlinear transducer functions tested thus far, the form of the PST histogram in response to clicks is qualitatively quite similar to the data obtained from fibers. These similarities include: (i) the appearance of a number of peaks in the histograms; (ii) the intervals of time between peaks equal 1/CF; (iii) the values of these intervals are relatively insensitive to changes of the intensity of the stimulus; (iv) the times of occurrence of peaks in the response of the model to clicks of opposite polarity interleave in time; and (v) the times of occurrence of these peaks relative to the onset of the stimulus decrease (by a duration less than 1/(4 CF)) when the intensity of the stimulus is increased. The intensity range required for the appearance of successive peaks in the PST histogram is, however, larger for the model than for the VIIIth-nerve data. We feel that this discrepancy can also be accounted for by our not knowing the actual nonlinear transducer function of the hair cells. Furthermore, the same form of transducer function appears capable of improving the discrepancies of the response of model and fiber to sinusoidal as well as to click stimuli. This function appears to be a sigmoid function.

Data generated by the model appear to approximate the fiber data for the three experimental conditions that we have considered. At this stage in the research, the agreement is, for the most part, qualitative, or perhaps semiquantitative, but agreement holds for a relatively broad class of stimulus conditions and parameters. The particular model presented in this work should be considered as a first, and a very primitive, attempt to account for the data, on the basis of a mechanistic model of the peripheral system.

6.2 APPRAISAL OF THE MODEL AND SUGGESTIONS FOR FURTHER STUDY

This study suggests that the peripheral auditory system can be represented to a first-order approximation by a model consisting of three functional constituents: (i) a linear mechanical system; (ii) a nonlinear transducer; and (iii) a probabilistic threshold device with refractory properties. Such a model appears to be consistent with much of the known anatomy and physiology of the peripheral auditory system. In particular, this model generates both spontaneous events and responses to stimuli that appear to be in agreement with many of the data obtained from VIIIth-nerve fibers. As might be expected, the parts of the model that appear to be responsible for the quantitative

discrepancies that exist between model and fiber data correspond to the parts of the peripheral auditory system that are least understood. More precisely, the excitation process involving the hair cell-neuron junction is not understood precisely. We propose to extend our studies of models of the excitation process. For instance, we are considering a model that attributes the probabilistic mechanism in the peripheral system to "synaptic noise," rather than to noise in the membrane potential of the fiber as we have assumed in the model presented here.

The results obtained from the model have suggested some novel ways to analyze the spike activity generated by nerve fibers. The D_n criterion, discussed in section 5.3, is a measure of the amount of time-locked spike activity present in a record of data. This measure is somewhat independent of the spontaneous rate of firing. A "threshold of firing" to a stimulus can be defined by using the D_n measure, and the significant variations of D_n from its mean value can be computed.

Another method of analysis of the spike activity of VIIIth-nerve fibers has suggested itself as a result of working with the model. The interaction between the refractory effects of the model neuron and the nonlinearities in the system (both those included in the transducer model and those in the model neuron) have led to many conceptual difficulties in this study. Both the refractory effects and the nonlinearities affect the pattern of firing of the model in response to stimuli. The separation of the effects of these two components on the response of the model to stimuli would simplify the study of the model. One procedure for eliminating the refractory effects and studying only the effects of the rest of the system is to consider only those events (in the model) or spikes (generated by a fiber) that are preceded by long intervals of time during which no firing occurs. For instance, a PST histogram of the response to acoustic clicks could be generated by counting only those firings that are preceded by intervals of time equivalent to the time needed for a fiber to recover completely from the last firing. Such modified PST histograms of the response of model and fiber to acoustic stimuli might, we feel, lead to interesting insights on the nature of the excitation process.

Further extensions of this work have suggested themselves. For instance, the study of models of transducer-neuron junctions and models of the initiation of action potentials in simple peripheral structures are of rather general interest. There are clearly analogous anatomical structures in many of the sensory modalities, as well as analogous physiological functions. We have not yet explicitly explored the relevance of this work to other physiological systems.

6.3 NOTE ON MODELS AND DIGITAL-COMPUTER SIMULATIONS

The research discussed here is patterned after a style of scientific investigation that we would like to describe more explicitly. First, we believe that precise answers to scientific questions can be obtained only when the questions themselves are precise. Furthermore, we find it desirable to phrase these questions in some context. We think

of this context as a formal or a conceptual structure: The word "model" is now in vogue to describe such a structure.

With the advent of the general-purpose digital computer, it has become possible to investigate models that do not necessarily lend themselves to more formal and analytic treatments. A much richer class of conceptual structures can thus be studied, at the cost, of course, of the elegance and economy that the formal models afford. This has particular importance in neurophysiology because few problems in this area have been reduced to an analytically manipulative form.

It is unfortunately true that many of the contemporary digital machines are taxed by even relatively simple models of relatively simple parts of the nervous system (such as the model of the peripheral auditory system presented here). Primarily, this is a consequence both of the design of these machines and the uses to which they have been put. Many of the large, general-purpose machines have been designed for business or military use, and this has made them somewhat unsuitable as research tools. Access to these machines has been limited largely to computer operators using punched cards.

This study has been made practical because of the existence of the TX-2 computer. This machine was designed and is administered as a research tool. Relatively large periods of time (hours instead of minutes) have been made available to individual investigators. An investigator can thus operate the machine in much the same manner as he might perform an experiment in the laboratory. Computations can be modified on the basis of results obtained. Also, the TX-2 computer has a flexible-order code, high-speed memories and a rich selection of input-output devices. We hopefully expect that bigger and better "scientific" machines will be built to serve the needs of the biological investigator.

APPENDIX A

A Discussion of the Distribution of Spontaneous Events

Deriving the distribution of intervals between events generated by the model (for the spontaneous-event case) is equivalent to deriving the distribution of axis crossings of a Gaussian process, for which the axis is not constant but is a function of time. The axis-crossing problem has not been solved in general, although considerable attention has been directed to this problem.

The distribution of intervals between spontaneous events generated by the model for a white noise process is discussed here. Consider the set of events $\{E_k\}$ occurring at times $k(\Delta t)$, where k is an integer. The event E_k is defined as occurring at k if the noise exceeds the threshold, $n_k \geq r_k$. The noise has a Gaussian distribution with

$$E[n_k] = 0$$

and

$$E[n_j n_k] = \begin{cases} 0 & \text{if } j \neq k \\ \sigma^2 & \text{if } j = k \end{cases}$$

The value of the threshold r_k is determined by the time of occurrence of the last event. If the previous event occurred at j, then the threshold is a function only of the time elapsed since the last event, $r_k = a_{k-j}$. The probability of the occurrence of an event at k+j, given that an event occurred at time k, is

$$(p_{k+j})_k = \Pr\left[n_{k+1} < r_{k+1}, n_{k+2} < r_{k+2}, \ldots, n_{k+j-1} < r_{k+j-1}, n_{k+j} \geq r_{k+j} / n_k \geq r_k\right].$$

An event occurred at k and the noise is assumed to be stationary; therefore

$$(p_{k+j})_k = p_j = \Pr\left[n_1 < a_1, n_2 < a_2, \ldots n_{j-1} < a_{j-1}, n_j \geq a_j / n_o \geq a_i\right].$$

The noise process is white; therefore

$$p_j = \int_{-\infty}^{a_1} p(n_1)\, dn_1 \int_{-\infty}^{a_2} p(n_2)\, dn_2 \cdots \int_{-\infty}^{a_{j-1}} p(n_{j-1})\, dn_{j-1} \int_{a_j}^{\infty} p(n_j)\, dn_j.$$

The n_k are identically distributed; therefore

$$p_j = \prod_{k=1}^{j-1} \left[\int_{-\infty}^{a_k/\sigma} d\Phi\right]\left[\int_{a_j/\sigma}^{\infty} d\Phi\right]$$

$$p_j = \prod_{k=1}^{j-1} \Phi(a_k/\sigma)\left[1-\Phi(a_j/\sigma)\right],$$

where

$$\Phi(x) = \int_{-\infty}^{x} (1/\sqrt{2\pi})\, e^{-(y^2/2)}\, dy$$

$$p_j = \Phi^{j-1}(a_j/\sigma)[1-\Phi(a_j/\sigma)] \prod_{k=1}^{j-1} [\Phi(a_k/\sigma)/\Phi(a_j/\sigma)].$$

Assume $\lim_{j\to\infty} a_j = a$ and $a_1 > a_2 > \ldots > a_j > a$. Therefore $\lim_{j\to\infty} \Phi(a_j/\sigma) = q$ (a constant).

Then for large j

$$p_j = q^{j-1}(1-q) \prod_{k=1}^{j-1} [\Phi(a_k/\sigma)/\Phi(a_j/\sigma)],$$

and

$$\prod_{k=1}^{j-1} [\Phi(a_k/\sigma)/\Phi(a_j/\sigma)]$$

is a typical term of a monotone bounded sequence, and therefore the sequence converges to a limit as $j \to \infty$. Therefore,

$$p_j \sim q^{j-1}(1-q); \qquad j \to \infty$$

and the distribution of intervals between events approaches the geometric distribution (exponential) in the limit of large intervals.

APPENDIX B

Derivation of Statistics of D_n^2

Consider a histogram with η_i elements in the i^{th} bin, $i = 1, \ldots, n$, and a total number of elements equal to $\sum_{i=1}^{n} \eta_i = N$. Define the counting random variable,

$$x_{ij} = \begin{cases} 1 & \text{if the } j^{th} \text{ element goes into the } i^{th} \text{ bin} \\ 0 & \text{otherwise} \end{cases}$$

Consider the case in which the probability that the j^{th} element goes into the i^{th} bin is independent of j and i, and equals $p = 1/n$. Then the number of elements in the i^{th} bin is given by the Bernoulli distribution. The mean and variance of η_i are then given by

$$E[\eta_i] = Np = N(1/n)$$

$$\text{var}[\eta_i] = Np(1-p) = (N/n)(1-1/n),$$

or they can be derived by means of the counting random variables as follows:

$$\eta_i = \sum_{j=1}^{N} x_{ij}$$

$$E[\eta_i] = E\left[\sum_{j=1}^{N} x_{ij}\right] = \sum_{j=1}^{N} E[x_{ij}]$$

but $E[x_{ij}] = 1 \cdot p + 0 \cdot (1-p) = p$; therefore, $E[\eta_i] = Np = N/n$. Similarly,

$$\text{var}[\eta_i] = \text{var}\left[\sum_{j=1}^{N} x_{ij}\right],$$

but the x_{ij} are a set of independent random variables. Therefore,

$$\text{var}[\eta_i] = \sum_{j=1}^{N} \text{var}[x_{ij}]$$

$$\text{var}[x_{ij}] = E[x_{ij}^2] - E^2[x_{ij}]$$

$$E[x_{ij}^2] = 1^2 \cdot p + 0^2 \cdot (1-p) = p$$

$$\text{var}[x_{ij}] = p - p^2 = p(1-p)$$

$$\text{var}[\eta_i] = Np(1-p) = (N/n)(1-1/n).$$

Define

$$D^2 = (1/n) \sum_{i=1}^{n} (\eta_i - E[\eta_i])^2$$

$$E[D^2] = E\left[(1/n) \sum_{i=1}^{n} (\eta_i - E[\eta_i])^2\right]$$

$$= (1/n) \sum_{i=1}^{n} E[(\eta_i - E[\eta_i])^2]$$

$$= (1/n) \sum_{i=1}^{n} \text{var}[\eta_i] = \text{var}[\eta_i]$$

$$= (N/n)(1-1/n)$$

$$\text{var}[D^2] = E[(D^2)^2] - E^2[D^2]$$

$$E[(D^2)^2] = (1/n^2) \sum_{i=1}^{n} \sum_{k=1}^{n} E[(\eta_i - E[\eta_i])(\eta_k - E[\eta_k])].$$

Expansion of the term in the brackets yields terms such as $E[\eta_i^2 \eta_k^2]$. By using the counting random variables, this term can be expanded:

$$E[\eta_i^2 \eta_k^2] = \sum_{j,p,\ell,m}^{N} E[x_{ij} x_{ip} x_{k\ell} x_{km}].$$

There are several cases to be considered in order to evaluate this sum.

Case 1. All terms different $j \neq p \neq \ell \neq m$

$$E[x_{ij} x_{ip} x_{k\ell} x_{km}] = E[x_{ij}]\, E[x_{ip}]\, E[x_{k\ell}]\, E[x_{km}]$$
$$= p^4$$

There are $(N)(N-1)(N-2)(N-3) = (N!)/(N-4)!$ such terms.

Case 2. All terms equal $j = p = \ell = m$

$$E[x_{ij} x_{ip} x_{k\ell} x_{km}] = E[x_{ij}^2 x_{kj}^2]$$
$$= \begin{cases} 0 & \text{if } i \neq k \\ E[x_{ij}^4] = p & \text{if } i = k \end{cases}$$

There are N such terms.

Case 3. Only one pair of equal terms

(a) Pair corresponds to same bin, that is, $j = p$, $\ell \neq m$, $j \neq \ell \neq m$

$$E[x_{ij}x_{ip}x_{k\ell}x_{km}] = E[x_{ij}^2 x_{k\ell}x_{km}]$$
$$= E[x_{ij}^2]\,E[x_{k\ell}]\,E[x_{km}]$$
$$= p^3$$

There are (N)(N-1)(N-2) = (N!)/(N-3)! such terms and two ways to pick the equal pair.

(b) Pair corresponds to different bins, that is, $j = \ell \neq p \neq m$

$$E[x_{ij}x_{ip}x_{k\ell}x_{km}] = E[x_{ij}x_{kj}]\,E[x_{ip}]\,E[x_{km}]$$
$$= \begin{cases} 0 & \text{if } i \neq k \\ p^3 & \text{if } i = k \end{cases}$$

There are (N)(N-1)(N-2) = (N!)/(N-3)! such terms and four ways to pick the equal pair.

The other cases can be dealt with in similar fashion.

Case 4. Two pairs of two equal terms

Case 5. Three equal terms

The other terms in the equation for $E[(D^2)^2]$ can be similarly expanded. When all of these terms are expanded and the results collected, the variance reduces to

$$\text{var}[D^2] = \frac{2N(N-1)}{n^3}\left[1 - \frac{1}{n}\right]$$
$$= \left(\frac{2(N-1)}{n^2}\right)\left(\frac{N}{n}\left[1 - \frac{1}{n}\right]\right)$$
$$= \left(\frac{2(N-1)}{n^2}\right) E[D^2]$$

$$\sigma[D^2] = \frac{\sqrt{2(N-1)\,E[D^2]}}{n}.$$

APPENDIX C

A Description of the Computer Programs

When a choice was necessary, the computer programs for this investigation were written to achieve greater flexibility of the programs, rather than to decrease the time required to run them. The programs are flexible in two different senses. First, there is a great deal of program control available to the operator of the machine. This control includes typewriter control of the parameters of the computation, toggle-switch control of various options in the computation, toggle-switch control of the initiation of a series of runs to be done automatically, push-button control of various displays of the computations that can be shown while the computation proceeds, and so forth. Second, it is relatively simple to make program modifications that accommodate, rather gross changes in the model. Thus a wide variety of models of the peripheral auditory system can be studied with relatively minor changes of program. Flexibility is an essential feature in the kind of research presented here. It is important for the research worker to interact with the machine directly, since the problems do not remain static but change as the system under investigation is further explored.

The TX-2 computer was chosen for this project for a number of reasons. Foremost among them is the philosophy of its design and administration. It has been regarded primarily as a research tool rather than as an overgrown calculating device. As such, it incorporates a highly flexible order code, a multiplicity of easily manipulative input and output devices, together with a large high-speed memory. Furthermore, computer time has been made available for large enough intervals of time to make on-line concept formation possible.

No discussion of computer programs can be complete without a presentation of a logical flow diagram of the programs. Figure 49 is such a diagram. The programs are divided into four major functional blocks: (1) main sequence, (2) miscellaneous input and output sequence, (3) display sequence, and (4) subroutine for handling numerical and alphabetical characters. The main sequence controls all of the computation associated with generating the required data. The miscellaneous input and output sequence can be used to select the desired display mode (without essentially interrupting the computation), or to stop the computation at any desired time. The display sequence is controlled by the miscellaneous input and output sequence and can be used to display a number of the results of the computation. The subroutine for handling characters (written by Lt. C. E. Molnar) is used in a variety of ways whenever alphabetical, numerical or other characters are to be manipulated by the machine. For instance, this subroutine can be used to display characters on the oscilloscope display tube in order to provide a title for the particular computation that is to be displayed. Examples of the use of this subroutine were shown in many of the figures in Section V. This subroutine is also utilized by a program that sets the parameters of the computation according to the keys struck on a keyboard. All of these sequences can be run virtually concurrently in the

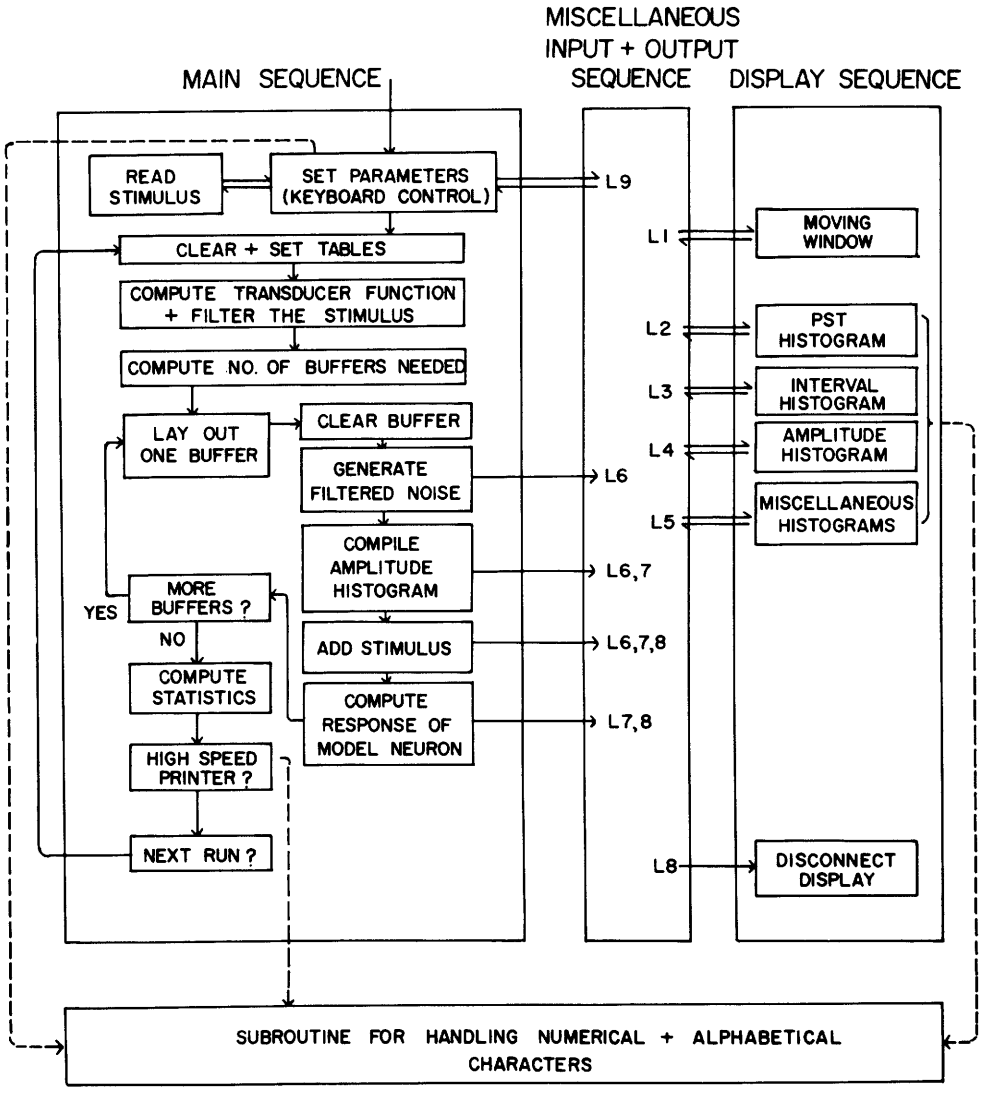

Fig. 49. Logical flow diagram of the computer programs. L1, L2, . . . , L9 is a set of lights and push buttons. The lights and push buttons are independent. The lights can be used as indicators from the machine to the operator, and the push buttons can be used as indicators from the operator to the machine. The "Moving Window" display program (written by Lt. C. E. Molnar) is used to view the contents of memory of the machine. (Figure 24 shows six pictures of data generated by the machine as displayed on the oscilloscope display tube with the Moving Window program used.)

machine. That is, the computations can be viewed and/or the results printed as they are produced. This is achieved in the TX-2 computer by the existence of interleaved programs. The control of the interleaving is performed almost automatically by the machine.

When the main sequence is actuated, control can be transferred to a program that has three uses: (i) to set the parameters of the computation (parameters are set according to keys struck on the keyboard); (ii) to read stimuli into the memory through a photoelectric tape reader; and (iii) to add any desired titles associated with the run or set of runs. In the next step an area of the memory that is used to hold the results of the computation is cleared and the locations of tables holding the results of the computation (such as histograms, mean firing rates, other statistics, etc.) are defined. Next, a specified nonlinear function of the stimulus (displacement of the basilar membrane) can be computed. The stimulus (which is a table of numbers stored in the memory) is then lowpass-filtered. Several different nonlinear functions have been used and the program has been written so that these different nonlinear functions can be selected by toggle switches.

The program then computes the number of buffers needed to compute the number of data points called for by the operator. Several distinct computations are performed on each buffer of data. First, the buffer is cleared; then filtered Gaussian noise is loaded into the buffer. (The filtered noise is obtained by sampling a noise generator, which produces noise with a uniform distribution. Several samples of this uniform-distribution noise are added and the sum is then filtered in two stages – a highpass stage followed by a lowpass stage. Both of these filtering operations are accomplished by difference equations that simulate RC filters.) When the buffer has been filled with noise, an amplitude histogram of the noise is compiled. The transformed and filtered stimulus is then added to the noise. Finally, the subroutine that is used to determine the response of the model neuron to this signal is activated. This subroutine compares the value of the signal plus noise to the value of the threshold at each point in time. The threshold value is determined by a "table look-up" scheme and the computer determines the value of the threshold by retaining the amount of time that has elapsed since the last event. An event occurs when the value of the signal plus the noise exceeds the threshold value. When an event occurs the appropriate entries are made in tables representing the PST histogram, the interval histogram, and the two-dimensional interval histogram. The counter, which is used to retain the value of the time elapsed since the last event, is reset, thus effectively resetting the threshold to its maximum value. If the threshold value is larger than the sum of signal and noise, no event occurs and the counter is indexed; this effectively changes the value of the threshold to its new value.

When these computations are completed on one buffer, the process is continued until the specified number of data points has been completed. At the end of these computations various other statistics are derived. The results can then be printed (in plotted form when desirable) on a high-speed printer. The high-speed printer has been used to obtain

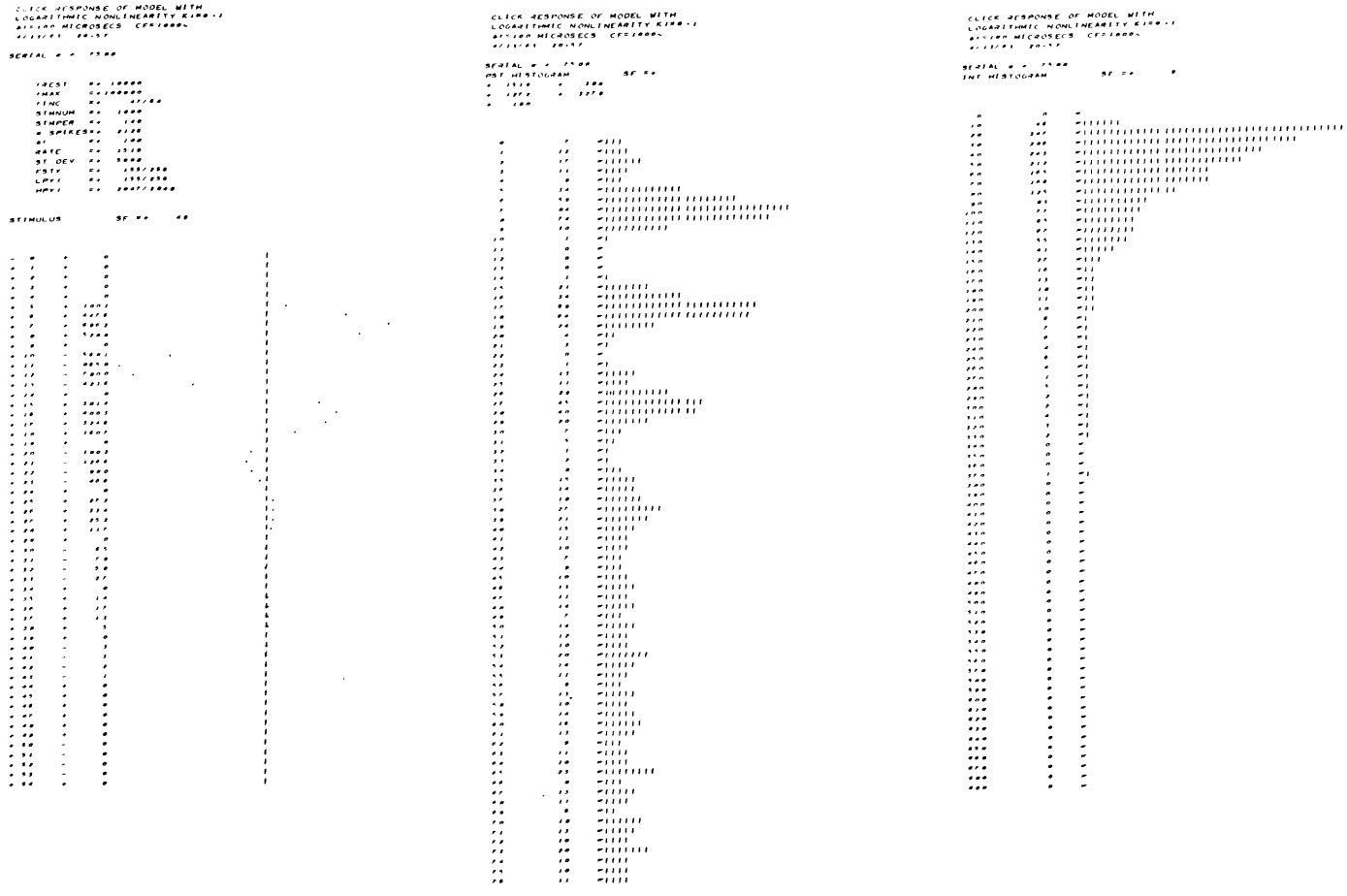

Fig. 50. High-speed printer display of the results of a typical computation. Left portion is a list of the parameters of the computation: tREST = R_R, tMAX = R_M, tINC = $\exp(-\Delta t/\tau_R)$, STMNUM = number of stimuli presented, STMPER = period of the stimulus, ST DEV = σ, etc. Also, the response of the cochlear partition is shown (for a point tuned to 1000 cps, in this case). Middle portion is the PST histogram. Right portion is the interval histogram.

a fast permanent record of each run. An example of a typical display available on the high-speed printer is shown in Fig. 50.

After (or while) the data for one run are being printed the next run can be started automatically. A number of options are available. For instance, a series of runs with varying intensity of stimulation can be automatically actuated, by using a set of toggle switches to specify the change in signal intensity. Similarly, a series of runs for different spontaneous rates can be actuated, and so on.

The time required for a typical run is two or three minutes. This run generates data equivalent to approximately one minute of similar data obtained from the physiological preparation. The time required to obtain the results of a computation on the model is thus equivalent to the time required to obtain and process the physiological data. No particular significance is attached to this result except in a comparative sense. Furthermore, programming changes calling for a change of speed of at least a factor of five are envisioned at present. The bulk of the two-minute time interval is consumed by the programs that generate the filtered noise and this time can be reduced in a number of ways. For instance, the filtered noise could be stored on digital tape and read into the machine on command.

At present, the programs occupy approximately 5000 registers of core memory. The bulk of this storage is required for the programs concerned with input and output devices, including the programs used for the various displays, the programs used to print the results on the high-speed printer, the programs used to read information into the machine through the photoelectric tape reader, the programs used to decode information coming into the machine through the keyboard, and the programs used to type information on a typewriter.

Acknowledgement

It is a pleasure to acknowledge the guidance and assistance of a few of the many people who have contributed to the completion of this work. I am most indebted to Dr. Nelson Y-S. Kiang for suggesting the topic of this research and for his constant counsel. The data that he has been able to obtain have made possible the formulation of models and theories. Professor Moise H. Goldstein, Jr., who supervised my thesis, Professor W. M. Siebert, Professor W. T. Peake, Dr. G. L. Gerstein, and Mr. Joseph L. Hall II were very generous with their time and provided critical appraisal of the work when it was needed. The members of the Communications Biophysics Group of the Research Laboratory of Electronics provided a stimulating intellectual environment in which to work. This atmosphere of freedom of inquiry is a consequence of the leadership of Professor Walter A. Rosenblith. I am grateful for the opportunity of working and learning in this environment.

The TX-2 computer was generously made available by Lincoln Laboratory, M. I. T. In particular, I wish to thank Mr. W. A. Clark for his efforts in my behalf. The friendship and assistance of Lt. C. E. Molnar is also acknowledged.

Bibliographical Note

The volume by G. von Békésy entitled Experiments in Hearing, edited by E. G. Weaver (New York, McGraw-Hill Book Company, 1960) is a compilation of the major publications of von Békésy in the field of hearing during the period from 1928 to 1958. For the reader's convenience, some of these publications, selected for their pertinence to this report, are listed here.

Zur Theorie des Hörens; Die Schwingungsform der Basilar-membran, Physik. Z. 29, 793-810 (1928).

Zur Physik des Mittelohres und über das Hören bei fehlerhaftem Trommelfell, Akust. Z. 1, 13-23 (1936).

Über die Messung der Schwingungsamplitude der Gehörknöchelchen mittels einer kapazitiven Sonde, Akust. Z. 6, 1-16 (1941).

Über die Elastizität der Schneckentrennwand des Ohres, Akust. Z. 6, 265-278 (1941); On the elasticity of the cochlear partition, J. Acoust. Soc. Am. 20, 227-241 (1948).

Über die Schwingungen der Schneckentrennwand beim Präparet und Ohrenmodell, Akust. Z. 7, 173-186 (1942); The vibration of the cochlear partition in anatomical preparations and in models of the inner ear, J. Acoust. Soc. Am. 21, 233-245 (1949).

Über die Resonanzkurve und die Abklingzeit der verschiedenen Stellen der Schneckentrennwand, Akust. Z. 8, 66-76 (1943); On the resonance curve and the decay period at various points on the cochlear partition, J. Acoust. Soc. Am. 21, 245-254 (1949).

Über die mechanische Frequenzanalyse in der Schnecke verschiedener Tiere, Akust. Z. 9, 3-11 (1944).

The variation of phase along the basilar membrane with sinusoidal vibrations, J. Acoust. Soc. Am. 19, 452-460 (1947).

The sound pressure difference between the round and the oval windows and the artificial window of labyrinthine fenestration, Acta Oto-laryngol. 35, 301-315 (1947).

D-C potentials and energy balance of the cochlear partition, J. Acoust. Soc. Am. 22, 576-582 (1950).

Microphonics produced by touching the cochlear partition with a vibrating electrode, J. Acoust. Soc. Am. 23, 29-35 (1951).

D-C resting potentials inside the cochlear partition, J. Acoust. Soc. Am. 24, 72-76 (1952).

Gross localization of the place of origin of the cochlear microphonics, J. Acoust. Soc. Am. 24, 399-409 (1952).

Direct observation of the vibrations of the cochlear partition under a microscope, Acta Oto-laryngol. 42, 197-201 (1952).

Description of some mechanical properties of the organ of Corti, J. Acoust. Soc. Am. 25, 770-785 (1953).

Shearing microphonics produced by vibrations near the inner and outer hair cells, J. Acoust. Soc. Am. 25, 786-790 (1953).

Paradoxical direction of wave travel along the cochlear partition, J. Acoust. Soc. Am. 27, 155-161 (1955).

References

1. G. von Békésy, Experiments in Hearing, edited by E. G. Wever (McGraw-Hill Book Company, Inc., New York, 1960).

1a. Ibid., p. 101.

1b. Ibid., p. 102.

1c. Ibid., p. 113.

1d. Ibid., pp. 99-100.

1e. Ibid., p. 432.

1f. Ibid., pp. 472-473.

1g. Ibid., pp. 476, 510.

1h. Ibid., pp. 466-469.

1i. Ibid., p. 407.

1j. Ibid., pp. 443-446.

1k. Ibid., pp. 458-460.

1ℓ. Ibid., pp. 447-464.

1m. Ibid., pp. 447-448.

1n. Ibid., pp. 442, 500-508.

1p. Ibid., p. 454.

1q. Ibid., p. 461.

1r. Ibid., p. 455.

1s. Ibid., p. 448.

1t. Ibid., pp. 510-534.

1w. Ibid., pp. 651-654.

1x. Ibid., pp. 680-684.

1y. Ibid., pp. 504-509.

1z. Ibid., pp. 442, 504-508.

1α. Ibid., pp. 448, 462.

2. G. von Békésy and W. A. Rosenblith, The early history of hearing – observations and theories, J. Acoust. Soc. Am. 20, 728 (1948).

3. E. A. Blair and J. Erlanger, A comparison of the characteristics of axons through their individual electrical responses, Am. J. Physiol. 106, 524-564 (1933).

4. W. A. Clark, The Lincoln TX-2 computer development; J. M. Frankovich and H. P. Peterson, A functional description of the Lincoln TX-2 computer; J. W. Forgie, The Lincoln TX-2 input-output system; R. L. Best, Memory units in the Lincoln TX-2; K. H. Olsen, Transistor circuitry in the Lincoln TX-2. Consecutive articles in Proc. Western Joint Computer Conference, February 26-28, 1957, pp. 143-171.

5. H. Davis, Biophysics and physiology of the inner ear, Physiol. Rev. 37, 1-49 (1957).

6. H. Davis, A mechano-electrical theory of cochlear action, Ann. Otol. Rhinol. Laryngol. 67, 789-802 (1958).

7. H. Davis, Some principles of sensory receptor action, Physiol. Rev. 41, 391-416 (1961).

8. H. Davis, B. H. Deatherage, D. H. Eldredge, and C. A. Smith, Summating potentials of the cochlea, Am. J. Physiol. 195, 251-261 (1958).

9. H. Engström, Electron micrographic studies of the receptor cells of the organ of corti, Neural Mechanisms of the Auditory and Vestibular Systems, edited by G. L. Rasmussen and W. Windle (Charles C. Thomas, Publisher, Springfield, Illinois, 1960), pp. 48-64.

10. H. Engström, H. W. Ades, and J. E. Hawkins, Structure and functions of the sensory hairs of the inner ear, J. Acoust. Soc. Am. 34, 1356-1363 (1962).

11. P. Fatt and B. Katz, Spontaneous subthreshold activity at motor nerve endings, J. Physiol. 117, 109-128 (1952).

12. W. Feller, An Introduction to Probability Theory and Its Applications (John Wiley and Sons, Inc., New York, 1950), p. 278.

13. C. Fernandez, The innervation of the cochlea (guinea pig), Laryngoscope 61, 1152-1172 (1951).

14. J. Fex, Augmentation of cochlear microphonics by stimulation of efferent fibers to the cat, Acta Otolaryngol. 50, 540-541 (1959).

15. J. Fex, Auditory activity in centrigufal and centripetal cochlear fibers in cat, Acta Physiol. Scand. (Stockholm) Vol. 55, Suppl. 189, 1962.

16. J. L. Flanagan, Models for approximating basilar membrane displacement, Bell System Tech. J. 39, 1163-1192 (1960).

17. J. L. Flanagan, Computational model for basilar membrane displacement, J. Acoust. Soc. Am. 34, 1370-1376 (1962).

18. H. Fletcher, On the dynamics of the cochlea, J. Acoust. Soc. Am. 23, 637-645 (1951).

19. L. S. Frishkopf, A Probability Approach to Certain Neuroelectric Phenomena, Technical Report 307, Research Laboratory of Electronics, M. I. T., March 1, 1956.

19a. Ibid., p. 63.

20. L. S. Frishkopf and W. A. Rosenblith, Fluctuations in Neural Thresholds, Symposium on Information Theory in Biology, edited by H. P. Yockey (Pergamon Press, London and New York, 1958), pp. 153-168.

21. R. R. Gacek and G. L. Rasmussen, Fiber analysis of the statoacoustic nerve of guinea pig, cat and monkey, Anat. Rec. 139, 455-463 (1961).

22. R. Galambos, Suppression of auditory nerve activity by stimulation of efferent fibers to cochlea, J. Neurophysiol. 19, 424-437 (1956).

23. R. Galambos, Studies of the auditory system with implanted electrodes, Neural Mechanisms of the Auditory and Vestibular Systems, edited by G. L. Rasmussen and W. Windle (Charles C. Thomas, Publisher, Springfield, Illinois, 1960), pp. 137-151.

24. G. L. Gerstein, Mathematical models for the all-or-none activity of some neurons, IRE Trans. on Information Theory, Vol. IT-8, 137-143, 1962.

25. G. L. Gerstein and N. Y-S. Kiang, An approach to the quantitative analysis of electrophysiological data from single neurones, Biophys. J. 1, 15-28 (1960).

26. D. D. Greenwood, Critical bandwidth and the frequency coordinates of the basilar membrane, J. Acoust. Soc. Am. 33, 1344-1356 (1961).

27. D. D. Greenwood, Approximate calculation of the dimensions of traveling-wave envelopes in four species, J. Acoust. Soc. Am. 34, 1364-1369 (1962).

28. L. D. Harmon, Studies with artificial neurons, I: properties and functions of an artificial neuron, Kybernetik 1, 89-101 (1961).

29. J. E. Hind, Unit activity in the auditory cortex, Neural Mechanisms of the Auditory and Vestibular Systems, edited by G. L. Rasmussen and W. Windle (Charles C. Thomas, Publisher, Springfield, Illinois), p. 203.

30. A. L. Hodgkin and A. F. Huxley, A quantitative description of membrane current and its application to conduction and excitation in nerve, J. Physiol. 117, 500-544 (1952).

31. M. Kac and D. Slepian, Large excursions of gaussian processes, Ann. Math. Statist. 30, 1215-1228 (1959).

32. Y. Katsuki, Neural mechanism of hearing in cats and insects, Electrical Activity of Single Cells, edited by Y. Katsuki (Igaku Shoin, Tokyo, 1960), pp. 53-75.

33. Y. Katsuki, N. Suga, and Y. Kanno, Neural mechanism of the peripheral and central auditory system in monkeys, J. Acoust. Soc. Am. 34, 1396-1410 (1962).

34. N. Y-S. Kiang, Spontaneous activity of single auditory nerve fibers in cats (Abstract), J. Acoust. Soc. Am. 35, 793 (1963).

35. N. Y-S. Kiang, T. Watanabe, E. C. Thomas, L. F. Clark, Stimulus coding in the cat's auditory nerve, Ann. Otol. Rhinol. Laryngol. 71, 1009-1027 (1962).

36. N. Y-S. Kiang, T. Watanabe, E. C. Thomas, and Louise F. Clark (monograph in preparation).

37. K. Küpfmuller and F. Jenik, Über die nachrichtenverarbeitung in der nervenzelle, Kybernetik 1, 1-6 (1961).

38. J. C. R. Licklider, Basic correlates of the auditory stimulus, Handbook of Experimental Psychology, edited by S. S. Stevens (John Wiley and Sons, Inc., New York, 1951), p. 995.

39. J. A. McFadden, The axis-crossing intervals of random functions, IRE Trans. on Information Theory, Vol. IT-2, pp. 146-150, 1956; The axis-crossing intervals of random functions II, Vol. IT-4, pp. 14-24, 1958; The fourth product moment of infinitely clipped noise, Vol. IT-4, pp. 159-162, 1958; The axis crossings of a stationary gaussian markov process, Vol. IT-7, pp. 150-153, 1961.

40. W. J. McGill and W. A. Rosenblith, Electrical responses to two clicks: A simple statistical interpretation, Bull. Math. Biophys. 13, 69-77 (1951).

41. A. Møller, Bilateral Contraction of the Tympanic Muscles in Man, Report No. 18, Speech Transmission Laboratory, Royal Institute of Technology, Stockholm, Sweden, February 20, 1961.

42. A. Møller, Network model of the middle ear, J. Acoust. Soc. Am. 33, 168-176 (1961).

43. A. Møller, personal communication, 1963.

44. A-M. Monnier and H. H. Jasper, Recherche de la relation entre les potentiels d'action élémentaires et la chronaxie de subordination. Nouvelle démonstration du functionnement par 'tout ou rien' de la fibre nerveuse, Compt. rend. Soc. Biol. 110, 547-549 (1932).

45. R. Oetinger and H. Hauser, Ein elektrischer kettenleiter zur untersuchung der mechanischen schwingungsvorgange in innenohr, Acustica 11, 161-177 (1961).

46. W. T. Peake, An Analytic Study of Electric Responses at the Periphery of the Auditory System, Technical Report 365, Research Laboratory of Electronics, M. I. T., March 17, 1960.

47. C. Pecher, La fluctuation d'excitabilite de la fibre nerveuse, Arch. Int. Physiol. 49, 129-152 (1939).

48. S. L. Polyak, The Human Ear in Anatomical Transparencies, Sonotone Corporation, Elmsford, New York, 1946.

48a. Ibid., p. 103.

48b. Ibid., p. 107.

48c. Ibid., p. 109.

49. O. F. Ranke, Physiologie des gehors, Gehör. Stimme Sprache (Lehrbuch der Physiologie, W. Trendelenburg and E. Schutz, eds.) (Springer-Verlag, Berlin, 1953).

50. G. L. Rasmussen, Efferent fibers of the cochlear nerve and cochlear nucleus, Neural Mechanisms of the Auditory and Vestibular Systems, edited by G. L. Rasmussen and W. Windle (Charles C. Thomas, Publisher, Springfield, Illinois, 1960), pp. 105-115.

51. S. O. Rice, Mathematical analysis of random noise, Selected Papers on Noise and Stochastic Processes, edited by N. Wax (Dover Publications, Inc., New York, 1954), pp. 133-294.

52. R. J. Ruben, U. Fisch, and W. Hudson, Properties of the eighth nerve action potential, J. Acoust. Soc. Am. 34, 99-102 (1962).

53. A. Rupert, G. Moushegian, and R. Galambos, Unit responses to sound from auditory nerve of the cat, J. Neurophysiol. 26, 449-465 (1963).

54. H. F. Schuknecht, Neuroanatomical correlates of auditory sensitivity and pitch discrimination in the cat, Neural Mechanisms of the Auditory and Vestibular Systems, edited by G. L. Rasmussen and W. Windle, op. cit., pp. 86-87.

55. W. M. Siebert, Models for the dynamic behavior of the cochlear partition, Quarterly Progress Report No. 64, Research Laboratory of Electronics, M. I. T., January 15, 1962, pp. 242-258.

56. D. Slepian, The one-sided barrier problem for gaussian noise, Bell System Tech. J. 41, 463-501 (1962).

57. Catherine A. Smith and F. S. Sjöstrand, Structure of the nerve endings on the external hair cells of the guinea pig cochlea as studied by serial sections, J. Ultrastructure Research 5, 523-556 (1961).

58. S. S. Stevens and H. Davis, Hearing (John Wiley and Sons, Inc., New York, 1938), pp. 310-332.

59. I. Tasaki, Nerve impulses in individual auditory nerve fibers of guinea pig, J. Neurophysiol. 17, 97-122 (1954).

60. I. Tasaki, Conduction of the nerve impulse, Handbook of Physiology (J. Field, ed.), Vol. I. Neurophysiology, Sec. 1. (American Physiological Society, Washington, D. C., 1959), p. 85.

61. I. Tasaki, H. Davis, and D. H. Eldredge, Exploration of cochlear potentials in guinea pig with a microelectrode, J. Acoust. Soc. Am. 26, 765-773 (1954).

62. I. Tasaki, H. Davis, and J. P. Legouix, The space time pattern of the cochlea microphonics (guinea pig), as recorded by differential electrodes, J. Acoust. Soc. Am. 24, 502-519 (1952).

63. D. C. Teas, D. H. Eldredge, and H. Davis, Cochlear responses to acoustic transients: an interpretation of whole-nerve action potentials, J. Acoust. Soc. Am. 34, 1438-1459 (1962).

64. M. ten Hoopen, A. den Hertog, and H. A. Reuver, Fluctuation in excitability of nerve fibres – A model study, Kybernetik 2, 1-8 (1963).

65. M. ten Hoopen and A. A. Verveen, Nerve-model experiments on fluctuation in excitability, Nerve, Brain and Memory Models, edited by Norbert Wiener and J. P. Schadé (Elsevier Publishing Company, Amsterdam, 1963), pp. 8-21.

66. A. A. Verveen, On the fluctuation of threshold of the nerve fibre, Structure and Function of the Cerebral Cortex, edited by D. B. Tower and J. P. Schadé, Proc. Second International Meeting of Neurobiologists, Amsterdam, 1959 (Elsevier Publishing Company, Amsterdam, 1960), pp. 282-288.

67. A. A. Verveen, Fluctuation in Excitability (Drukkerij Holland N. V., Amsterdam, 1961).

67a. Ibid., pp. 60-64.

68. A. A. Verveen, Axon diameter and fluctuation in excitability, Acta Morph. Neerl.-Scand., Vol. V, pp. 79-85, 1963.

69. L. J. Viernstein and R. G. Grossman, Neural discharge patterns in the transmission of sensory information, Information Theory, edited by C. Cherry (Butterworths Scientific Publications, London, 1961), pp. 252-269.

70. C. Wansdronk, On the Mechanism of Hearing (Ph. D. Thesis, University of Leyden, November, 1961), Philips Research Reports Supplements No. 1, Philips Research Laboratories, The Netherlands, 1962.

71. E. G. Wever and M. Lawrence, Physiological Acoustics (Princeton University Press, Princeton, N. J., 1954).

71a. Ibid., p. 113.

71b. Ibid., pp. 271-282.

71c. Ibid., p. 154.

71d. Ibid., p. 195.

71e. Ibid., pp. 154, 167.

72. F. M. Wiener and D. A. Ross, The pressure distribution in the auditory canal in a progressive sound field, J. Acoust. Soc. Am. 18, 401-408 (1946).

73. J. Zwislocki, Theorie der Schneckenmechanik, Acta Oto-laryngol., Supplement LXXII, 1948.

74. J. Zwislocki, Review of recent mathematical theories of cochlear dynamics, J. Acoust. Soc. Am. 25, 743-751 (1953).

75. J. Zwislocki, Some impedance measurements on normal and pathological ears, J. Acoust. Soc. Am. 29, 1312-1317 (1957).

76. J. Zwislocki, Analysis of the middle-ear function. Part I. Input impedance, J. Acoust. Soc. Am. 34, 1514-1523 (1962).

77. J. Zwislocki, Analysis of the middle-ear function. Part II. Guinea pig ear, J. Acoust. Soc. Am. 35, 1034-1040 (1963).

78. J. Zwislocki and A. S. Feldman, Post-mortem acoustic impedance of human ears, J. Acoust. Soc. Am. 35, 104-107 (1963).